

Syracuse University

**SURFACE**

---

Dissertations - ALL

SURFACE

---

5-14-2017

## EXPERIMENTAL AND MODELING STUDY OF IGNITION-RESISTANT FUELS

Apeng Zhou  
*Syracuse University*

Follow this and additional works at: <https://surface.syr.edu/etd>



Part of the [Engineering Commons](#)

---

### Recommended Citation

Zhou, Apeng, "EXPERIMENTAL AND MODELING STUDY OF IGNITION-RESISTANT FUELS" (2017).

*Dissertations - ALL*. 730.

<https://surface.syr.edu/etd/730>

This Dissertation is brought to you for free and open access by the SURFACE at SURFACE. It has been accepted for inclusion in Dissertations - ALL by an authorized administrator of SURFACE. For more information, please contact [surface@syr.edu](mailto:surface@syr.edu).

## ABSTRACT

This research investigates relative ignition behavior of some oxygenated fuels and their blends with gasoline surrogates. It seeks to identify fuels with higher resistance to ignition and validate tentative kinetic models intended to predict their combustion chemistry. It also develops a method for simplified ignition delay time correlation that can allow for a more rapid estimation of the ignition behavior of a given fuel at known thermodynamic conditions.

The work is motivated by the fact that in spark-ignition (SI) engines, increasing energy conversion efficiency through increasing the engine compression ratio is limited by the phenomenon of undesired autoignition known as engine knock. This is controlled by the chemical kinetics of the fuels which can be modified toward higher resistance using fuels of higher ignition resistance. In this study, the ignition behavior of the representative fuels is studied using both shock tube experiments and simulations of the kinetics of homogeneous chemical reactors. Specifically, we study: 1) propanol isomers, which are alcohols with three carbon atoms and promising alternative fuels for gasoline fuels; 2) MTBE and ETBE, which are effective ignition-resistant fuel components; 3) blends of a gasoline with ETBE or *iso*-propanol, to establish the kinetic interactions. The resulting experimental data are used to validate current chemical kinetics models of the individual fuels. To further facilitate the use of fuel blends suggested by this study, combined chemical kinetic models are developed of *iso*-octane as a gasoline surrogate and each of ignition resistant fuels identified.

In order to reduce the computational cost of using the validated detailed models of the fuels studied, reduced kinetic models are developed. These reduced versions are of two kinds. The first uses the model reduction method known as Alternate Species Elimination (ASE) to derive smaller versions of the detailed models. The second reduction approach focuses on the prediction of the chemical time scale associated with ignition. Here a generalized ignition format is developed and detailed model simulations are used to obtain the constraining data. This makes it possible to predict ignition time scales based on knowledge of temperature, pressure, and composition of the combustible mixture.

The work advances understanding of biofuels combustion by characterizing ignition properties of promising fuel additives and the effects of fuel blend on ignition. The resulting experimental data sets are useful for validating existing and future kinetic models. The combined models will allow for better insight into the combustion chemistry of ignition-resistant fuels formed from blending *iso*-octane with *iso*-propanol or ETBE.

EXPERIMENTAL AND MODELING STUDY OF IGNITION-RESISTANT FUELS

by

Apeng Zhou

B.S., Hefei University of Technology, 2010

M.S., Xi'an Jiaotong University, 2013

Dissertation

Submitted in partial fulfillment of the requirements for the degree of

Doctor of Philosophy

in

Mechanical and Aerospace Engineering

Syracuse University

June 2017

© Copyright 2017

Apeng Zhou

All Rights Reserved

## ACKNOWLEDGMENTS

I would like to express my deepest and sincere gratitude to my advisor, Prof. Ben Akih-Kumgeh, for his enlightening guidance and sage advice throughout my PhD study. From the discussions we had, I have gradually learned how to think critically and construct newly proposed ideas. His patience and support helped me finish this dissertation, and more importantly, overcome many challengeable situations during my progress in academic research.

I am indebted to Prof. Lawrence Tavlarides, Prof. Edward Bogucz, Prof. Thong Dang, Prof. Jianshun Zhang, and Prof. Melissa Green for graciously agreeing to be on my thesis committee. I am extremely grateful for their time in reviewing and commenting on my dissertation.

None of this would have been possible without the love and support from my family, who always encourage me in all of my pursuits and inspire me to follow my dreams.

I am very fortunate to study with several colleagues, including Mazen Eldeeb, Shirin Jouzdani, Nathan Peters, Deshawn Coombs, and David Zheng. Their efforts have helped complete the ideas in this dissertation. I would like to thank all of my friends for the good time we had together. The friendship has been an important piece in my life. Last but not least, I would like to give my special thanks to my dearly girlfriend, Meiling Zhao, who has supported me along the graduation journey and stood by me throughout the process.

## TABLE OF CONTENTS

	Page
ABSTRACT . . . . .	i
LIST OF TABLES . . . . .	viii
LIST OF FIGURES . . . . .	ix
1 Introduction and literature review . . . . .	1
1.1 Background and motivation . . . . .	1
1.2 Literature review . . . . .	6
1.2.1 Engine knock phenomena . . . . .	6
1.2.2 Research on ignition-resistant additive . . . . .	8
1.2.3 Research status of representative ignition-resistant fuels . . . . .	12
1.2.4 Engine knock modeling and prediction . . . . .	21
1.3 Objectives of this work . . . . .	26
2 Experimental and modeling approach . . . . .	29
2.1 Shock tube experiments . . . . .	29
2.1.1 Shock tube technique in ignition studies . . . . .	29
2.1.2 Experimental setup and procedure . . . . .	39
2.1.3 Data acquisition and processing . . . . .	42
2.1.4 Experimental uncertainties . . . . .	46
2.2 Ignition modeling approaches . . . . .	51
2.2.1 Chemical kinetic analysis of homogeneous constant volume reactor . . . . .	51
2.2.2 Mechanism reduction via Alternate Species Elimination (ASE) method . . . . .	57
2.2.3 Generalized ignition correlation method . . . . .	60
3 Ignition experiments . . . . .	64
3.1 Comparative ignition behavior: propanol isomers . . . . .	64
3.1.1 Experimental results and model validation . . . . .	64

	Page
3.1.2 Reduced chemical kinetic model . . . . .	75
3.2 Comparative ignition behavior: MTBE/ETBE . . . . .	85
3.2.1 Experimental studies and model validation . . . . .	85
3.2.2 Reduced chemical kinetic model . . . . .	99
3.3 Ignition behavior of gasoline-biofuel blends . . . . .	102
3.3.1 <i>Iso</i> -octane - <i>iso</i> -propanol blend . . . . .	102
3.3.2 <i>Iso</i> -octane - ETBE blend . . . . .	115
4 Generalized ignition correlation . . . . .	124
4.1 Demonstration . . . . .	124
4.2 Validation . . . . .	132
5 Conclusion and outlook . . . . .	141
LIST OF REFERENCES . . . . .	143
Vita . . . . .	155



## LIST OF TABLES

Table	Page
1.1 Oxygenates adding to gasoline [17] . . . . .	11
1.2 Fuel Economy and Octane . . . . .	16
1.3 Properties of ETBE and MTBE. . . . .	17
3.1 Composition of propanol mixtures used in this study. In the text, an ignition mixture is identified by the fuel type, its equivalence ratio, $\phi$ , and its argon/oxygen molar ratio, $D$ . . . . .	64
3.2 Composition of ethers mixtures used in this study. In the text, an ignition mixture is identified by the fuel type, its equivalence ratio, $\phi$ , and its argon/oxygen molar ratio, $D$ . . . . .	86
3.3 Composition of mixtures used for blend fuels study. In the text, an ignition mixture is characterized by the fuel type, its equivalence ratio, $\phi$ , and its argon/oxygen molar ratio, $D$ . . . . .	103
4.1 MD ignition correlation parameters (four switches) based on model by Herbinet et al. [149]. . . . .	130
4.2 Princeton jet fuel surrogate ignition correlation parameters (four switches) based on model by Dooley et al. [109]. . . . .	131
4.3 Aachen jet fuel surrogate ignition correlation parameters (four switches) based on model by Honnet et al. [150]. . . . .	132
4.4 Gasoline ignition correlation parameters (four switches) based on model by Mehl et al. [107]. . . . .	132
4.5 <i>n</i> -Octanol correlation parameters (four switches) based on model by Cai et al. [151]. . . . .	132
4.6 Ethanol/gasoline blend correlation parameters (four switches) based on model by Cai et al. [27]. . . . .	133
4.7 HCCI Engine Simulation Parameters. . . . .	137

## LIST OF FIGURES

Figure	Page
1.1 Chemical structures of representative anti-knock additives. . . . .	3
1.2 Spark ignition engine combustion processes and the mechanism for knocking combustion [3]. . . . .	8
1.3 Ignition delay times for stoichmetric n-heptane/air mixture in a wide range of temperatures at a pressure of 20 atm. Results are simulated using the n-heptane model by Mehl et al. [107]. . . . .	24
2.1 Shock tube used in this study. A laser diagnostic system for species concentration measurement during combustion processes is also displayed beneath the tube. . . . .	30
2.2 Distance, $x$ , versus time, $t$ , in a simple shock tube with gases at different states. (1) Initial test gas, (2) gas shocked by the incident shock wave, (3) driver gas behind contact surface, (4) initial driver gas, (5) test gas subjected to reflected shock wave [126]. . . . .	31
2.3 Schlieren images of a representative shock tube experiment. The test mixture is stoichmetric ETBE/O <sub>2</sub> /AR with a dilution ratio of 21.1; the average incident shock velocity is 725.2 m/s; test mixture at 10.2 atm and 1190 K. Ignition occurs around the 2.16 ms after onset of the reflected shock wave. . . . .	33
2.4 Schlieren images of ignition events after the reflected shock. The test mixture is stoichmetric ETBE/O <sub>2</sub> /AR with a dilution ratio of 21.1; test mixture at 10.2 atm and 1190 K. . . . .	34
2.5 Comparison of calculated and measured post-reflected shock pressure, $p_5$ , for sample reactive gas mixtures to establish the reliability of the shock relation method of temperature determination. . . . .	39
2.6 Representative signals from an experiment. . . . .	44
2.7 Representative shock wave arrival time measurement. . . . .	45
2.8 Representative shock velocity profile, indicating shock attenuation. . . . .	45
2.9 Representative ignition delay time measurement. Shown are the sidewall pressure and CH emission signals, for a <i>iso</i> -propanol/O <sub>2</sub> /Ar mixture with $\phi = 1.0$ , $p = 12.6$ atm, $T = 1068$ K and ratio of argon to oxygen, $D$ , is 3.76. . . . .	45

Figure	Page
2.10 Simplified mechanism for the oxidation of a general alkane, RH. QOOH is an alkyl hydroperoxide radical, produced from RO <sub>2</sub> by H atom transfer [99]. . . . .	53
3.1 comparison with <i>n</i> -propanol experiment correlations [25, 54] at 3.5 atm. . . . .	66
3.2 comparison with <i>iso</i> -propanol experiment correlation [54] at 3.5 atm. . . . .	66
3.3 Comparison with <i>n</i> -propanol experiment correlations [25, 54] at 5 atm. . . . .	67
3.4 comparison with <i>iso</i> -propanol experiment correlation [54] at 5 atm. . . . .	67
3.5 isomer effect on propanol ignition (3.5 atm). . . . .	67
3.6 isomer effect on propanol ignition (5 atm). . . . .	67
3.7 Comparison of measured <i>n</i> -propanol ignition delay times at 3.5 atm with model predictions. . . . .	69
3.8 Comparison of measured <i>iso</i> -propanol ignition delay times at 3.5 atm with model predictions. . . . .	69
3.9 Comparison of measured <i>n</i> -propanol ignition delay times at 5 atm with model predictions. . . . .	69
3.10 Comparison of measured <i>iso</i> -propanol ignition delay times at 5 atm with model predictions. . . . .	69
3.11 Comparison of measured <i>iso</i> -propanol ignition delay times at three equivalence ratios with predictions of model by Sarathy et al. [56]. . . . .	70
3.12 Comparison of measured <i>iso</i> -propanol ignition delay times at three equivalence ratios with predictions of model by Sarathy et al. [56]. . . . .	70
3.13 Isomer effect on ignition of stoichiometric mixtures at a higher average pressure of 12 atm and less dilute condition ( $D = 3.76$ ). Model simulations: Sarathy et al. [56]. . . . .	71
3.14 Species sensitivity analysis of <i>n</i> -propanol ignition. Shown are the 20 most important species at the condition $\phi = 1.0$ , $D = 21.0$ , $p = 15$ atm, and $T = 1050$ K. . . . .	73
3.15 Species sensitivity analysis of <i>iso</i> -propanol ignition. Shown are the 20 most important species at the condition $\phi = 1.0$ , $D = 21.0$ , $p = 15$ atm, and $T = 1050$ K. . . . .	73
3.16 Reaction pathway for <i>n</i> -propanol ignition ( $\phi = 1$ , 1% fuel, $D = 21$ , $p = 3$ atm) using the model by Sarathy et al. [56] at temperatures of 1475 K (top) and 1230 K (bottom). . . . .	74
3.17 Reaction pathway for <i>iso</i> -propanol ignition ( $\phi = 1$ , 1% fuel, $D = 21$ , $p = 3$ atm) using models by Sarathy et al. [56] with temperatures of 1510 K (top) and 1310 K (bottom). . . . .	75

Figure	Page
3.18 Methanol and ethanol: comparison of detailed and reduced model with respect to ignition delay time prediction at three equivalence ratios and pressure of 20 atm. . . . .	78
3.19 Propanol isomers: comparison of detailed and reduced model with respect to ignition delay time prediction at three equivalence ratios and pressure of 20 atm. . . . .	78
3.20 <i>n</i> - And <i>iso</i> -butanol isomers: comparison of detailed and reduced model with respect to ignition delay time prediction at three equivalence ratios and pressure of 20 atm. . . . .	78
3.21 <i>n</i> - And <i>s</i> -butanol isomers: comparison of detailed and reduced model with respect to ignition delay time prediction at three equivalence ratios and pressure of 20 atm. . . . .	78
3.22 Methanol and ethanol: comparison of detailed and reduced model with respect to ignition delay time prediction at two different pressures and higher dilution level. . . . .	79
3.23 <i>n</i> - and <i>iso</i> -propanol isomers: comparison of detailed and reduced model with respect to ignition delay time prediction at two different pressures and higher dilution level. . . . .	79
3.24 Methanol and ethanol; propanol isomers: Comparison of detailed and reduced models with respect to burning velocity prediction for fuel/air mixtures at 1.0 atm and 400 K. . . . .	80
3.25 Binary blends of butanol isomers: Comparison of detailed and reduced models with respect to burning velocity prediction for fuel/air mixtures at 1.0 atm and 400 K. . . . .	80
3.26 Concentration correlation function based on fuel and CO concentrations. The time to maximum captures the global chemical kinetics of the pyrolysis process and can be used to investigate effects of temperature, pressure, and fuel concentration. . . . .	81
3.27 Comparison of pyrolysis time for 1% fuel (equal proportions of methanol and ethanol) at a pressure of 3.0 atm. . . . .	82
3.28 Comparison of pyrolysis time for 1% fuel (equal proportions of <i>n</i> - and <i>iso</i> -propanol) at a pressure of 3.0 atm. . . . .	82
3.29 Simulation of a Homogeneous Charge Compression Ignition cycle at an engine speed of 1000 rpm from an initial state of 400 K and 1.0 atm. The combustible mixture is a stoichiometric fuel/air mixture, with the fuel as equal molar proportions of methanol and ethanol. . . . .	83

Figure	Page
3.30 Simulation of a Homogeneous Charge Compression Ignition cycle at an engine speed of 1000 rpm from an initial state of 400 K and 1.0 atm. The combustible mixture is a stoichiometric fuel/air mixture, with the fuel as equal molar proportions of <i>n</i> - and <i>s</i> -butanol. . . . .	83
3.31 Validation of MTBE experiment against literature data by Fieweger et al. [95,96] and comparison with model predictions using models by the Galway [83], the CNRS [87] and the Milano [86] groups. . . . .	87
3.32 Relative ignition behaviors of MTBE and ETBE at average pressures of 3.5 atm and 13 atm. . . . .	88
3.33 Bond dissociation energies (BDEs) of MTBE/ETBE calculated by direct atomization (CBS QB3 method) using the Gaussian 09 software package. The values are in units of kcal/mol. . . . .	90
3.34 Comparison of measured MTBE ignition delay times at 3.5 atm with model predictions. . . . .	91
3.35 Comparison of measured ETBE ignition delay times at 3.5 atm with model predictions. . . . .	91
3.36 Comparison of measured ETBE ignition delay times at 13 atm with model predictions. . . . .	91
3.37 Comparison of measured MTBE ignition delay times at three equivalence ratios with predictions of Galway model [83]. . . . .	92
3.38 Comparison of measured ETBE ignition delay times at three equivalence ratios with predictions of Galway model [83]. . . . .	92
3.39 Comparison of measured ignition delay times for stoichiometric MTBE mixtures at two different dilution ratios with model predictions. . . . .	94
3.40 Comparison of measured ignition delay times for lean MTBE mixtures at two different dilution ratios with model predictions. . . . .	94
3.41 Comparison of measured ignition delay times for stoichiometric ETBE mixtures at two different dilution ratios with model predictions. . . . .	95
3.42 Species sensitivity analysis of MTBE ignition. Shown are the 20 most important species at the condition $\phi = 1.0$ , $D = 21.0$ , $p = 15$ atm, and $T = 1050$ K. . . . .	96
3.43 Species sensitivity analysis of ETBE ignition. Shown are the 20 most important species at the condition $\phi = 1.0$ , $D = 21.0$ , $p = 15$ atm, and $T = 1050$ K. . . . .	96
3.44 The four-center elimination reaction for MTBE [87]. . . . .	97
3.45 Reaction pathways for MTBE ignition ( $\phi = 1$ , $D = 3.76$ ) using the model by Galway group [83] at pressures of 3.5 atm (top) and 13 atm (bottom). . . . .	98

Figure	Page
3.46 Reaction pathways for ETBE ignition ( $\phi = 1$ , $D = 3.76$ ) using the model by Galway group [83] at pressures of 3.5 atm (top) and 13 atm (bottom). . . . .	99
3.47 Reaction pathways for MTBE ignition ( $\phi = 1$ , $D = 3.76$ ) using the model by CNRS group [87] at pressures of 3.5 atm (top) and 13 atm (bottom). Contrary to the Galway model, features more reactive channels. . . . .	100
3.48 Reaction pathways for ETBE ignition ( $\phi = 1$ , $D = 3.76$ ) using the model by CNRS group [87] at pressures of 3.5 atm (top) and 13 atm (bottom). Contrary to the Galway model, features more reactive channels. . . . .	100
3.49 MTBE and ETBE: comparison of detailed and reduced model with respect to ignition delay time prediction at three equivalence ratios and pressure of 20 atm. The Ar/O <sub>2</sub> , $D$ , is 3.76. . . . .	101
3.50 MTBE and ETBE: comparison of detailed and reduced model with respect to ignition delay time prediction at two different pressures and higher dilution level than used in model reduction. . . . .	101
3.51 Validation of <i>iso</i> -octane experiment against data previously measured by our group [138,139]. . . . .	104
3.52 Relative ignition behavior of stoichiometric fuel/O <sub>2</sub> /Ar mixtures of <i>iso</i> -propanol and <i>iso</i> -octane at a pressure of 12 atm. . . . .	104
3.53 Relative ignition behavior of <i>iso</i> -octane, <i>iso</i> -propanol, 50/50 and 75/25 blends of both (by liquid volume) at a pressure of 12.0 atm. The experimental data has same level of uncertainty as shown before. . . . .	105
3.54 Relative ignition behavior of <i>iso</i> -octane/ <i>iso</i> -propanol (75/25 by liquid volume) blends at three equivalence ratios. . . . .	106
3.55 Isooctane: comparison of detailed and reduced model with respect to ignition delay time prediction at three equivalence ratios and pressure of 15 atm. . . . .	108
3.56 Isooctane: comparison of detailed and reduced model with respect to ignition delay time prediction at two different pressures and higher dilution level. . . . .	108
3.57 Comparison of <i>iso</i> -octane test with the model predictions from the blend models in this work and detailed model by Mehl et al. [107]. . . . .	110
3.58 Comparison of <i>iso</i> -propanol test data with the model predictions from the blend model in this work and detailed model by Sarathy et al. [159]. . . . .	110
3.59 Comparison of test for stoichiometric <i>iso</i> -octane/ <i>iso</i> -propanol (50/50) mixture with the model predictions from the blend model in this work and model by Milano group [24]. . . . .	111

Figure	Page
3.60 Comparison of test for stoichiometric <i>iso</i> -octane/ <i>iso</i> -propanol (75/25) mixture with the model predictions from the blend model in this work and model by Milano group [24]. . . . .	111
3.61 Comparison of test for rich <i>iso</i> -octane/ <i>iso</i> -propanol (75/25) mixture with the model predictions from the blend model in this work and model by Milano group [24]. . . . .	111
3.62 Reaction pathways for <i>iso</i> -octane, <i>iso</i> -propanol, and a blend of equal liquid volume proportions during ignition process ( $\phi = 1$ , $D = 3.76$ ) using the combined model at a pressure of 12 atm. Shown are the results close to the onset of the reactor. . . . .	112
3.63 Reaction pathways for <i>iso</i> -octane, <i>iso</i> -propanol, and a blend of equal liquid volume proportions during ignition process ( $\phi = 1$ , $D = 3.76$ ) using the combined model at a pressure of 12 atm. Shown are the results of the reactor midway to the ignition instance. . . . .	113
3.64 Reaction pathways for <i>iso</i> -octane, <i>iso</i> -propanol, and a blend of equal liquid volume proportions during ignition process ( $\phi = 1$ , $D = 3.76$ ) using the combined model at a pressure of 12 atm. Shown are the results very close to ignition onset. . . . .	114
3.65 Relative ignition behavior of stoichiometric fuel/O <sub>2</sub> /Ar mixtures of ETBE and <i>iso</i> -octane at two pressures of 5 and 12 atm. The experimental data has same level of uncertainty as shown before. . . . .	116
3.66 Relative ignition behavior of <i>iso</i> -octane, ETBE, 50/50 and 75/25 blends of two ratios at a pressure of 12.0 atm. . . . .	117
3.67 Relative ignition behavior of <i>iso</i> -octane, ETBE, 50/50 blend of both (by liquid volume) at a pressure of 5.0 atm. . . . .	117
3.68 Comparison of ETBE test with the model predictions from the blend model in this work and detailed model by Galway group [83]. . . . .	118
3.69 Comparison of test for stoichiometric <i>iso</i> -octane/ETBE (50/50) mixture with the model predictions from the blend model in this work, and models by Milano [86] and Tokyo [93] groups. . . . .	119
3.70 Comparison of test for stoichiometric <i>iso</i> -octane/ETBE (75/25) mixture with the model predictions from the blend model in this work, and models by Milano [86] and Tokyo [93] groups. . . . .	119
3.71 Reaction pathways for <i>iso</i> -octane, ETBE, and a blend of equal liquid volume proportions during ignition process ( $\phi = 1$ , $D = 3.76$ ) using the combined model at a pressure of 12 atm. Shown are the results close to the onset of the reactor. . . . .	120

Figure	Page
3.72 Reaction pathways for <i>iso</i> -octane, ETBE, and a blend of equal liquid volume proportions during ignition process ( $\phi = 1$ , $D = 3.76$ ) using the combined model at a pressure of 12 atm. Shown are the results of the reactor midway to the ignition instance. . . . .	121
3.73 Reaction pathways for <i>iso</i> -octane, ETBE, and a blend of equal liquid volume proportions during ignition process ( $\phi = 1$ , $D = 3.76$ ) using the combined model at a pressure of 12 atm. Shown are the results very close to ignition onset. . .	122
4.1 Representative ignition simulations for methyl decanoate (MD) correlation development based on model by Herbinet et al. [149]. . . . .	125
4.2 Dependence of cross-over temperatures on reactor pressures. . . . .	125
4.3 a. Simulated methyl decanoate (MD) ignition delay times and correlation predictions in the three regions. b. Comparison of MD ignition correlation predictions with simulated delay times using two switches at cross-over temperatures. . . .	127
4.4 Comparison of simulated MD ignition delay times with ignition predictions using the empirical correlation proposed by Vandersickel et al. [121,122]. . . . .	127
4.5 Merging of MD ignition correlations of the three sub-regions using the sine function. . . . .	128
4.6 Graphic description of hyperbolic tangent function. . . . .	128
4.7 a. Comparison of correlation predictions with simulated ignition delay times (four switches). b. Test of the correlation at pressures not used in its development. .	131
4.8 Comparison of the model-based correlations with experimental data. a). Methyl decanoate shock tube ignition data by Wang et al. [167] and Li et al. [168]. b. Gasoline surrogate RCM data by Kukkadapu et al. [169] and shock tube data by Gauthier et al. [152]. . . . .	135
4.9 Comparison of the model-based correlations with experimental data. a. <i>n</i> -Octanol shock tube data taken by Cai et al. [151]. b. Ethanol/Gasoline surrogate shock tube data by Fikri et al. [153]. . . . .	136
4.10 By modifying correlation parameters, the model-based correlation for Princeton Jet Fuel Surrogate can be brought to better agreement with experimental data. Experimental data taken from Dooley et al. [109] . . . . .	136
4.11 Cases for comparison between Livengood-Wu integral ignition prediction and engine combustion pressure profiles. . . . .	138
4.12 Comparison of the predicted ignition times for gasoline surrogates using Livengood-Wu integral method and engine simulation results. . . . .	139
4.13 Simulation for MD ignition under various dilution and equivalence ratios. . . .	140



# 1. INTRODUCTION AND LITERATURE REVIEW

## 1.1 Background and motivation

The spark-ignition (SI) engine has achieved a high level of success since the invention of the first Otto engine over a century ago [1]. However, these internal combustion engines convert only about 20-30 % of the energy in the fuel to motive power [2]. Theoretically, this is far lower than the maximum efficiency of an ideal heat engine which can be as high as 70 %. Due to limited fossil fuel reserves and more stringent emission regulations, increasing the efficiency of engines used in transportation represents a significant opportunity to reduce future demand for oil, while also reducing our carbon footprints. Faced with these challenges, researchers and engineers are working toward more advanced combustion systems. These advanced combustion engine should have very high efficiencies and low emissions [3].

Uncontrolled ignition in spark-ignition (SI) engines is known as engine knock. This is an abnormal combustion phenomenon which can limit engine life span and reduce thermal efficiency [4]. In SI engines, normal combustion depends on the operating conditions and fuel chemistry. In this normal mode, which is initiated solely by a timed spark discharge, the initiated flame front propagates through the cylinder volume in a uniform manner. Depending on the evolution of thermodynamic conditions in the end-gas, the fuel reactivity and the rate of development of the flame, the abnormal combustion mode, engine knock,

can result. Engine knock is well known as a major barrier to further improvement of the SI engine thermal efficiency. If knock occurs over a long period of time, it causes damage to the engine hardware, and so it must to be avoided.

This undesired autoignition can be effectively suppressed by various methods such as increasing in-cylinder turbulence, reducing the end-gas temperature by decreasing chamber wall temperature and decreasing the initial combustible gas temperature, introducing more inert gases, increasing the fuel octane number, etc. [5]. Each approach has its own advantages and weakness. Previous studies have shown that various fuels have different ignition-resistance capabilities. Thus fuel design technology for SI engines today seeks alternative fuels for sustainability while also targeting those fuel options with good ignition resistance. For practical comparison of fuels, a fuel's ignition resistance is described using the octane number. This octane number essentially refers to the percentage of *iso*-octane in an *iso*-octane/*n*-heptane mixture which would have similar ignition behavior as the fuel in question. For decades, engineers have used fuel additives to gasoline in order to increase the resulting fuel's octane number [6]. From a chemical perspective, these additives can be viewed as increasing the activation energy for the combustion of the gasoline mixture. Activation energy is the minimum applied energy required to effect a chemical reaction. Including ignition-resistance additives in gasoline fuel modifies the chemical reactivity of the fuel so that combustion can proceed smoothly without the uncontrolled self ignition. Ignition-resistance additives were introduced in the 1920s and were instrumental in increasing engine compression ratios to levels which yielded higher efficiency and durable performance.

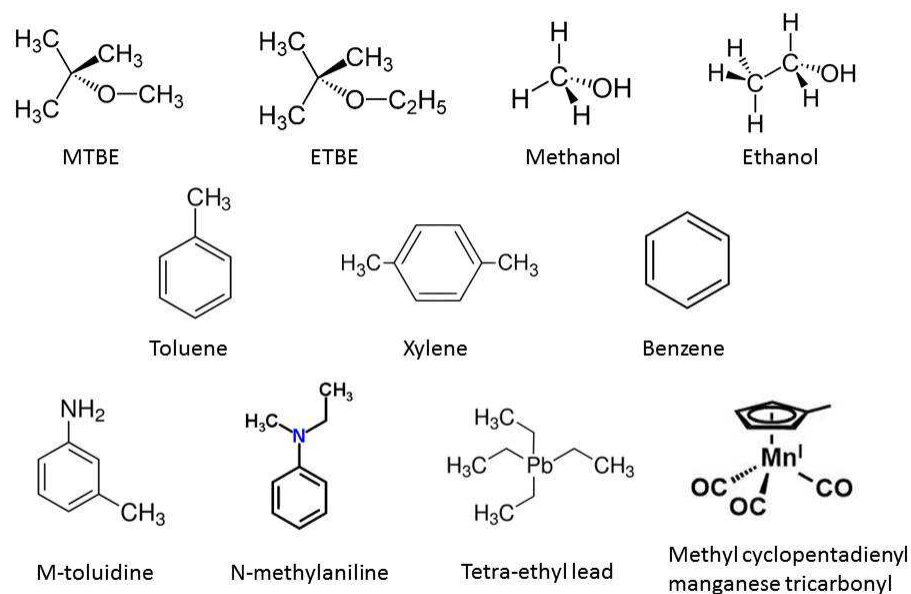


Fig. 1.1.: Chemical structures of representative anti-knock additives.

There is a wide spectrum of ignition-resistant additives [7], among which are oxygenated hydrocarbons, aromatic hydrocarbons, aromatic amines, and organometallic carbonyl compounds. Molecular structures of representative anti-knock additives are shown in Fig. 1.1. These are briefly described below.

a. Oxygenates: These include ethers such as methyl tertiary-butyl ether (MTBE), ethyl tertiary-butyl ether (ETBE), tertiary-amyl methyl ether (TAME), di-isopropyl ether (DIPE); alcohols such as methanol, ethanol, tertiary butyl alcohol (TBA). Because they are added in large amounts (e.g. 3% vol. methanol to 15% vol. MTBE), these oxygenates are often considered as fuel compounds and not just fuel additives.

b. Aromatic hydrocarbons (aromatics): These include toluene, xylene, and benzene. The last one is toxic (including carcinogenicity) and therefore its amount is restricted to

1% vol. The maximum allowable concentration of aromatics in gasoline is 35% vol. This is because in addition to toxicity, aromatics have lower lubricating effectiveness and so, can cause problems to fuel supply systems.

c. Aromatic amines: These are not widely used today; they were mostly used in aviation gasoline during World War II. Examples of these include *m*-toluidine, *p*-toluidine, *p*-tert-butylaniline, technical pseudocumidine, *N*-methylaniline, and cumidines.

d. Organometallic carbonyl compounds: These are organic compounds with metallic inclusion. Examples include tetra-ethyl lead (TEL), methyl cyclopentadienyl manganese tricarbonyl, iron pentacarbonyl, and ferrocene. One of the most effective organometallic, tetra-ethyl lead (TEL), is based on Pb, while other additives also are based on metals such as Mn and Fe. Most organometallic additives have adverse effects on human health and the environment.

Nowadays most ignition-resistant fuel are oxygenates and aromatics and research engineers continue to explore ignition-resistant agents that are better suited for next-generation engines and without negative effects on humans or the environment. It is therefore of great interest to investigate and study possible alternative ignition-resistant fuels or fuel additives for suppressing uncontrolled ignition in engines.

The focus on ignition-resistant fuels of renewable origin is linked to the fact that crude oil is an exhaustible energy source. Biofuels is the term generally applied to fuels derived from biomass and they often contain oxygen [8–10]. Biomass is biological material (plant and animal) from living or recently living matter, such as wood, various types of plants, grass, algae (microorganisms) and organic wastes. Two main subclasses of biofuels are bioalcohols and biodiesel. They can be used as substitutes of or as additives to

conventional fuels. For instance, bioalcohols can be added to gasoline and biodiesel can be added to diesel fuel. Among alcohols, four alcohols are commonly used as biofuels: methanol, ethanol, propanols, and butanols. Currently, there is need for improved understanding of the fundamental combustion properties of these fuels in order to properly apply them in combustion technologies.

An optimal approach to fuel design is developing alternative fuels that can be blended with conventional fuels, imparting improved ignition resistance and reduced emission levels. For each of the additives, a reliable model is needed for ignition prediction in order to understand and avoid uncontrolled ignition conditions in the engine during design and real time engine control. Detailed and reduced chemical kinetics models of fuel combustion can be used to simulate autoignition processes under known conditions. However, they are associated with high computational costs. To simplify ignition prediction for hydrocarbon and biofuels, it is necessary to develop highly reduced and simplified versions of the detailed models that can reduce the computational cost for ignition prediction with a prediction accuracy that is comparable with that of the detailed kinetic models. Part of the proposed research will therefore seek reduced models of some fuels of interest.

In terms of potential bio-derived fuels that can retard ignition, bioalcohols and ethers appear to be good candidates. In particular, alcohols such as propanol isomers and the ethers, such as MTBE and ETBE need serious considerations. Their ignition behavior can be investigated using a shock tube facility. Existing chemical kinetic models of these fuels are not yet sufficiently accurate and they have been validated using a limited set of experimental data. The effect of blending biofuels of interest with gasoline is yet to be explored, especially with respect to the ignition resistance. Further, the reactivity

differences revealed by ignition studies of these compounds can be used to improve understanding and modeling. Detailed and reduced models of the combustion kinetics of biofuel-gasoline blends are needed to advance computational analysis.

## **1.2 Literature review**

This review puts into context the objective of the proposed work. It focuses on two closely related topics: understanding and modeling uncontrolled ignition phenomena as well as fundamental and applied combustion study of biofuels and other oxygenates as ignition-resistant fuels.

### **1.2.1 Engine knock phenomena**

Many research activities in the past on engine knock have focused on understanding the nature and causes of uncontrolled ignition in SI engines [3,4,11]. There are two generally accepted theories of engine knock: "auto-ignition" and "detonation" theories. The auto-ignition theory of engine knock relates to the ignition of so-called hot spots in the unburned compressed combustible gas. These hot spots are formed due to non-uniformity in temperature or fuel concentrations. After spark ignition, the unburned gas is compressed by the expanding burned gas, further compressed or expanded by the moving piston, heated by radiation from the flame front, and cooled or heated by the surrounding boundaries. At the point where the temperature and pressure of the end gas exceed its auto-ignition point, the end gas would ignite spontaneously, starting at one or more points with front propagation velocities that are higher than 2000 m/s as shown in Figure 1.2. A

violent explosion will occur in the end gas, causing pressure waves to oscillate in the combustion chamber, often perceived as a pinging sound. The detonation theory, on the other hand, assumes that engine knock occurs due to the propagation of the flame front that accelerates from the spark plug to the other end of the cylinder. A shock wave is generated by the wrinkled flame as it propagates and it reflects from one side of the cylinder wall to the other within the combustion chamber. The impact pressures are short in duration but high in magnitude, leading to uncontrolled ignition.

It is now generally accepted that "engine knock" can be understood to be the result of auto-ignition in the compressed end-gas before it is reached by the flame front propagating from the spark plug [12–14]. Because of the compositional and thermal heterogeneity of the unburned end-gas, the auto-ignition is seldom homogeneous, it usually occurs randomly at localized centers. When it occurs, pressure waves are generated, which can lead to the formation of detonation waves. Sometimes auto-ignition does not necessarily give rise to the violent knock. There are three basic modes of propagation from the auto-ignition centers, depending on the temperature gradients [15]. These include (a) a weak pressure rise, (b) sequence of nearby hot spot ignition, and (c) shock-driven detonation.

a). When the end-gas has low temperature and steep temperature gradients, it will produce a weak pressure rise, which propagates from the center and is attenuated, combustion then undergoes a gradual transition to knock. The resulting flame travels with average speeds of  $v = 50 - 200$  m/s. In this phase, we have non-knocking combustion.

b). When the end-gas has high temperatures and small temperature gradients, ignition occurs locally and is immediately followed by ignition of nearby spots. At the onset of the main heat release, the average speed can be up to  $v = 500$  m/s. There is a clear correlation

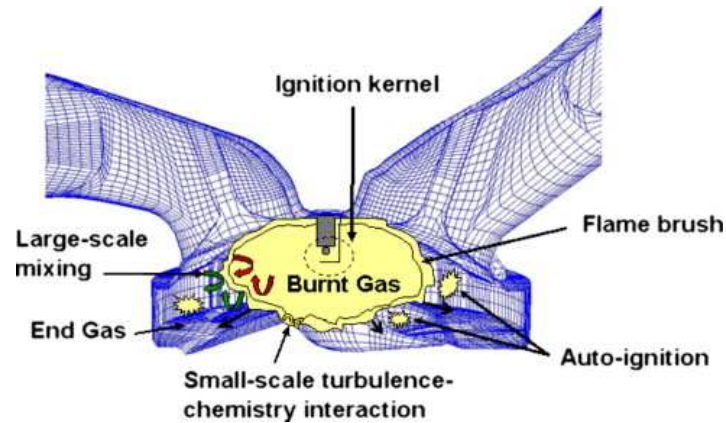


Fig. 1.2.: Spark ignition engine combustion processes and the mechanism for knocking combustion [3].

between the propagation velocity and the knock intensity: the faster the flame front of main heat release propagates, the higher the knock intensity.

c). In this case, local heat release by a large enough volume generates shock waves. A shock wave that is strong enough eventually leads to detonation of the mixture.

These three basic modes can represent limiting conditions and are associated with trace, moderate, severe engine knock, respectively. Therefore, a complete understanding of knock and exploring possible knock reduction methods can be of great importance with respect to the future emission levels as well as engine development costs. Since auto-ignition is "central" to each of the theorized "knock mechanisms", characterizing ignition properties of fuels can lead to identification of those fuels which are likely to inhibit knock.

### 1.2.2 Research on ignition-resistant additive

Combustion involves a very rapid series of chemical chain reactions between fuel vapors and oxygen. Factors that increase the rates of combustion reactions would also favor



uncontrolled ignition or knocking. These factors include higher temperatures, higher pressures, and longer residence times after spark ignition. Ignition-resistant additives interrupt and slow down the chain reactions that lead to unexpected auto ignition.

The relative ignition resistance of a fuel is assessed using the octane number, an empirical metric. The octane number scale is defined by two pure reference fuels: normal heptane (*n*-heptane) with an octane number of zero, and *iso*-octane (2,2,4-trimethylpentane) with an octane number of 100. The octane number of a blend of these two reference compounds, *n*-heptane and *iso*-octane, is equal to the volume percentage of *iso*-octane it contains. The octane number of a given fuel is then determined as the percentage of the *iso*-octane in the blend of the two reference fuels so that the blend has comparable engine knock behavior with the fuel. For instance, a gasoline fuel with an octane number of 87 has the same knock as a mixture of 87 % vol. *iso*-octane and 13 % vol. *n*-heptane. A fuel with a high octane number exhibits better resistance to auto ignition. Typical octane values for gasoline used in passenger cars are between 80 and 100. Since this scale is arbitrary, there are ignition-resistant fuels with octane numbers that are higher than 100 (e.g. benzene, toluene, xylene, methanol, ethanol, some ethers). Scientists and engineers continue to explore additives to gasoline which can increase the resulting fuel's octane number and ignition-resistance.

There are different measurement methods resulting in different octane ratings. The most common one is the Research Octane Number (RON). It is deduced by running the fuel in a variable compression ratio test engine under defined operating conditions, and comparing the results with those for mixtures of *iso*-octane and *n*-heptane. Another type of octane rating, Motor Octane Number (MON), a better measure of how the fuel behaves

when under load, is measured at 900 rpm engine speed instead of the 600 rpm for RON. A similar test engine is used in MON and RON testing, however, the fuel mixture in MON test is preheated and the engine runs at variable ignition timing to further stress the fuel's ignition resistance. Depending on the fuel composition, the MON is typically about 8 to 10 points lower than the RON, but there is no direct link between them. Normally, both a minimum RON and a minimum MON are needed to specify a fuel. In many countries, including all of Europe and Australia, the octane rating is based on the RON. But in the United States, Canada, and some other countries, people use the Anti-Knock Index (AKI), which is the average of the RON and the MON. Due to the 8 to 10 point difference mentioned above, the octane shown in US is 4 to 5 points lower than the same fuel elsewhere: for instance, 87 octane fuel, the "regular" gasoline in the US and Canada, is equivalent to 91-92 in Europe.

Fuel with high ignition resistance may have other unwanted effects. High octane number fuel additives based on metals (Pb, Mn and Fe) have some disadvantages (in addition to toxicity of lead) [10, 16]. These organometallic additives are not fully burned since ash is formed and accumulates in engines or in catalytic converters, or emitted into the atmosphere. In contrast, organic compounds (oxygenates and aromatic solvents) used to increase the octane number of gasoline are fully burned, without ash formation during the combustion process. The disadvantage of these organic compounds is that large quantities (up to 15% vol. oxygenates and 35% vol. aromatic solvents) are needed for noticeable effect on gasoline ignition propensity while very small amounts (around 100 ppm) are needed for the organometallic additives. Strictly speaking, because of the high proportions, these organic compounds are not additives but are considered to be the components of gasoline.

Ignition-resistant aromatic solvents such as benzene, toluenes, ethyl benzene, and xylenes (BTEX), are restricted because of their negative attributes [7]. Benzene is toxic, and thus is an undesirable component of gasoline. The maximum allowable concentration of benzene is 1% vol. and other aromatics is 35% vol. in gasoline. Oxygenated organic compounds (with at least one oxygen atom in molecule) are considered as good solutions. Relevant oxygenates are alcohols and ethers that are generally soluble in gasoline. Fuel oxygenates have been increasingly used since 1970s as octane enhancers to replace the toxic tetraethyl lead (TEL) and are now accepted components of gasoline, often referred to as reformulated gasoline. Common oxygenates are shown in Tab. 1.1. Regarding the use of alcohols as potential ignition-resistant additives, one of the main topics for this study, a relevant review is presented in the next section.

Chemical type	Name	Short name	Formula	Maximum % vol.
Ether	Methyl Tertiary-Butyl Ether	MTBE	$(\text{CH}_3)_3\text{COCH}_3$	15
	Ethyl Tertiary-Butyl Ether	ETBE	$(\text{CH}_3)_3\text{COC}_2\text{H}_5$	15
	Tertiary-Amyl Methyl Ether	TAME	$\text{C}_2\text{H}_5\text{C}(\text{CH}_3)_2\text{OCH}_3$	15
	Tertiary-Hexyl Methyl Ether	THEME	$\text{C}_3\text{H}_7\text{C}(\text{CH}_3)_2\text{OCH}_3$	15
	Tertiary-Amyl Ethyl Ether	TAAE	$\text{C}_2\text{H}_5\text{C}(\text{CH}_3)_2\text{OC}_2\text{H}_5$	15
	Diisopropyl ether	DIPE	$(\text{CH}_3)_2\text{CHOCH}(\text{CH}_3)_2$	10
	Tertiary Octyl Methyl Ether	TOME	$\text{C}_5\text{H}_{11}\text{C}(\text{CH}_3)_2\text{OCH}_3$	15
Alcohol	Methanol	MeOH	$\text{CH}_3\text{OH}$	3
	Ethanol	EtOH	$\text{C}_2\text{H}_5\text{OH}$	5
	isopropanol	iPOH	$(\text{CH}_3)_2\text{CHOH}$	10
	n-propanol	nPOH	$\text{CH}_3\text{CH}_2\text{CH}_2\text{OH}$	
	n-butanol	BuOH	$\text{CH}_3\text{CH}_2\text{CH}_2\text{CH}_2\text{OH}$	
	tert-butanol	GTBA	$(\text{CH}_3)_3\text{COH}$	7
	Iso-butyl alcohol	IBA	$(\text{CH}_3)_2\text{CHCH}_2\text{OH}$	10
	sec-Butanol		$\text{CH}_3\text{CHOHCH}_2\text{CH}_3$	

Table 1.1: Oxygenates adding to gasoline [17]

### 1.2.3 Research status of representative ignition-resistant fuels

The fuels included in this "review" are "bioalcohols" (ethanol, methanol and mainly focus on propanol isomers), methyl tertiary-butyl ether (MTBE) and ethyl tertiary-butyl ether (ETBE), as well as gasoline representative (*iso*-octane).

Biofuels, including bio-alcohol, bio-hydrogen, bio-diesel are potential substitutes for fossil fuel as the main fuel or as additives due to their renewability. Their use can lead to lower greenhouse gas emissions, and less PAH and soot formation [18–20]. Among the various biofuels, alcohols have received greater attention. Historically, ethanol ( $C_2H_5OH$ ) was used as fuel in internal combustion engines by the German inventor, Nikolaus August Otto, in 1876 and by the US engineer, Henry Ford, in his first automobile, in 1896. Nowadays, ethanol accounts for over 90% of the total biofuel production in the US and Brazil [21] because of their low cost and advanced production techniques. Mixtures of 90% vol. gasoline and 10% vol. ethanol (named gasohol) are used in the USA.

Alcohols from biomass sources can improve the sustainability of transportation and they offer attractive combustion properties such as high ignition resistance [18, 19, 22], as shown in the Tab. 1.2 [23], where the alcohols usually display higher octane number and ignition-resistant capability. The short-chain alcohols, methanol and ethanol, have been extensively studied [20, 21]. Short-chain alcohols, often referred to as "first-generation" bioalcohol fuels, have the drawback that they have low energy content per liter and could possibly lead to corrosion in engine fuel supply systems [20, 23]. In comparison, higher molecular weight alcohols, including propanol and butanol, are considered to have better properties; they are also considerably less toxic and less volatile than methanol [24]. As a

result, there is growing interest in higher molecular weight alcohols [25–32]. Some physical properties of the higher alcohols (e.g. boiling point) must, however, be comparable with those of gasoline for optimal performance in engines. Propanol isomers are therefore attractive to combustion engines because of their combined favorable energy density and appropriate fuel volatility. It has been found that these isomers can be commercially produced through fermentation of biomass and from processing petrochemical feed stocks [33,34]. Based on octane numbers as a global measure of resistance to uncontrolled ignition, some bioalcohols have higher research octane numbers (RON) than conventional gasoline (with RON less than 100): for instance, methanol - 109 [35]; ethanol - 108 [36] or 109 [35]; *n*-propanol - 105 [36]; and *iso*-propanol - 113 [36].

The performance of propanol isomers as potential gasoline additives has been investigated in both SI and Homogeneous Charge Compression Ignition (HCCI) engines. Results show that their addition also results in lower CO and unburned hydrocarbons (HC) emissions [37,38]. It has been observed that combustion of alcohols, such as propanol isomers, can also lead to undesirable increase in aldehyde and ketone emissions [39,40]. The inhibition effects of *iso*-propanol addition to *n*-heptane combustion in an HCCI engine was studied by Lu et al. [41] and Uyumaz [42]. The work by Lu et al. [41] showed that increasing the volume fraction of *iso*-propanol in *n*-heptane/*iso*-propanol blends up to 30 - 40% would lead to incomplete combustion in HCCI engines. Further addition can even result in misfires, attributed to the suppression of low-temperature chemical reactions by *iso*-propanol. Uyumaz [42] investigated the effects of blending *iso*-propanol with *n*-heptane on HCCI combustion under different inlet air temperatures. Decreased CO and HC emissions were observed with near zero NO<sub>x</sub> emissions under most test conditions. The

results also suggest that *iso*-propanol has a higher resistance to engine knocking phenomena, compared to *n*-butanol. There is also interest in using the more reactive propanol isomer, *n*-propanol, as a diesel fuel additive [43,44].

Despite the growing interest in propanols, only a few kinetic studies of their oxidation are reported in the literature. Some of the reported studies have focused on the relative reactivities of the two isomers, establishing the expected trend that *n*-propanol is more reactive than *iso*-propanol as a result of the weaker secondary C-H bonds in the former.

Oxidation studies of propanol isomers have been reported in a number of experimental studies. The intermediate species profiles of premixed flames of propanol isomers were recently measured [45,46], highlighting key differences in their combustion chemistry. Frassoldati et al. [24] measured the structures of counterflow non-premixed flames of *n*- and *iso*-propanol. A chemical kinetic model capable of describing the observed profiles was developed.

Following that, Togbe et al. [47] and Galmiche et al. [48] studied propanol oxidation in a jet-stirred reactor (JSR) at 10 atm over the temperature range of 770 K - 1190 K and equivalence ratios,  $\phi = 0.35 - 4.0$ . Premixed laminar flames at pressures of 1 - 10 atm were also investigated. Results show that the two isomers have substantially different major chemical intermediates. Subsequently, counterflow laminar premixed and non-premixed flames of both *n*- and *iso*- propanol were studied by Veloo and Egolfopoulos [49] to determine isomer effects on their burning velocities and extinction strain rates. It was established that *n*-propanol premixed flames are faster than those of *iso*-propanol and that the extinction strain rates of *n*-propanol are consistently higher than those of *iso*-propanol in both premixed and non-premixed flames. In analysis of the underlying chemical kinetics,

some differences were found, such as the higher concentrations of propene in *iso*-propanol/air flames which lead to the relatively non-reactive allyl radicals, thereby retarding the overall reactivity of *iso*-propanol. It was found that in *n*-propanol/air flames, formyl radicals formed from higher concentrations of formaldehyde resulted in enhanced reactivity. Further laminar burning velocities of *n*-propanol were also determined in recent work by Beeckmann et al. [50] and Gong et al. [51].

Regarding the auto-ignition study of the isomers, Johnson et al. [52] measured the first reported ignition delay times behind reflected shock waves at temperatures of 1350-2000 K, equivalence ratios of 0.5, 1.0 and 2.0, and pressures of 1.2 atm. Their study shows that *n*-propanol is more reactive than *iso*-propanol. Noorani et al. [25] and Akih-Kumgeh et al. [53], in their comparative investigations of ignition of C1 - C4 primary alcohols and C3 oxygenated hydrocarbons, measured the ignition delay times of *n*- and *iso*-propanol under pressures of 1.0 - 12 atm. These studies provided ignition delay times at higher pressures, placing the observed trends in ignition delay times in a broader context. To further extend the range of test conditions for both isomers, Man et al. [54] measured the ignition delay times behind reflected shock waves at pressures of 1.2 to 16 atm and temperatures of 1100 - 1500 K. The authors also proposed a modified chemical kinetic model based on the earlier model by Johnson et al. [52]. Analysis of their model showed that H-abstraction reactions are mainly responsible for propanol consumption. *n*-Propanol produces ethanol, ethane and propene, while *iso*-propanol produces acetone and propene. The ignition delay results have also been used in their recent study, comparing ignition delay times with those of propanal and propane [55].

Progress in the characterization of propanol and other alcohols as potential biofuels have recently been reviewed by Sarathy et al. [56]. A number of chemical kinetic models for both propanol isomers have been established, such as the models by Johnson et al. [52], Sarathy et al. [56], and Man et al. [54]. However, there are still outstanding issues regarding the performance of these models over a wide range of thermodynamic conditions. This knowledge could facilitate analysis and improvement of existing models whose predictions of various combustion properties are at variance with measurements at a number of test conditions. In the context of this work, previous results on propanol isomers are verified and the data set extended.

The other set of fuels considered in this work are ethers. High octane rated ethers are widely used today as gasoline additives to increase the ignition-resistant performance of the resulting fuel blends [57, 58]. The use of those ethers such as methyl tert-butyl ether (MTBE) and ethyl tert-butyl ether (ETBE) could lead to higher engine efficiency by means of higher compression ratios. It can also reduce engine combustion emissions as a result of the oxygen content [59]. Methyl tert-butyl ether (MTBE) can be produced from reactions between methanol and iso-butylene [60]. It was introduced in 1970s as gasoline additives

Fuel	Energy Density (MJ/L)	Average Octane (AKI rating/RON)
Gasoline	33	85-96/90-105
Methanol	16	98.65/108.7
Ethanol	20	99.5/108.6
Propanol	24	108/118
Butanol	30	97/103
AKI - Used in Canada and US RON - Used in Australia and most of Europe		

Table 1.2: Fuel Economy and Octane



since it is non-toxic and has a higher octane rating than gasoline [61]. Initially, it was added to gasoline at low concentrations to replace tetra-ethyl lead as an octane enhancer [61] and later was also blended in higher proportions to meet the clean air requirement [62].

However, MTBE is linked to ground water contamination problem and has come under regulation [61,63]. ETBE, another ether that is less soluble in water, has been considered a possible substitute. As can be seen from Tab. 1.3 [61], ETBE has a higher octane number, higher boiling point and lower vapor pressure compared with MTBE. Another attractive feature of ETBE is that it can be produced from renewable sources such as bio-ethanol and biomass [64,65]. Although the octane number indicates potential higher ignition resistance, its fundamental kinetic behavior needs to be established.

Despite the phase-out for gasoline additives in United States, MTBE, because of its lower production cost and greater compatibility with the hydrocarbons in gasoline, is still adopted in many parts of the world [66]. There have been studies on the effects of MTBE or ETBE addition to gasoline in engines [67–75]. The key findings have been reviewed in a number of work [59, 76–78] and it was concluded that within certain blending limits, MTBE or ETBE addition can improve engine brake thermal efficiency and reduce brake

Properties	ETBE	MTBE
Octane number	112	109
Boiling point	69 - 70 °C	55.2 °C
Flash point	- 19 °C	- 10 °C
Blending Reid vapor pressure	27.56 kPa	55 kPa
Oxygen content	15.7 %	18.2 %
Water solubility	23.7 mg/L	42 mg/L

Table 1.3: Properties of ETBE and MTBE.

specific fuel consumption. The CO and unburnt hydrocarbon (HC) emissions decrease as the increased oxygenate contents from those oxygenates. Various results for NO<sub>x</sub> emissions were found even though slightly increased NO<sub>x</sub> emissions were more frequently observed for both MTBE and ETBE. In addition, increased formaldehyde emission for MTBE fuel was reported.

The gas-phase oxidation of pure MTBE and ETBE has been examined using several techniques, such as static reactors [79], flow reactors [80], shock tubes [81–83], research engines [84], constant volume reactors [82] and jet-stirred reactors [85–87]. Recently, the low-temperature oxidation characteristics and products of MTBE and ETBE were examined using a calorimetry coupled with a gas chromatography-mass spectrum analysis [88,89]. Previous studies revealed that the superior anti-knock quality of MTBE/ETBE can be attributed to the presence of highly branched tertiary butyl group attached to the ether group. The presence of this group greatly increases the number of primary H bonds. It is also found that the *iso*-butene chemistry dramatically influences the overall reactivity due to its strong inhibiting effect [90]. There are also a number of investigations on the chemical effects of blending MTBE and ETBE into primary reference fuels (PRF: n-heptane and *iso*-octane). For instance, Dagaut et al. [91] studied the oxidation of mixtures of n-heptane and MTBE or ETBE in a jet stirred reactor at 10 atm, for a residence time of 0.5 s and an equivalence ratio of 1.0. The test was conducted in the conditions covering the low and high temperature oxidation regimes (570–1150 K). MTBE and ETBE are observed to reduce the mixture reactivity in the low temperature regime (570 - 800 K). The findings support that the use of MTBE and ETBE as gasoline additives by virtue of their ability to reduce the radical pool to slow down chain branching reactions

which lead to ignition. However, it is noted that the experiment here and also many others were only carried out at very low fuel concentrations (e.g. 0.1% here). The simulated results from the model by Battin - Leclerc et al. [92] was reported to properly capture the experimental results and a similar level of agreement was obtained in comparison with experimental results for oxidation of pure MTBE and ETBE [87]. Ogura et al. [93] developed a detailed oxidation mechanism of primary reference fuels with ETBE or ethanol as octane improver. The model was validated with experimental results from literature using shock tubes, a jet-stirred reactor, and a flow reactor. It was found that the model could reproduce the ignition-resistance variations of PRF and ETBE/ethanol blend. Similar effects on ignition-resistance between ETBE and ethanol were observed.

There has been limited work on the ignition of MTBE and ETBE using shock tubes. Regarding MTBE, the Galway group measured ignition delay time of MTBE mixtures behind reflected shock conditions at temperatures of 1100 - 1900K, equivalence ratios of 0.15 - 2.4, and pressures of 2.0 - 3.5 atm [81,94]. A detailed chemical kinetic model was proposed for MTBE combustion. Fieweger et al. [95,96] determined the ignition time of stoichiometric MTBE/air mixtures under high pressures at 13 and 40 atm. After shifting attention from MTBE to ETBE in the 2000s, Yahyaoui [82] determined the ignition delay times and laminar flame speeds of ETBE in a shock tube and a constant volume reactor, respectively. In their study, mixtures containing 0.1 - 0.4 % of fuel were oxidized over the temperature range 1280 - 1750 K and for pressures of 0.2 and 1 MPa. The equivalence ratio was varied from 0.25 to 1.5. A chemical kinetic model was built and validated using these data and earlier jet stirred reactor and shock tube experimental data. Most recently, pyrolysis and oxidation of MTBE and ETBE were studied by Yasunaga et al. [83] using a

shock tube facility. A reaction mechanism was constructed and tested against shock tube experimental data in the pressure range of 1.0 - 3.5 atm. It was found that uni-molecular elimination reactions have a larger influence on the pyrolysis and oxidation of MTBE and ETBE compared to EME (ethyl methyl ether) and DEE (di-ethyl ether) at high temperatures. As can be seen from above, the previous work were done under limited experimental conditions (mostly at low test pressures up to 3.5 atm), low oxygen concentration in the test had generally been adopted, which limits the regime of validity of the proposed models.

There are a number of chemical kinetics models for modeling MTBE/ETBE oxidation in the literature, as recently reviewed [97,98]. However, a large part of research on combustion of acyclic ethers (ethers with straight chain carbons such as MTBE and ETBE) was carried out before 2000, even though MTBE and ETBE are widely applied worldwide in the automotive industry as fuel additives today. The resulting models have not yet been comprehensively validated because there are few experimental data available. The differences and similarities among these models, including their various prediction capabilities have not been thoroughly evaluated. To fill the gap, in the present work, the ignition characteristics of MTBE and ETBE are established using a shock tube facility. Factors in determining the ignition times of both additives are explored. Kinetic analysis are carried out to better understand the underlying combustion chemistry.

As can be seen from this review, there has been very limited study of the effect of biofuels on ignition resistance of gasoline so far. The current chemical models need to be further validated and improved. Thus, there is need for further investigations in order to enable the use of those fuels as substitutes and ignition-resistant additives to gasoline.

Also, work on fundamental experimental study and combined chemical kinetic model development for blends of ignition-resistant fuels and gasoline are needed.

Since gasoline fuel is a complex mixture of many types of hydrocarbons, it is impractical to model and simulate the chemistry of all the species included in a model [99]. A "surrogate" fuel, a mixture usually with fewer chemical species, is then proposed to simplify kinetic modeling of the real fuel. The chosen surrogate fuel is expected to match the chemical and physical properties of the real fuel, such as density, carbon and hydrogen amounts, volatility (boiling range and flash point) and molecular transport properties, and combustion properties ( such as heat of combustion, flammability limits, and laminar premixed flame burning rate) [100]. The goal is to replicate the behavior of practical fuels during engine combustion [101]. A widely used surrogate for gasoline is a mixture of *n*-heptane and *iso*-octane. Other more complex gasoline surrogates include these two fuels and other hydrocarbons. A review of gasoline surrogate components has been presented by Pitz et al. [102]. In this work, *iso*-octane is used as a representative of gasoline in the blend fuel study for simplicity.

#### **1.2.4 Engine knock modeling and prediction**

Although it is understood that uncontrolled ignition is central to engine knock, describing and even predicting knock in an engine is complex; it requires a good understanding of the processes within the combustion chamber. Research indicates that the combustion mechanisms associated with knock are not fully understood because of the complexity of the phenomena involved. Engine knock simulations based on

zero-dimensional (0D), one-dimensional (1D), three-dimensional (3D) formulations have been used in many studies [5, 103, 104]. It is understandable that 3D simulations are better suited to capture the various physical and chemical processes that are characteristic of practical engines. It is, however, also recognized that 1D engine cycle simulations with lower computational requirements equally play an essential role in the conceptual design and calibration of combustion engines.

Regarding the prediction of auto ignition in various simulations, ignition models can be classified into three categories: 1). Ignition prediction using detailed chemical mechanisms, 2). Ignition prediction using reduced or simplified mechanisms and 3). phenomenological ignition time models [105]. Sustained research activities in combustion chemistry have yielded detailed chemical kinetic models. However, the detailed or even the reduced mechanisms are often very large; discouraging the application of these models in real engine design and control processes.

Detailed chemical kinetic models have been developed to simulate the combustion properties of a number of fuels. For instance, comprehensive models have been proposed for diesel and gasoline fuel surrogates [106–108], as well as aviation kerosene surrogates [109, 110]. This approach is also pursued in modeling biodiesel and fuels for SI engines. For example, Sarathy et al. [56] have recently reviewed the state of fundamental characterization of alcohol combustion chemistry and proposed a validated detailed chemical kinetic model for C1-C5 alcohols with 4100 elementary reactions among 600 species. In general, these kinds of large chemical kinetic models do not readily lend themselves to analysis of combustion flows or homogeneous reactors undergoing

compressive heating. It is therefore necessary to deduce smaller versions of the detailed models for realistic combustion design and analysis.

It has been recognized that the high dimensionality that is characteristic of detailed chemical kinetic models (a high number of species and reactions) can be reduced by appropriately probing the chemical models to identify insensitive reactions and species. These insensitive reactions and species can be eliminated without loss of relevant predictive power of the model. A number of model reduction approaches have been developed and are routinely used in model reduction while research for other simpler and more effective reduction methods continues. Among the available methods are the Directed Relation Graph method [111] and its related variants [112, 113], the reaction flux analysis, the Principal Component Analysis [114], and the Alternate Species Elimination (ASE) [115] methods. Such reduced models enable more complex Computational Fluid Dynamics (CFD) investigations of engine combustion as shown in a few recent studies [116–118].

A sensitivity based model reduction approach, the Alternate Species Elimination (ASE) method, has been developed by Akih-Kumgeh and Bergthorson [115], and used to generate reduced models for various fuels [119, 120]. This method aims to identify those species with marginal importance in simulating a given combustion property, such as ignition delay time, based on species sensitivity analysis. It is achieved by evaluating the effect of eliminating reactions of a given species on predicting a combustion property. The ASE method reduces the size of the original model by removing the species which do not significantly affect transition of the chemical system from an unburnt state to a burnt state. The method is simple, easily implemented in the CANTERA software package, and allows for rapid derivation of a number of reduced chemical kinetic models. The reduced

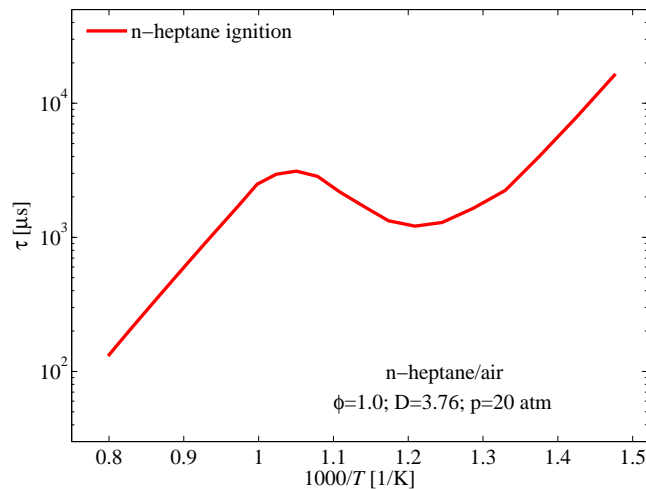


Fig. 1.3.: Ignition delay times for stoichiometric n-heptane/air mixture in a wide range of temperatures at a pressure of 20 atm. Results are simulated using the n-heptane model by Mehl et al. [107].

models are obtained on the basis of ignition delay times in this work but also prove to be adequate for predicting burning velocities and non-premixed flame structures.

Regarding the phenomenological ignition time model development, the simplest auto ignition model is an empirical or model-based generalized correlation. Ignition delay time correlations generally adopt a format such as the reciprocal of the reaction rate constant of an Arrhenius-type first order global reaction.

$$\tau = Ap^n \exp\left(\frac{E_a}{RT}\right) \quad (1.1)$$

where  $p$  and  $T$  are pressure and temperature of the mixture and  $A$ ,  $n$ ,  $E_a$  are the fitting coefficients. The complex behavior of large hydrocarbons found in practical fuels requires further considerations given that the temperature sensitivity does not follow a simple one step Arrhenius behavior as shown in Fig. 1.3.



There is need for analytic ignition models which cover a wide temperature range as encountered in engines. An empirical ignition correlation capable of capturing the complex temperature and pressure dependence of ignition delay times for long-chain hydrocarbons has been proposed by Vandersickel et al. [121, 122]. It comprises separate correlations for the low-, high-, and intermediate-temperature or NTC regions. This approach has recently been used by Gowdagiri and Oehlschlaeger [123] to obtain generalized ignition correlations for alternative jet fuel and diesel. The main ignition correlation is obtained from sub correlations using the relation:

$$\frac{1}{\tau} = \frac{1}{\tau_{low} + \tau_{mid}} + \frac{1}{\tau_{high}}, \quad (1.2)$$

which can also be written as:

$$\tau = \frac{\tau_{high}(\tau_{low} + \tau_{mid})}{\tau_{low} + \tau_{mid} + \tau_{high}} \quad (1.3)$$

Ignition delay times in the low-, intermediate-, and high-temperature regions correspond to asymptotic cases of eqn. 1.3. This form of the equation indicates that in the region where a change in temperature sensitivity is experienced, non-negligible deviations would be observed between the correlations and the original data on which it is based. Such a correlation method can also be applied to simulated ignition delay times using the detailed chemical kinetic model in order to obtain simplified ignition models. It would be also useful if other chemical kinetic features such as cross over temperatures could be explicitly accounted for in the ignition model to provide further insight on the chemical kinetic effects. Combining these reduced ignition model development with autoignition

studies can yield better understanding and effective suppression of undesirable ignition in engine design.

### 1.3 Objectives of this work

In line with the discussion in the literature review, there are important motivations for further exploration of alternative ignition-resistant agents and investigation of the effect of biofuels on ignition resistance. Engine knock is closely related to the ignition phenomena. On the one hand, the relative ignition behavior and reactivity trends of promising knock-resistant fuels such as propanol isomers and ETBE need to be further investigated. Moreover, the chemical effect of blending propanol and ETBE with gasoline surrogates is still poorly studied and has not been thoroughly analyzed in literature. On the other hand, regarding chemical kinetic modeling, the current models of these potential additives need to be further validated and improved. Systematic analysis and possible model revisions when necessary are beneficial to improved understanding of the potential of these fuels as additives or replacement for gasoline. Furthermore, to simulate blend combustion, a combined model needs to be constructed to analyze the chemical kinetic effects of blending propanol with gasoline. Lastly, to predict and avoid knock uncontrolled-ignition operation, there is need for a simplified method of ignition delay time estimation that can reduce the high computational cost involved in current knock modeling and prediction.

Specifically, the objectives of this thesis are to:

a). Study the ignition behavior and establish the reactivity trends between propanol isomers using measured shock-tube ignition delay times. Subsequently, we will explore the effect of adding propanol to gasoline.

b). Explore suitable alternatives to MTBE as ignition-resistant agents based on the comparative ignition investigation of methyl and ethyl tert butyl ethers.

c). Carry out the chemical kinetic analysis of the fuel oxidation process and use experimental data to validate and improve current models of fuels studied. This will also include developing combined kinetic models to study the blend effects of representative ignition-resistant fuels with gasoline.

d). Construct reduced combustion models for prediction of key combustion properties. This involves developing and evaluating reduced models and empirical ignition correlations for engine knock prediction.

In the first part of this work, the relative ignition behavior of representative ignition-resistant fuels is studied using the shock tube technique. Mixture compositions (including fuel concentration, equivalence ratio and dilution ratio) and test conditions (pressure and temperature) are carefully designed to gain a general understanding of reactivity trends under various conditions. Based on the experimental results above, alternative ignition-resistant agents will be evaluated and proposed.

The second part of this thesis focuses on the comparative ignition investigation of the more ignition resistant fuels and *iso*-octane which is a gasoline surrogate. Differences in the ignition delay times of their blends will be quantified. Further, combined chemical kinetic models of *iso*-octane and the additives are developed based on the most recent models from the literature for *iso*-propanol, ETBE and *iso*-octane. Detailed analysis of these separate

and combined models will be carried out for further insight on the oxidation process of the individual fuels and their blends. Furthermore, those models are validated and improved upon based on the measured experimental data.

Lastly, simplified ignition delay time correlations for representative transportation fuels such as alcohols, gasoline and biodiesel surrogates are developed and used for rapid and "accurate" engine autoignition prediction. Their performance is assessed and compared with detailed engine auto-ignition simulations.

## 2. EXPERIMENTAL AND MODELING APPROACH

The experiments in this thesis are carried out using a shock tube. The facility and data acquisition processes are described here. The section concludes with a description of how the objectives outlined above will be attained.

### 2.1 Shock tube experiments

The shock tube is a reactor operated using shock waves for various studies. Combustion chemistry is one such area which makes use of the shock tube.

#### 2.1.1 Shock tube technique in ignition studies

Combustion properties such as ignition delay times and laminar flame speeds are valuable indicators of the reactivities of both conventional and alternative fuels. They are widely used in detailed chemical kinetic model construction and validation [124]. Shock tube, as a vital experimental tool for high temperature gas-phase kinetics study, has been extensively used by chemical kineticists because of its ability to establish very high temperatures in a rapid manner. Other reactors are rapid compression and perfectly stirred reactors but these are not capable of establishing good temperature conditions above 1000 K.

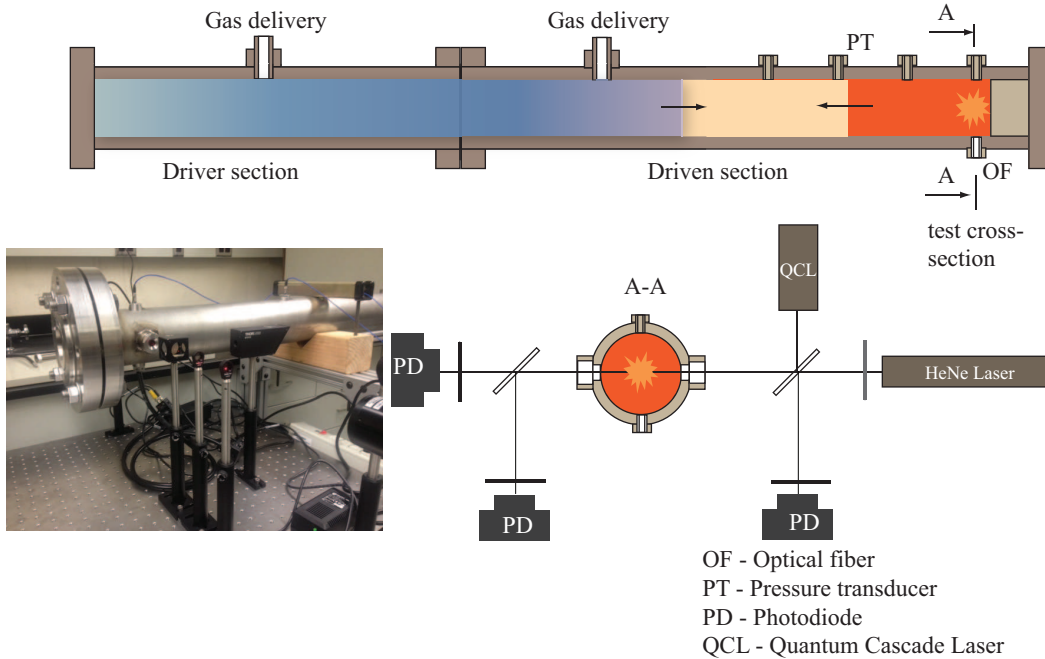


Fig. 2.1.: Shock tube used in this study. A laser diagnostic system for species concentration measurement during combustion processes is also displayed beneath the tube.

Considering the significant role of ignition in combustion processes, shock tubes are used to measure ignition data during the development and verification of combustion reaction mechanisms [125].

The Syracuse shock tube facility is shown in Fig. 2.1. The simple shock tube consists of two sections, separated by a diaphragm. The test section contains the test mixture at low pressure. The high pressure section uses a light gas to drive the process. A shock wave is normally formed when the diaphragm separating the high and low pressure sections ruptures. The subsequent wave processes are as shown in Fig. 2.2. In the test driven section, the incident shock wave propagates toward the end of the driven section while heating and compressing the test gases. Alongside the incident shock, an expanded expansion wave appears and propagates to the opposite end of the driver section. After

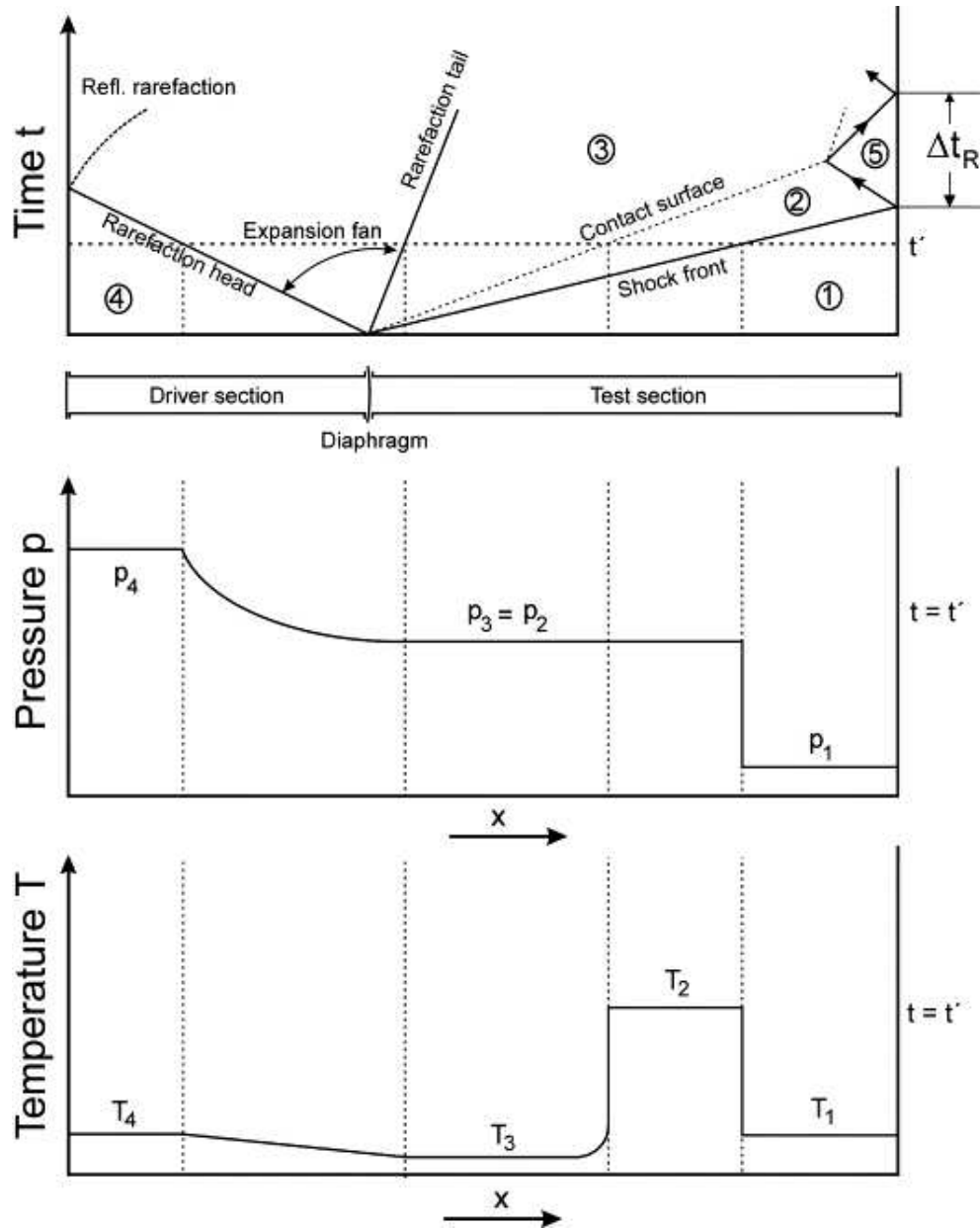


Fig. 2.2.: Distance,  $x$ , versus time,  $t$ , in a simple shock tube with gases at different states.

(1) Initial test gas, (2) gas shocked by the incident shock wave, (3) driver gas behind contact surface, (4) initial driver gas, (5) test gas subjected to reflected shock wave [126].

incident shock wave reaches the endwall, the reflected shock wave causes additional heating and compression of the test gases which forms a stagnant gas column. It is this high pressure, high temperature, stagnant region that is the region of observation, or the test

region. One therefore studies the evolution of this reactor at high temperature and pressure as it evolves chemically. The test condition typically lasts about 1 - 3 ms before the hot gases are cooled by the reflected expansion waves from the other end of the tube. This test condition is often studied and modeled as a constant volume reactor for combustion study [127]. Beside, it is worth mentioning that, a shock tube with increased experimental test times could be a versatile tool and employed in the study of combustion chemistry at low temperatures. This can be done by tailoring the interface between the driver and driven gas. One way to increase the test time is to tailor the driver gas by mixing helium with a heavier gas such as nitrogen [128,129].

Investigation of ignition using a shock tube can be regarded as two consecutive experiments in one realization. The first experiment consists in creating the conditions after reflected shock passes through. The second one can be viewed as a constant volume reactor with the combustible mixture rapidly subjected to the temperature and pressure jumps. The evolution of the chemical reactor can then compared with the predictions of simulations using a detailed reaction mechanism.

The shock tube can be equipped with optical windows for laser absorption spectroscopy or for visualization of the gas dynamic and ignition processes. Visualization techniques include density gradient methods such as Schlieren imaging. Examples of these visualizations are shown in Figs. 2.3 and 2.4. Fig. 2.3 shows incident and reflected shock waves in a test mixture of ETBE/O<sub>2</sub>/AR captured using a high-speed camera. The incident shock front propagates from right to left and after reflecting from the endwall, it travels from left to right. The pressure increases behind the reflected shock and the higher pressure is reflected in the smaller shock front size. After establishing the high pressure



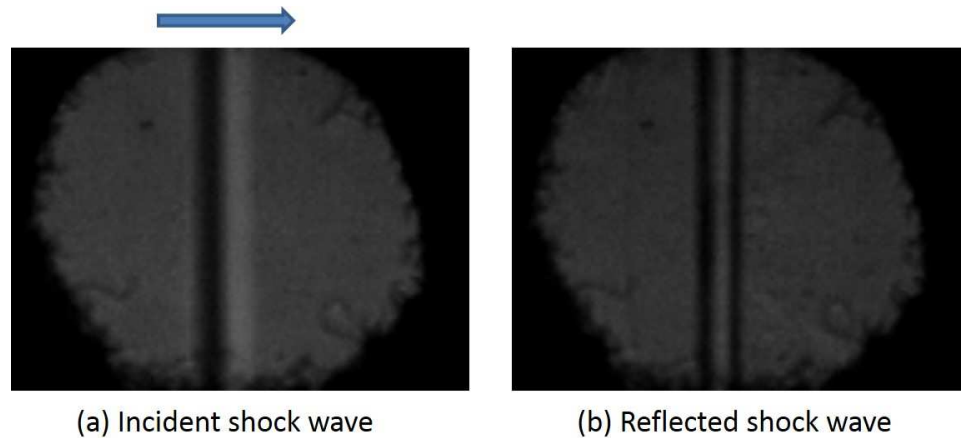


Fig. 2.3.: Schlieren images of a representative shock tube experiment. The test mixture is stoichiometric ETBE/O<sub>2</sub>/AR with a dilution ratio of 21.1; the average incident shock velocity is 725.2 m/s; test mixture at 10.2 atm and 1190 K. Ignition occurs around the 2.16 ms after onset of the reflected shock wave.

and temperature conditions behind the reflected shock wave, a time elapses before ignition occurs. Fig. 2.4 shows the ignition event after the characteristic ignition delay time. The ignition event is accompanied by light emission and propagation of the edges of the ignition kernel.

Here, we need to first discuss the difference between incident and reflected shock and their effects on the combustible mixture before proceeding to the details about shock tube experiments. Even though the temperature and pressure of the gas rise when both incident and reflected shock pass through, the temperature behind the incident shock wave is generally very low, and not sufficient to induce substantial chemical reactions, compared to the temperature behind the reflected shock wave. Because of this, the chemical system is assured to be compositionally frozen until the gases have been processed by the reflected shock wave.

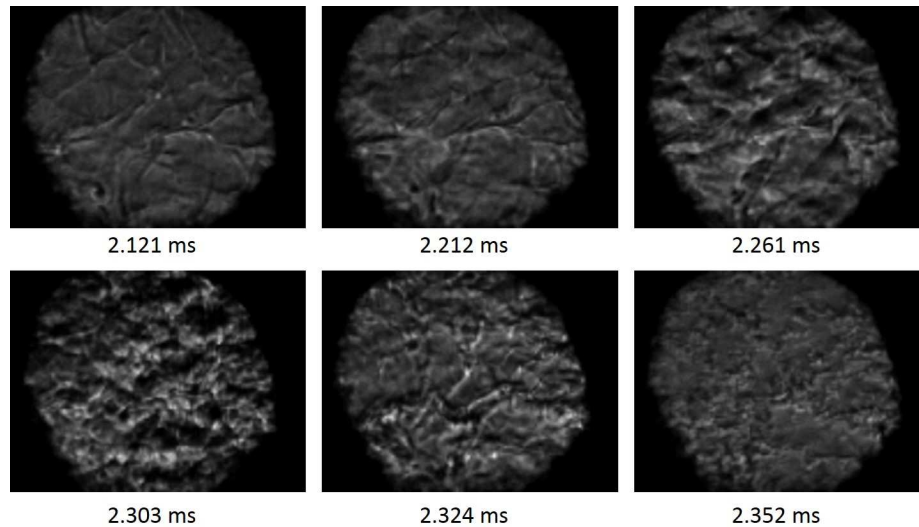


Fig. 2.4.: Schlieren images of ignition events after the reflected shock. The test mixture is stoichiometric ETBE/O<sub>2</sub>/AR with a dilution ratio of 21.1; test mixture at 10.2 atm and 1190 K.

The observables from each shock tube experiments are the shock arrival times and pressure signals measured using fast-response pressure transducers and high-speed digitizers. Ignition times can be determined from light emission. It is, however, challenging to measure the temperature behind the reflected shock since the response time of thermocouples is generally too slow to accurately track the rapid temperature changes. Some attempts to use laser spectroscopic methods to measure temperature yield results that are comparable or less accurate than the gas dynamic method [130–132].

One often relies on gas dynamic relations to deduce the shock conditions given knowledge of shock velocity and test gas composition. The measured and calculated shock pressure are compared to check the accuracy of the method. The following assumptions are adopted for shock tube gas dynamics [126]:

- (1) The flow inside the shock tube is one-dimensional along the axis;

(2) We can neglect the influences of viscous flow and heat loss;

(3) We assume that the diaphragm ruptures instantaneous, that the contact surface rapidly attains speed and that no heat exchange occurs with the walls;

(4) The flow expansion process is considered to be isentropic;

(5) Regions ahead of and behind the shock wave are adiabatic, thus energy of the flow is conservative in these regions;

(6) Ideal gas behavior is assumed for the test gases, in closing the transport equations.

By using a shock-fixed coordinates, i.e. with shock front as the stationary frame of reference, the basic continuity, momentum and energy equations below can be solved:

Continuity

$$\rho_1 u_1 - \rho_2 u_2 = 0 \quad (2.1)$$

Momentum conservation

$$(p_1 + \rho_1 u_1^2) - (p_2 + \rho_2 u_2^2) = 0 \quad (2.2)$$

Energy Conservation

$$(h_1 + \frac{1}{2}u_1^2) - (h_2 + \frac{1}{2}u_2^2) = 0 \quad (2.3)$$

where  $\rho$  is the density,  $u$  is the velocity in the shock frame of reference,  $p$  is the pressure and  $h$  is the mass specific enthalpy. As mentioned above, the ideal gas law, in most cases, can be used to appropriately relate the density, temperature and pressure at each state of the gas. However, at very high pressures, where ideal gas behavior cannot be assumed, determining shock conditions in this way can lead to larger errors [133]. An improved

equation of state is necessary to account for the real gas effects and other gas dynamic effects in the very high pressure shock tube [134, 135].

Using the initial conditions at driver and driven sections i.e. zone 4 and zone 1 as shown in Fig. 2.2, and assuming the constant specific heat, the relationship between the incident shock velocity or the incident Mach number ( $M_s$ ) and pressure ratio of zone 4 and zone 1,  $P_{41}$ , can be deduced as follows:

$$P_{41} = \frac{p_4}{p_1} = \left[1 + \frac{2\gamma_1}{\gamma_1 + 1}(M_s^2 - 1)\right] \left[1 - \frac{\gamma_4 - 1}{\gamma_1 + 1} a_{14} \left(M_s - \frac{1}{M_s}\right)\right]^{(-\frac{2\gamma_4}{\gamma_4 - 1})} \quad (2.4)$$

where  $\gamma_1$  and  $\gamma_4$  are the specific heat capacity ratios at zone 1 and zone 4,  $a_{14}$  is the ratio of sound speeds at zone 1 and zone 4, which can be expressed as:

$$a_{14} = \frac{a_1}{a_4} = \sqrt{\frac{\gamma_1 MW_4 T_1}{\gamma_4 MW_1 T_4}} \quad (2.5)$$

where  $a_1$  and  $a_4$  are the local sound speed at zone 1 and zone 4,  $MW_1$  and  $MW_4$  are the molecular weight at zone 1 and zone 4.

It should again be pointed out that the above calculation for incident shock velocity or mach number neglects a series of non-ideal effects such as non-ideal diaphragm rupture, shock wave decay, real gas effects, wall heat conduction and boundary layer effects. The obtained incident mach number ( $M_s$ ), thus, can only be used in experiment to estimate required filled pressures,  $P_4$ . In shock tube experiments, the velocity is usually measured with the piezoelectric pressure transducers. More details about this are elaborated in next section.

After deriving the incident mach number ( $M_s$ ), the thermodynamic conditions across shock wave front can be written as using 1-D normal shock equation:

$$P_{21} = \frac{p_2}{p_1} = 1 + \frac{2\gamma_1}{\gamma_1 + 1}(M_s^2 - 1) \quad (2.6)$$

$$T_{21} = \frac{T_2}{T_1} = \frac{[2\gamma_1 M_s^2 - (\gamma_1 - 1)][(\gamma_1 - 1)M_s^2 + 2]}{(\gamma_1 + 1)^2 M_s^2} \quad (2.7)$$

where  $T_1$  and  $T_2$  are the temperatures at zone 1 and zone 2.

Using the relationship between the reflected shock and the normal shock, the reflected shock Mach number,  $M_r$ , can then be obtained as:

$$M_r = \sqrt{\frac{2M_s^2 - (\gamma_1 - 1)}{(\gamma_1 - 1)M_s^2 + 2}} \quad (2.8)$$

Finally, the reflected shock condition at zone 5 can be solved as the functions of  $M_s$  and  $\gamma_1$ .

$$P_{51} = \frac{p_5}{p_1} = \frac{[2\gamma_1 M_s^2 - (\gamma_1 - 1)][(3\gamma_1 - 1)M_s^2 - 2(\gamma_1 - 1)]}{(\gamma_1 + 1)[(\gamma_1 - 1)M_s^2 + 2]} \quad (2.9)$$

$$T_{51} = \frac{T_5}{T_1} = \frac{[2(\gamma_1 - 1)M_s^2 - (\gamma_1 - 3)][(3\gamma_1 - 1)M_s^2 - 2(\gamma_1 - 1)]}{(\gamma_1 + 1)^2 M_s^2} \quad (2.10)$$

In reality, the specific heat capacities of these gases depend on temperature. To obtain a solution to the shock equations, the enthalpy is often represented using temperature dependent specific heat capacities instead of assuming that they are constant. The

temperature-dependent enthalpy can be determined from the specific heat capacity at constant pressure,  $c_p$ , and the reference enthalpy,  $h_{ref}$  as in Eqn. 2.11.

$$h = h_{ref} + \int_{T_{ref}}^T c_p(T) dT \quad (2.11)$$

More conveniently, the thermodynamic parameters for the species involved in this study are usually given in the form of coefficients NASA polynomial in chemical kinetic models [54, 83]. Their fitted thermodynamic database entries are estimated using the Group Additivity method [136]. The NASA polynomials for thermodynamic properties,  $c_p$ ,  $h$ , and entropy ( $s$ ), have the form:

$$\frac{c_p}{R} = a_1 + a_2T + a_3T^2 + a_4T^3 + a_5T^4 \quad (2.12)$$

$$\frac{h}{RT} = a_1 + \frac{a_2}{2}T + \frac{a_3}{3}T^2 + \frac{a_4}{4}T^3 + \frac{a_5}{5}T^4 + \frac{a_6}{T} \quad (2.13)$$

$$\frac{s}{RT} = a_1 \ln T + a_2T + \frac{a_3}{2}T^2 + \frac{a_4}{3}T^3 + \frac{a_5}{4}T^4 + a_7 \quad (2.14)$$

where the coefficients  $a_1$  to  $a_7$  are supplied for each species in the model's thermodynamic file. Two sets of coefficients are provided for low-temperature and high-temperature ranges. The input data for the system of equations are the initial species concentrations, initial pressure, and initial temperature of the test mixture, as well as the shock velocity. The solution yields thermodynamic conditions behind the incident wave and after the reflected wave, the latter being the desired initial condition. The accuracy of the calculated properties is confirmed by comparing the calculated post-reflected shock

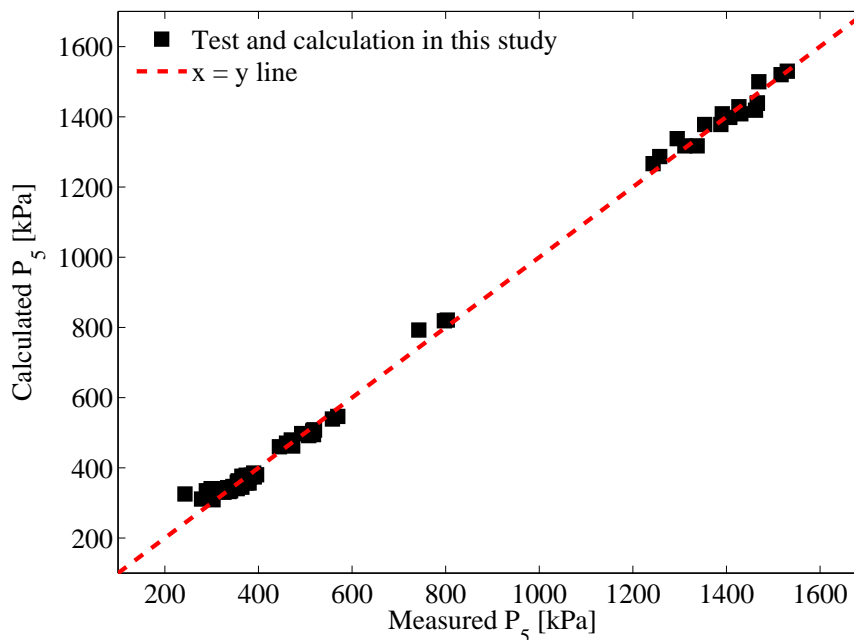


Fig. 2.5.: Comparison of calculated and measured post-reflected shock pressure,  $p_5$ , for sample reactive gas mixtures to establish the reliability of the shock relation method of temperature determination.

pressure with that measured using fast-response pressure transducers. Figure 2.5 is an example of this comparison, highlighting the reliability of the method and therefore reliability of the calculated temperature.

### 2.1.2 Experimental setup and procedure

The experiments in this study are carried out in a newly-built shock tube reactor with an internal diameter of 10 cm, a test section length of 6 m and a total length of 9 m. The setup of the shock tube is shown below in Fig. 2.1. This shock tube has been previously described in other works [137–139]. High purity helium is used as the high pressure driver gas (Airgas, > 99.999%) while high purity oxygen and argon are used to prepare the test

mixtures. The test mixtures contain the research grades samples of the investigated fuels from Sigma-Aldrich. In this work, these include research grades of propanol isomers (n-propanol,  $\geq 99.9\%$ ; *iso*-propanol, 99.5%), MTBE (99.8%), ETBE (99%), and *iso*-octane ( $\geq 99\%$ ). Although normal combustion occurs in air (mainly nitrogen and oxygen), in shock tube experiments nitrogen is replaced by argon as the diluent gas. This replacement improves the quality of experiments because it eliminates temperature uncertainties associated with long vibrational relaxation times of nitrogen behind shock waves.

The test mixtures of fuel, oxygen, and argon are prepared manometrically in a 150 L stainless steel mixing tank. Before the mixture preparation, the fuel tank is vacuumed out to a near vacuum using a geared vacuum pump (Edwards, RV12). According to the manufacturer, vacuum pressures as low as  $2 \times 10^{-3}$  mbar can be attained. Each component of the mixture is delivered through a valve-controlled manifold, connected to the tank. Proportions of each component is determined through partial pressures measured using a 1000-Torr high precision MKS Baratron pressure transducer which is accurate to 0.12% of its reading. In the mixture preparation, the liquid fuel is first drawn and dispensed into the tank using a Hamilton gas-tight syringe. In order to avoid fuel condensation in the tank, the liquid fuel volume is chosen such that its partial pressure in the mixing tank does not exceed 1/2 of its saturated vapor pressure at the given room temperature. Oxygen is then introduced into the tank based on the required equivalence ratio and finally the argon gas is added to achieve the desired dilution ratio. The fuel mixture is then allowed to homogenize for at least 14 hours.

Each experimental realization using a volume of the test mixtures follows a number of steps. To start the experiment, a polycarbonate diaphragm with a thickness to yield an



intended test pressure, is placed between the driver and driven sections of the shock tube. Next, the tube sections are vacuumed out to ultimate pressures of  $2 \times 10^{-3}$  mbar using a vacuum pump (Edwards, RV12). The gas leak rate from the shock tube is regularly checked and found to be consistently less than 1 Pa/min. This means that the test gas mixture is not compromised between introduction into the tube and actual experimental realization. This is also demonstrated by the similar ignition test results achieved while repeating the experiments at different time intervals between filling the tube with the test mixtures and initiating the experiment by bursting the diaphragm. The waiting times range from a few minutes up to one hour. To minimize possible error from the residual air, the test section is first flushed with the test gas mixture. Afterward, the test section is carefully filled with the test mixture to a pressure most likely to produce the target test pressure behind reflected shock. This estimate of fill pressure is made by empirical calculations based on earlier shock tube calibration and validation experiments. The initial fill pressure at test section is dictated by the driver gas pressure, diaphragm strength, and the target test conditions of the experiments.

After the desired gas amount is introduced into the test section, the valves to the shock tube are closed. Helium is then gradually filled into the driver section and the pressure difference across the diaphragm builds up until it exceeds the yield strength of the diaphragm material, which causes the diaphragm to rupture and thereby induces the shock wave. The resulting shock wave traverses along the driven section, while increasing the pressure and temperature of the test fuel mixture. To get a sense of the pressures involved, we can consider an experiment for which the pressure behind reflected shock wave should be 5 atm, the test section is filled with the fuel mixture (e.g. 1% fuel, 4.5% O<sub>2</sub>, and 94.5% Ar)

to a pressure of about 18 kPa. One would use a diaphragm of 0.003 inch thickness which ruptures at helium pressure of about 480 kPa, producing the desired test pressure at 5 atm.

After each experiment, the exhaust gas inside the tube is thoroughly evacuated and then filled with air to atmospheric pressure. To minimize disturbances to the shock wave, hence experimental uncertainties, the tube is cleaned out after 2-3 experiments. For subsequent experimental realizations, the diaphragm is chosen according to the desired nominal pressure. The temperature effect on ignition can be examined by varying the initial fuel mixture pressure in the tube which leads to shocks of different strengths, whereas the effect of pressure can be studied by varying the diaphragm thickness. In the next section, the instrumentation used for data acquisition is described.

### **2.1.3 Data acquisition and processing**

#### **Data acquisition**

As discussed before, the condition behind reflected shock are deduced from the gas composition, initial thermodynamic conditions in the test section, and the incident shock velocity. The shock tube is equipped with four units of fast-response PCB pressure transducers to determine the shock velocity as in Fig. 2.1. Those transducers are mounted at separations of 40 cm from each other, near the end of test section. The transducers are powered by a signal conditioner from which the pressure signals are also collected using BNC cables. The pressure signal from those sensors indicate the shock arrival time at each test location, and by calculating the time difference between the shock wave passing

through two successive pressure transducers, the shock velocity can be obtained from the equation:

$$V = \frac{\Delta x}{\Delta t} \quad (2.15)$$

where  $\Delta x$  is the distance between two successive pressure transducers and  $\Delta t$  is the time interval between the arrival of the incident shock wave. The shock velocity is then considered to be the shock velocity at the midway location between the transducers. The velocity at the test location is obtained by extrapolation of a linear fit of the decaying velocities linear fit. Because of the viscous boundary layers involves, the strength of the shock wave decreases as it propagates toward the end wall. The shock velocity attenuation of this facility is generally less than 1.5% / m. Because the pressure measurements are crucial in verifying the gas dynamic calculations used to infer the test temperature, the high frequency PCB pressure sensors are calibrated and certificated by the manufacturer with the measurement uncertainty within 1.3% at a level of confidence of approximately 95%.

Ignition is detected by a photodiode in the sidewall with a  $430 \pm 10$  nm narrow band filter selective to light emission by the CH radical. The maximum concentration of this excited radical occurs at the instant of ignition and thus serves as an ignition marker. All voltage output from the pressure transducers and the photodiodes are acquired by a National Instruments 100 MHz data acquisition card (NI PCI-5105). A LabVIEW program is written to interface the DAQ card and DAQ computer. During the experiment, data acquisition is triggered by a positive gradient of the pressure registered by a designated sensor near the endwall. Figure 2.6 illustrates the data obtained from a typical

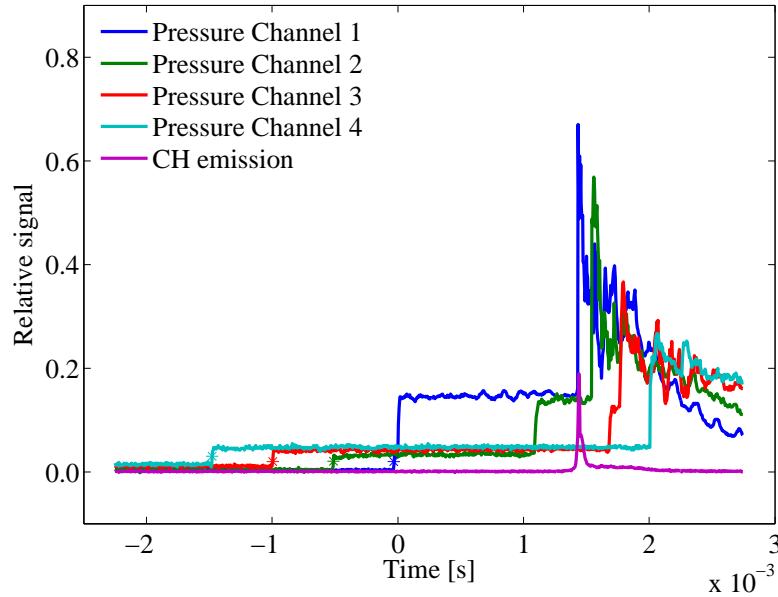


Fig. 2.6.: Representative signals from an experiment.

experimental realization. From these five signals, information about the shock velocity, test pressure, and ignition delay time needs to be extracted.

### Data processing

The extraction of information about ignition delay time, the shock velocity, and the post-reflected shock pressures is done using MATLAB programs. Figure 2.7 illustrates the identification of the shock arrival time at a pressure transducer location. The code identifies the "arrival times" by capturing the intersection of the maximum gradient line with the initial baseline pressure signal.

The calculated shock velocities are fitted to a line and used to estimate the shock velocity at the test section, as shown in Figure 2.8. The shock attenuation rate is also calculated and illustrated in the figure.

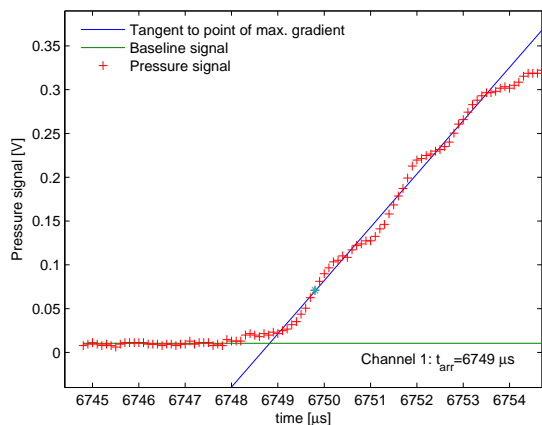


Fig. 2.7.: Representative shock wave arrival time measurement.

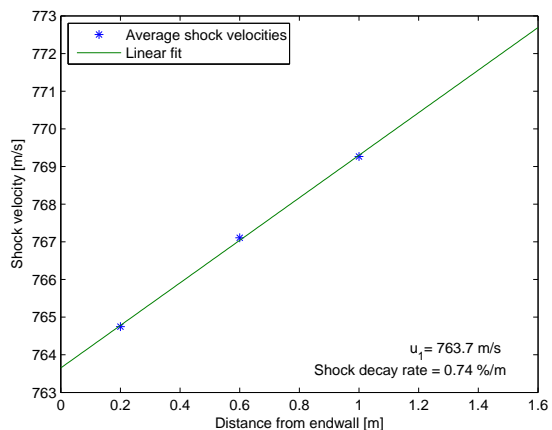


Fig. 2.8.: Representative shock velocity profile, indicating shock attenuation.

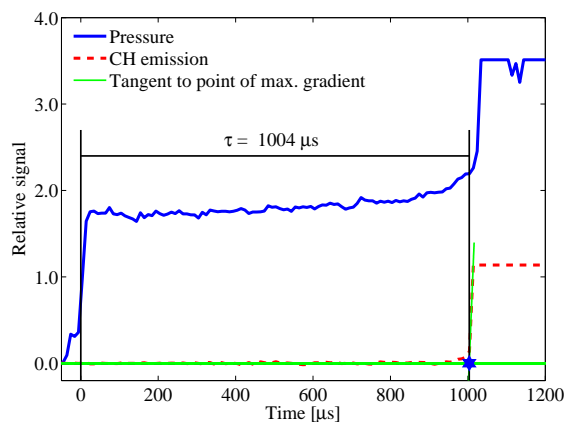


Fig. 2.9.: Representative ignition delay time measurement. Shown are the sidewall pressure and CH emission signals, for a *iso*-propanol/ $\text{O}_2$ /Ar mixture with  $\phi = 1.0$ ,  $p = 12.6$  atm,  $T = 1068$  K and ratio of argon to oxygen,  $D$ , is 3.76.

As shown in Fig.2.9, the onset of ignition is determined by extrapolating the maximum slope line of the CH\* emission profile to the baseline. Time zero refereed in the graph is the moment when the incident shock reflects from the end wall and forms the test condition, which subjects the fuel mixture to a combustion leading environment. The

ignition delay time herein is defined as the time between the pressure rise due to the arrival of the shock wave at the test location and the maximum gradient of the photodiode signal.

Using the shock velocity and initial state of the test mixture, the post-reflected shock temperature and pressure are determined from shock relations using the CalTech detonation tool kit in the MATLAB version of the CANTERA thermochemical solvers with thermodynamic parameters taken from chemical kinetic models [54,83]. The experimental post-reflected shock pressures are compared to values calculated by the code and have been found to be reasonably close. The agreement between the calculated and measured  $p_5$  further verify the validity of the estimated temperature.

#### 2.1.4 Experimental uncertainties

In this section, relevant experimental uncertainties are discussed, including their quantitative estimations. The uncertainties of reflected temperature and overall ignition delay time can be estimated by using the statistical error approaches [140] or conservative method as done by Zhukov et al. [141], both assuming a known Arrhenius dependence of ignition delay time on pressure, equivalence ratio, and temperature of the form:

$$\tau = Ap^\alpha \phi^\beta \exp\left(\frac{E_a}{RT}\right) \quad (2.16)$$

where  $\alpha$ ,  $\beta$  and  $E_a$  are the fitting coefficients.

The uncertainty of ignition delay time is thus understood to be caused by the uncertainties in reflected pressure and temperature, mixture compositions, pressure change by non-ideal gas dynamic effects, and the determination of the ignition time from sidewall

pressure and  $\text{CH}^*$  emissions signals. It is found that uncertainties of ignition times are more sensitive to errors in the conditions of the reactor than the actual of measurement of the delay as in Fig. 2.9. Among all the reactor factors, temperature uncertainty predominates the uncertainties. It is thus important that the post-reflected shock conditions are determined as accurately as possible, particularly the temperature due to the exponential dependence of ignition and chemical kinetic rates on temperature.

To deduce the test gas temperature, as mentioned earlier, the method used in the shock tube experiments is to measure the incident shock velocity and use the normal shock equations with appropriate thermodynamic properties. The underlying uncertainty of the test temperature, therefore, also lies in the accuracy of the shock velocity determination. This is due to the fact that errors in mixture compositions are small because of the highly accurate pressure transducers. Also, the thermodynamic data obtained from group additivity methods have been found to be sufficiently accurate. The uncertainties in the shock velocity arise from uncertainties in transducer separations, the time intervals detected between the successive sensors, and incident shock attenuation rate. The attenuation of the incident shock speed ranges from approximately 0.5 to 1.5 % per meter. It is therefore assumed that the incident shock velocity is fairly constant in the test section considering that combined with the short test times, the temperature rise behind reflected shock due to the boundary layer effect would be negligible.

The overall uncertainty in incident shock speed and test temperature are assessed using two methods: the maximum-error method and statistical methods [142, 143]. The maximum-error method calculates the error by assuming the maximum possible error in each of the variables in that function. The statistical method is more commonly used to

evaluate the error in functions with variables whose uncertainties are independent. A previous study by Petersen et al. [140] pointed out that results from the maximum-error method are generally more conservative while the statistical method is more realistic for uncertainty calculation. The statistical method is therefore used in the following shock tube uncertainty analysis.

For the purpose of uncertainty analysis in this section, we shall adopt the simplified equation, assuming constant specific heat capacity and ideal gas behavior. From the 1D shock tube relations, the reflected temperature is calculated as a function of the initial gas temperature,  $T_1$ , the test gas specific heat ratio,  $\gamma$ , and the incident shock Mach number,  $M$ , as follows:

$$T_5 = T_1 \frac{[2(\gamma_1 - 1)M_s^2 - (\gamma_1 - 3)][(3\gamma_1 - 1)M_s^2 - 2(\gamma_1 - 1)]}{(\gamma_1 + 1)^2 M_s^2} \quad (2.17)$$

The driven gas used in this work is argon, which has a specific heat ratio,  $\gamma$ , of 1.67. The test mixture consists of fuel and  $O_2$  in addition to the inert gas argon, which reduces the overall specific heat ratio in the mixture. Since argon is the most abundant gas in the experiment and the fuel concentration is generally very low, the equation above can then be approximated at the initial temperature of 300 K to better suit the statistical method of uncertainty calculations as follows:

$$T_5 = 225.1M_s^2 + 149.85 - 74.99M_s^{-2} \quad (2.18)$$



The Mach number,  $M$ , is a function of the measured shock velocity,  $V_s$ , and the speed of sound in the driven gas per

$$M = \frac{V_s}{\sqrt{\gamma RT_1}} \quad (2.19)$$

where  $R$  is the specific gas constant of the driven gas, which could be deduced by dividing the universal gas constant by the molar mass of argon. The incident-shock velocity,  $V_s$ , is calculated from the distance and time between pressure transducers,  $\Delta x$  and  $\Delta t$ , as follows:

$$V_s = \frac{\Delta x}{\Delta t} \quad (2.20)$$

If we use the maximum-error method, the worst-case values of  $\Delta x$  and  $\Delta t$  are applied to the equations above to infer bounds of  $V_s$  and  $T_5$  values. However, for the statistical approach in this work, the standard root-mean-square (RMS) method is adopted which incorporates the uncertainty of each variable in the calculation of uncertainty for  $V_s$ , and then for  $T_5$ . For  $\Delta V_s$ , it is obtained as a function of  $\Delta x$ ,  $\Delta t$  combined with their uncertainties,  $\delta_{\Delta x}$ ,  $\delta_{\Delta t}$ . The separation between pressure transducers could be measured to an accuracy of 1 mm and the temporal resolution of the sensors is 1  $\mu s$ . The uncertainty in shock velocity is then calculated using:

$$\delta_{V_s} = \sqrt{\left(\frac{\partial V_s}{\partial(\Delta x)}\delta_{\Delta x}\right)^2 + \left(\frac{\partial V_s}{\partial(\Delta t)}\delta_{\Delta t}\right)^2} = \sqrt{\left(\frac{1}{\Delta t}\delta_{\Delta x}\right)^2 + \left(\frac{-\Delta x}{(\Delta t)^2}\delta_{\Delta t}\right)^2} \quad (2.21)$$

Similarly, the uncertainty of the temperature behind the reflected shock can be calculated below using the equations above, with the consideration that  $T_5$  is only a function of the incident Mach number for the given gas.

$$\delta_{T_5} = \frac{\partial T_5}{\partial M} \delta_M = (450.19M + 149.98M^{-3}) \frac{\delta V_s}{\sqrt{\gamma RT_1}} \quad (2.22)$$

It can be seen from the above analysis that for most dilute test mixtures, an incident shock velocity uncertainty of 1 m/s, which is equal to around 0.12% error in Mach number, can lead to the temperature uncertainty of 3-4 K.

As earlier discussed, the temperature uncertainty can be estimated conservatively or using statistical error approaches [140]. Typically, estimated temperature errors are of the order of 0.5-1 %. Uncertainty of the reflected shock temperature in the present study is about 20 - 30 K by conservative estimates. Using the more realistic statistical error estimate as discussed before, it is found that the temperature uncertainty is 10-15 K.

The overall uncertainty in the ignition delay time can then be estimated by using the method of Zhukov et al. [141] as follows:

$$\frac{\Delta \tau_{total}}{\tau_{ign}} \% = \sqrt{\left(\frac{\Delta \tau}{\tau_{ign}}\right)^2 + \left(\alpha \frac{\Delta p}{p}\right)^2 + \left(\beta \frac{\Delta \phi}{\phi}\right)^2 + \left(\frac{E_a \Delta T}{RT^2}\right)^2} \quad (2.23)$$

assuming a known dependence of ignition delay time on pressure, equivalence ratio, and temperature in the form in Eqn. 2.16. The uncertainties of the other parameter in the equation above are obtained through statistical variance analysis of sample test data. For instance, for propanol experiments in the present study, the uncertainty for ignition

determination is  $4 \mu s$  for ignition delay times of about  $500 \mu s$ , uncertainty for pressure is found to be within 0.85% and for equivalence ratio is 0.03%.

Using conservative estimates (maximum errors of influencing factors), the temperature uncertainty for propanol experiments in this study is about 20 - 30 K, translating to an ignition delay time uncertainty of up to 30% at 1000 K for an uncertainty of 25 K. These uncertainties are within the range of the those reported in the literature. It should also be noted that the uncertainty is mostly systematic and applies to all data points [144]. The more realistic statistical error analysis as stated before puts the temperature uncertainty at 10 - 15 K, which one would expect to lead to a lower overall uncertainty in the ignition time. One further way to check the quality of the data is repeatability. It has been found that similar shock tube data can be obtained using test mixtures prepared at other times and reproduced with different realizations under similar initial conditions.

## **2.2 Ignition modeling approaches**

### **2.2.1 Chemical kinetic analysis of homogeneous constant volume reactor**

Ignition of homogeneous reaction reactors is one of the fundamental problems of chemical kinetics. The associated time scale of the process is of importance to the design of combustion devices and their performance optimization. A fundamental treatment of ignition has been attempted with two perspectives: the thermal theory and the chain-reaction theory. In thermal theory, ignition is pictured as the result of rapid heat release that affects reaction rates and leads to further heat release. The chain-reaction theory views ignition as resulting from initial reactions which leads to chain reactions and

rapidly consumption of the reactants through intermediate species and their reactions. More recently, a more unified approach invoking chain reactions and exothermicity has been suggested as a proper description of how hydrocarbon combustion is initiated.

The transformation of fuel and oxidizer to combustion products is therefore described by detailed chemical kinetic mechanisms combined with elementary reaction rates and thermodynamic properties. For example, the oxidation of a general alkane, RH, proceeds through a number of elementary reactions that include a number of intermediate species, as shown in Figure 2.10. Essentially, the fuel reacts through unimolecular decomposition and bimolecular abstraction to form reactive intermediates. These further reacts in various ways until the resulting chemical species are small enough to participate in direct oxidation to H<sub>2</sub>O and CO<sub>2</sub>. A detailed chemical kinetic mechanism usually contains elementary reactions among a number of species. The main objective of mathematical modeling of combustion kinetics is therefore to predict the temporal evolution of the species compositions and the other thermodynamic properties until the main heat release through final oxidation.

Of interest in this work is the homogeneous reaction model in fundamental combustion kinetics, in which the time evolution of a chemical reactor, consisting of  $I$  elementary steps among  $k$  species, is represented by an initial-value problem governed by a set of first-order ordinary differential equations (ODEs), under adiabatic, constant-volume conditions [145]. These equations include: conservation of species:

$$\frac{dY_k}{dt} = \frac{\dot{\omega}_k W_k}{\rho} \quad (2.24)$$

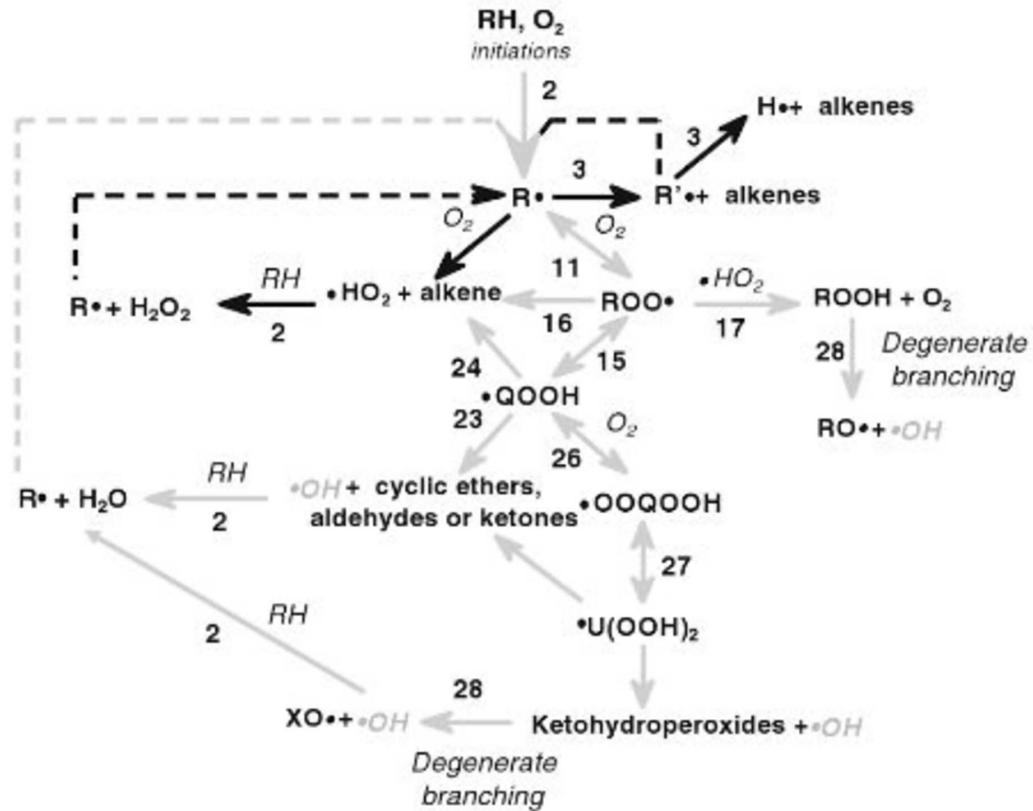


Fig. 2.10.: Simplified mechanism for the oxidation of a general alkane, RH. QOOH is an alkyl hydroperoxide radical, produced from  $RO_2$  by H atom transfer [99].

conservation of energy:

$$\rho c_v \frac{dT}{dt} + \sum_{k=1}^K e_k \dot{\omega}_k W_k = 0 \quad (2.25)$$

and an appropriate equation of state; such as the ideal gas law:

$$p = \rho \frac{R}{\bar{W}} T. \quad (2.26)$$

where  $Y_k$  is the mass fraction of the  $k$ th species,  $W_k$  is the molar mass of the  $k$ th species,  $e_k$  is the specific internal energy of the  $k$ th species,  $c_v$  is the constant volume specific heat capacity,  $\bar{W}$  is the mean molecular weight of the mixture, and  $\dot{\omega}_k$  is the molar rate of

production of the  $k$ th species by chemical reaction. The detailed chemical kinetic mechanisms for most large fuel molecules generally consist of hundreds of species and thousands of elementary reactions. As a result, chemical kinetic software packages, such as the CHEMKIN software and the CANTERA software packages, have been developed to solve these ODEs for temporal evolution of the species concentrations and temperature.

For the detailed chemical kinetic modeling of a combustion process, the underlying reaction mechanism and the rate coefficients of its elementary chemical steps have to be known. Reaction rate parameters can be obtained from experiments, analogies, and quantum chemical calculations. In many cases, however, an experimental determination of rate coefficients under combustion conditions using facilities such as shock tube and flow reactors is difficult or even impossible. Often only partial information such as relative rates or product branching ratios can be obtained, mostly restricted to rather narrow ranges of temperature and pressure. Thus, the analogies of reaction rates between similar classes of reactions, and a purely theoretical calculation of rate coefficients from first principles becomes more important as a very useful supplement to experimental studies. The common method of choice for the calculation of rate coefficients is the statistical rate theory, instead of establishing rate coefficients using quantum and classical dynamics calculations which is still currently restricted to small molecules (below six atoms).

Thermodynamic properties of participating molecules (heat of formation, specific entropies, and heat capacities) can be determined using experiments, statistical mechanics in conjunction with electronic structure theory, and by empirical rules such as group additivity of properties. Experimentally, enthalpies of formation, as an example, are derived from calorimetric experiments, which determine heat of reaction, yielding unique

products with known enthalpies of formation. However, measurement of the most important thermodynamic properties are not easy. Alternatively, there are two major approaches to determining thermodynamic properties of chemical species. One direction is ab initio calculations using electronic structure theory (quantum chemistry), which build on the treatment of the chemical system as an ensemble of atomic nuclei and electrons and numerically solution of the Schrödinger equation using the complex techniques and approximations. The other way of obtaining thermodynamic data without actual measurements is the so-called group additivity method, which is more empirical but very successful. It utilizes the fact that functional groups, especially in organic compounds, preserve not only their chemical characteristics from one molecule to the other, but also numerical values of their physical properties. This means the values of thermodynamic properties for the entire molecules could be closely approximated by summing the contributions of the constituting groups in the molecule.

The aim of chemical kinetic modeling is to accurately describe the evolution or concentrations profiles of important species and/or important features of the model predictions such as products of the reaction, and pollutant concentrations. It also involves predictions of time-to-ignition, and laminar flame velocities, among others. In building a detailed mechanism, the kineticist tries to include all the reactions and species that are relevant and necessary for the above predictions. When the detailed mechanism construction processes are applied, the resulting model contains many species and reactions, and the size increases with the carbon number and complexity of fuel molecules. It has been shown that modern detailed chemical kinetic models may contain up to several thousands of species and several thousands of elementary reaction steps [99, 111, 146].

The problem with such models is that they are too large for computational analysis of combustion. For computational reasons, large combustion models are still not adopted in two or three dimensions combustion flow simulations, where the applied combustion model often needs to be less than one hundred species. It is also observed that not all species are crucial for the prediction of combustion properties. Thus the key processes in such large mechanisms could be embedded in a network of many reaction steps with marginal importance. A first step to reducing the size of combustion chemical kinetic model is to determine species and reaction steps which are not crucial for accurate predictions of the target model outputs. Such approaches lead to the so-called skeletal chemical kinetic schemes. There are many different methods to identify the redundant species and reaction steps in the detailed kinetic model, including those based on sensitivity and Jacobian analyses, reaction rate comparison, intuitive guesses, and entropy production [146]. Another family of approaches is based on the investigation of reaction pathways such as the directed relation graph (DRG) and its derivatives, and the path flux analysis (PFA) method. From these skeletal schemes, further model reductions can be made via either species or reaction lumping.

To sum up, the process therefore is to develop detailed models, test these against experiments, and once the model is found to be reasonably accurate, then we can deduce simplified model versions to reduce computational costs. This work seeks to establish experimental trends, validate models, and provide simplified versions of the validated models for combustion analysis. The simplified models range from skeletal versions of the detailed models with fewer species and reactions to generalized correlations which capture chemical time scales as a function of thermodynamic conditions of the reactor. The skeletal



models are obtained using the reduction method called Alternate Species Elimination (ASE). Below, we describe the ASE reduction method and propose a generalized ignition correlation approach that is based on a validated detailed chemical mechanism.

### 2.2.2 Mechanism reduction via Alternate Species Elimination (ASE) method

To extract skeletal versions from a detailed chemical kinetic models, it is desirable to first identify the chemical species in the model that are crucial for the prediction of observed combustion phenomena. Our research group has successfully employed one of the reduction methods, Alternate Species Elimination (ASE), in generation of reduced models for various fuels [115, 119, 120]. This has been described in various publications from our research group, so only the outline is given here. In a nutshell, the ASE method seeks to examine the redundancy of individual species via a trial-and-error approach. A series of reduced mechanisms are created where in each one, all the reactions of the tested species involved were removed. If the resulting deviation between the solutions of the full and reduced models is small, then this species can be eliminated from the mechanism. The basis for this approach is that one considers the chemical system described by the set of ordinary differential equations, any ordinary dynamic system described by:

$$\frac{dX}{dt} = f(x_1, x_2, \dots, x_n) \quad (2.27)$$

In the equation,  $X$  is a column state vector with  $n$  variables, comprising temperature and concentrations of all the  $n - 1$  chemical species involved in the system. In conjunction with an appropriate equation of state, the temperature and concentrations permit the

thermochemical state of the system at each instance to be fully defined. The RHS is essentially a nonlinear function of species concentrations and reaction rate parameters in the Arrhenius format.

Special features of the chemically reacting systems encountered in combustion can be used to understand the geometry of their evolution in composition space. In the case of the homogeneous reactor, the chemical system transitions from an unburned state to a quasi-equilibrium state through a rapid ignition phase. Therefore, the initial solution of the system can be characterized by  $m$  nonzero components of the initial state vector,  $X_0$ .

$$X(t_0) = X_0(x_{10}, x_{20}, \dots, x_{m0}) \quad (2.28)$$

with  $m \ll n$ .

After ignition takes place, the system moves gradually to an equilibrium burned state,  $X_\infty$ , comprising of  $q$  components of the state vector,  $X_\infty$ , with equilibrium concentrations above a threshold such as a few parts per billion.

$$X(t_\infty) = X_0(x_{1\infty}, x_{2\infty}, \dots, x_{q\infty}) \quad (2.29)$$

The following inequality is generally valid:  $m < q < n$ , because a number of pollutant species is formed such as CO, soot, Unburned hydrocarbons, and other volatile organic compounds in addition to the main combustion products, CO<sub>2</sub> and H<sub>2</sub>O. Between the initial and equilibrium states, a large number of intermediates is formed, so that the number of nonzero components of the chemical system approach the number  $n$ , especially in the vicinity of ignition event.

Replacement of the complete chemical system comprising of  $n - 1$  species is possible with another system of smaller size with fewer species,  $r - 1$ , while keeping the predictive accuracy of the target combustion properties similar to that for which the detailed model was developed. These key properties contain global combustion properties, ranging from ignition delay times and burning velocities to concentration profiles of major species and pollutants. Reducing the number of species in the original chemical system can be achieved by getting rid of species and the irrelevant reactions as far as these have no effect on the prediction of target combustion properties.

To evaluate the effect of eliminating an individual species on the prediction of target global combustion properties, a normalized change in the combustion property is exploited. In the present work, the ignition delay time,  $\tau$ , is adopted as the desired combustion property. The normalized change,  $NC$ , is defined as

$$NC_i = \frac{\tau_i - \tau_0}{\tau_0} \quad (2.30)$$

where  $\tau_i$  and  $\tau_0$  are ignition time observed before and after eliminating the sub chemistry of the  $i$ th species under consideration.

All chemical species are then sorted and ranked by the absolute magnitude of their normalized changes,  $NC$ . The number of chemical species needed for predicting target combustion properties can be determined at a specified accuracy level with respect to the predictions of the detailed model.

The main aim of using the ASE method here is to generate a skeletal model from the original, detailed combustion models. It is obtained by assigning a user-defined threshold,

$NC_{thresh}$ , then suppressing sub chemistry of chemical species whose  $NC$ s are below the threshold. The  $NC_{thresh}$  can be examined by testing the reduced mechanism against the detailed one in terms of predicting other combustion properties of interest, in addition to prediction of ignition times. To match the flame propagation property, a lower threshold is often found necessary, compared to relatively simpler ignition delay times prediction. It has been observed that reasonably good predictions of flame propagation and ignition are ensured when less than or equal to  $1 \times 10^{-4}$  value for  $NC_{thresh}$  is chosen. A  $NC_{thresh}$  of  $5 \times 10^{-4}$  can generally satisfactorily capture the ignition behavior while some noticeable deviations in burning velocity predictions start to appear.

### 2.2.3 Generalized ignition correlation method

Per the discussion before, building simplified ignition correlation based on detailed chemical kinetic simulations or experimental data provides a cost-effective approach for realistic computer-aided combustor design and control. For example, the phenomenological models for engine combustion, heat release rate and heat loss have been widely used in the engine industry. Developing physics based simplified models or correlations have thus gained more attentions over the years among engine researchers and engineers [147, 148]. In this study, a correlation method is proposed and demonstrated by developing generalized correlations for selected fuels with the complex temperature behaviors based on simulations using detailed chemical kinetic models from the literature. The fuels considered are biodiesel, two jet fuel surrogates, a gasoline surrogate, *n*-octanol and ethanol/gasoline blends using data set from model simulations of constant volume homogeneous reactors.

The model for the biodiesel surrogate is by Herbinet et al. [149] that consists of 2878 species and 8555 elementary reactions. With respect to the jet fuel surrogates, two models each with a different formulation were considered here: the model by Dooley et al. [109] consists of 1599 species and 6633 reactions; a smaller model for kerosene by Honnet et al. [150] is also used in this work, it comprises 119 species and 527 reactions and uses *n*-decane and trimethylbenzene as a kerosene surrogate. In the case of the gasoline surrogate, we use the model by Mehl et al. [107] that comprises 1389 species and 5935 reactions. The model for *n*-octanol is that recently proposed by Cai et al. [151] which consists of 1281 species and 5510 reactions. Finally, a recent combined mechanism for ethanol/gasoline blends proposed by Cai et al. [27] with 339 species and 1690 reactions is used. The larger or relatively large size of these detailed or reduced models makes even simple combustion processes, such as the ignition of a homogeneous reactor, computationally time-consuming. The proposed generalized correlation consists of 20 parameters.

To develop the simplified ignition correlation, ignition delay times for stoichiometric fuel/air mixtures over a range of temperatures and pressures are first calculated using the CHEMKIN software package. The surrogate compositions used in this study for biodiesel is methyl decanoate. The jet fuel surrogate composition used for the Dooley et al. [109] is *n*-decane, *iso*-octane, and toluene in the ratio 42.67/33.02/24.31, referred to as the Princeton Jet Fuel Surrogate. The Aachen Jet Fuel surrogate composition, 80% *n*-decane and 20 % trimethylbenzene, is used to develop the correlation of the Aachen model. For gasoline we used surrogates proposed by Gauthier et al. [152] (63% *iso*-octane/20% toluene/17% *n*-heptane by liquid volume). The ethanol/gasoline surrogate compositions used in this study are from Fikri et al. [153] (62% *iso*-octane/18% *n*-heptane/20% ethanol

by liquid volume) with an Octane number of 92.0. In this study, the ignition delay time is defined as the time from reaction onset to the time when the maximum OH concentration is observed; with the verification that it is indeed the main ignition event.

After the ignition time database is built, we divide the ignition results into three temperature regimes (low, middle, and high temperature ranges) according to the negative temperature coefficient behaviors. In the vicinity of cross-over temperatures between the low-temperature/NTC and high-temperature/NTC regimes, a finer temperature resolution is used to precisely locate the cross-over temperature. We refer to cross-over temperatures here to be those that delimit the NTC regions from low- and high-temperature kinetics; we use this in the same context as Peters et al. [154]. For mixtures without NTC behavior, the temperatures delimiting high- from low-temperature kinetics could be determined as the inflexion points on plots of ignition delay times against temperature. A collection of the cross-over temperatures detected here by the temperature gradient change for various pressures is used to determine the relation between cross-over temperatures and pressures. This is needed for the generalized correlation.

In each region, the sub correlations are then developed and each one adopts an adapted format as the reciprocal of the reaction rate constant of an Arrhenius-type first order reaction rate for the global reaction.

$$\tau = Ap^\alpha \left( \frac{T}{T_{ref}} \right)^n \exp \left( \frac{E_a}{RT} \right) \quad (2.31)$$

where  $p$  and  $T$  are pressure and temperature of the mixture and  $A$ ,  $\alpha$ ,  $n$ ,  $E_a$  are the fitting coefficients. These coefficients are then derived by correlating the ignition data in each region using a Matlab script.

In this study, we combine the sub-correlations into a generalized ignition correlation by introducing the hyperbolic tangent as a switch function with parameters consisting of cross-over temperatures and a temperature difference over which the function transitions. With two switches at the cross-over temperatures, we evaluate the performance of the correlation with respect to reproducing the original simulation data. Our switches have the form  $\eta_1 = \frac{1}{2}(1 - \tanh[\frac{T-(T_L-10)}{10}])$ ,  $\eta_2 = \frac{1}{2}(1 - \tanh[\frac{T-(T_H+10)}{10}])$  and the generalized correlation has the form  $\tau = \tau_{low}\eta_1 + \tau_{mid}(1 - \eta_1)\eta_2 + \tau_{high}(1 - \eta_2)$ , capturing the whole temperature region.

While our suggested switch function is an improvement over the previous correlation approach, its performance in the vicinity of the critical cross-over points still needs further improvement. This is achieved here by means of a sine function around the transition points and four switches are effectively used to control the smooth change. The cross-over temperatures are used to center the sine wave around the point of interest and an amplitude function is included to capture the departure of the ignition dependence at various pressures. For the biodiesel surrogate model, these amplitudes,  $t_L$  and  $t_H$ , are found by further regression analysis of the form  $t \propto p^k$ . The final sine function,  $\tau_{sin}$ , takes the form as shown in the eqn. 4.4 and 4.5 in Chapter 4. The correlation approach is further illustrated and demonstrated in the discussion of the results in chapter 4.

### 3. IGNITION EXPERIMENTS

The results presented in this section are also part of a recent publication [155].

#### 3.1 Comparative ignition behavior: propanol isomers

##### 3.1.1 Experimental results and model validation

Presented here are the experimental results of the subtasks listed above for propanol isomers. To fully understand the ignition of propanol isomers, the test mixtures are carefully designed to investigate the effects of pressure dependence, equivalence ratio, fuel concentration and molecular structure on ignition time. The mixture compositions investigated in this study are shown in Tab. 3.1. Pressure and isomer effects on ignition behavior are explored. The experimental data are also compared with previous work and the relative reactivity of propanol isomers is examined.

Ignition mixtures	$\phi$	% fuel ( <i>n-</i> or <i>iso-</i> )	% O <sub>2</sub>	% Ar	$D$
1	1	1.00	4.500	94.500	21
2	0.5	0.5025	4.5226	94.9749	21
3	2	1.9802	4.4554	93.5644	21
4	1	4.4603	20.0714	75.4683	3.76

Table 3.1: Composition of propanol mixtures used in this study. In the text, an ignition mixture is identified by the fuel type, its equivalence ratio,  $\phi$ , and its argon/oxygen molar ratio,  $D$ .



Ignition delay times for propanol isomers are first presented. This is followed by comparison of model predictions with the measured time scales. Furthermore, sensitivity and reaction pathway analyses based on the most accurate combustion models are performed to interpret the experimental results and to shed light on the controlling chemical kinetic processes. Finally, reduced models for representative C1 - C4 alcohols including propanol isomers are constructed and widely validated with respect to predicting key combustion properties.

Ignition delay times for stoichiometric fuel/O<sub>2</sub>/Ar mixtures are measured under various pressure conditions to establish isomer and pressure effects. Lean ( $\phi=0.5$ ) and rich ( $\phi=2$ ) propanol mixtures are also studied at average pressures of 3.5 atm to explore the effect of equivalence ratio. A fixed argon to oxygen ratio,  $D = 21$ , is adopted so that the fuel molar fraction lies in the range of 0.5% - 2.0%, depending on the corresponding equivalence ratio. A further set of ignition delay measurements are obtained for less dilute stoichiometric mixtures ( $D=3.76$ ) at 12 atm to reflect the composition of air.

The shock tube ignition data are first compared with experimental ignition correlations developed by Noorani et al. [25] and Man et al. [54]. As for uncertainties in measured delay times discussed in the former chapter, they are estimated by propagating major uncertainty contributions: temperature uncertainties (1.0 - 1.5%), pressure uncertainties (1.0-1.5%), fits and ignition delay measurement (1%). The propagated uncertainties in ignition delay times are dominated by temperature uncertainties on account of their exponential dependence on temperature. Ignition uncertainties range from 10% to 20% and are indicated in the plots below. Uncertainties of ignition delay times calculated from literature correlations are of a comparable magnitude (not shown for clarity). The results

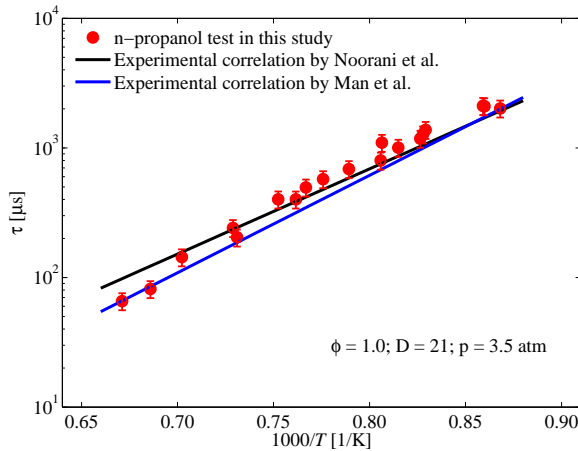


Fig. 3.1.: comparison with *n*-propanol experiment correlations [25, 54] at 3.5 atm.

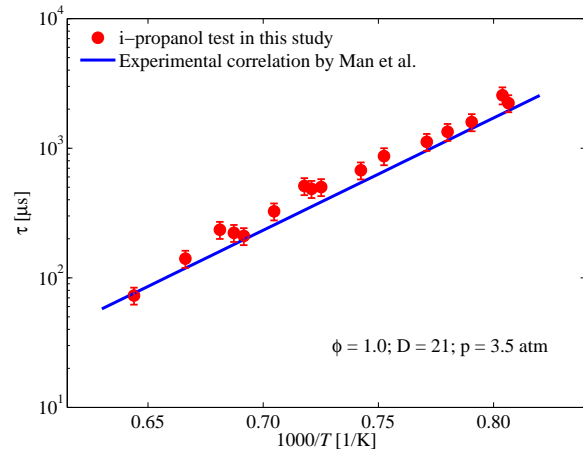


Fig. 3.2.: comparison with *iso*-propanol experiment correlation [54] at 3.5 atm.

for *n*-propanol ignition at pressures of 3.5 atm are shown in Fig. 3.1. It is observed that the correlation predictions agree with the current measurements within experimental uncertainties. The correlation by Noorani et al. [25] shows a lower activation energy such that longer delay times are predicted at higher temperatures.

With respect to *iso*-propanol, Figs. 3.2 shows that the measured delay times accord with calculated times from the correlation by Man et al. [54], with the latter showing slightly shorter delay times at 3.5 atm.

Similar trends and close agreements between the test data in this study and experiment correlations from literature are further demonstrated in the ignition study at a different pressure of 5 atm as shown in Figs. 3.3 and 3.4.

The isomer effect is established by carrying out ignition experiments using mixtures of similar compositions and at similar test conditions. The results are shown in Figs. 3.5 and Fig. 3.6 for pressures of 3 atm and 5 atm, respectively. As would be expected from the

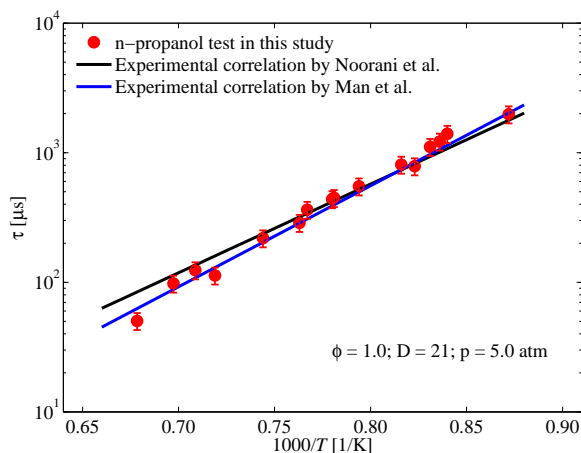


Fig. 3.3.: Comparison with *n*-propanol experiment correlations [25, 54] at 5 atm.

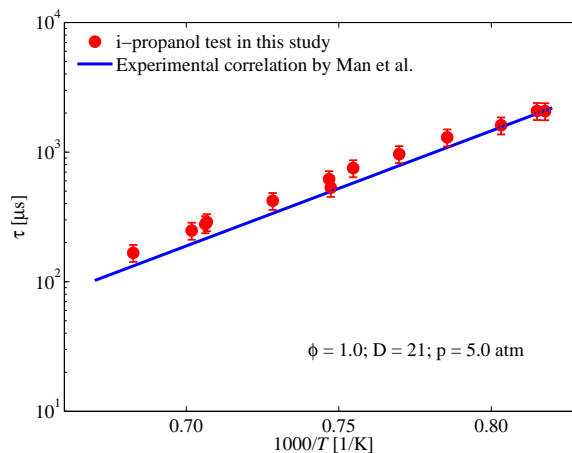


Fig. 3.4.: comparison with *iso*-propanol experiment correlation [54] at 5 atm.

chemical structure and in accordance with previous studies, *iso*-propanol has longer ignition delay times than *n*-propanol. This difference in reactivity is partially attributed to weaker secondary C-H bonds in *n*-propanol. Another reason for the observed difference is that *n*-propanol oxidation leads to formation of the highly reactive formaldehyde whereas

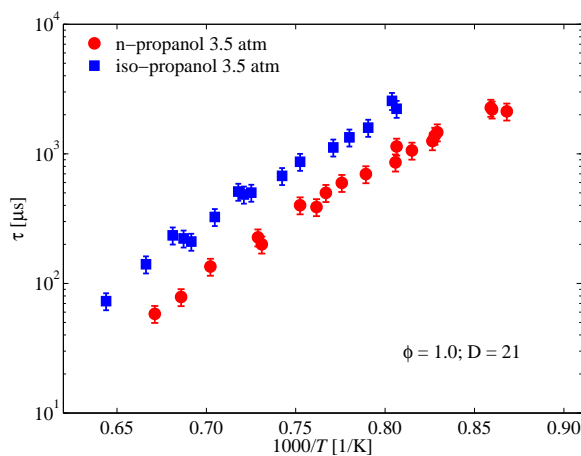


Fig. 3.5.: isomer effect on propanol ignition (3.5 atm).

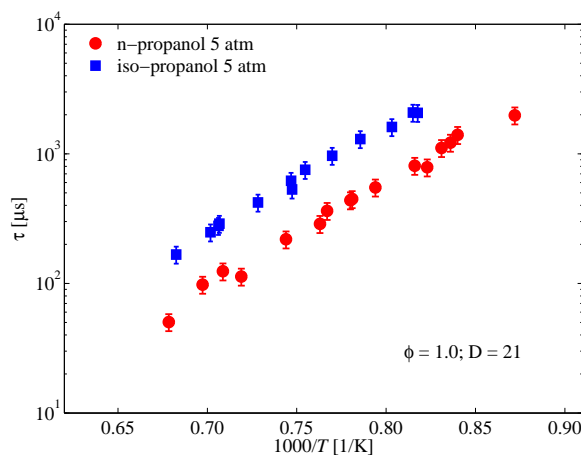


Fig. 3.6.: isomer effect on propanol ignition (5 atm).

the less reactive acetone is more readily formed during *iso*-propanol oxidation. These differences correlate with higher H atom formation rates in *n*-propanol than in *iso*-propanol, which further result in more rapid fuel consumption in *n*-propanol.

The observed ignition delay times are also compared with predictions obtained using three chemical kinetic models from the literature [52, 54, 56]. Figure 3.7 shows the comparison of model predictions with measured ignition delay times for stoichiometric mixtures of *n*-propanol at 3.5 atm. It is observed that the model by Johnson et al. [52] predicts much longer delay times than measured while the predictions of the models by Sarathy et al. [56] and Man et al. [54] are in closer agreement with the experimental observations. As discussed by the authors, the model by Man et al. [54] is an improved version of that by Johnson et al. [52]. It is also worth noting that Man et al. and Sarathy et al. models predict ignition delay times in close agreement albeit with slightly different global temperature sensitivities. A similar level of agreement is observed for *iso*-propanol as shown in Fig. 3.8. The comparison of experimental results with model simulations is also carried out for propanol isomers ignition at the pressure of 5 atm. Figs. 3.9 and 3.10 demonstrate the trends are consistent with earlier findings at 3 atm.

The equivalence ratio effect on ignition delay times is also examined by measuring ignition delay times under rich, lean, and stoichiometric conditions with a fixed  $D$  of 21 at 3.5 atm and the results are compared with predictions of the model by Sarathy et al. model [56]. This model is chosen to examine the equivalence ratio effect on account of the close agreement between simulations and measured delay times at stoichiometric conditions, discussed above. In the case of *n*-propanol, Fig. 3.11 shows that under the chosen conditions, there is a weak dependence on equivalence ratio. Ignition delay times

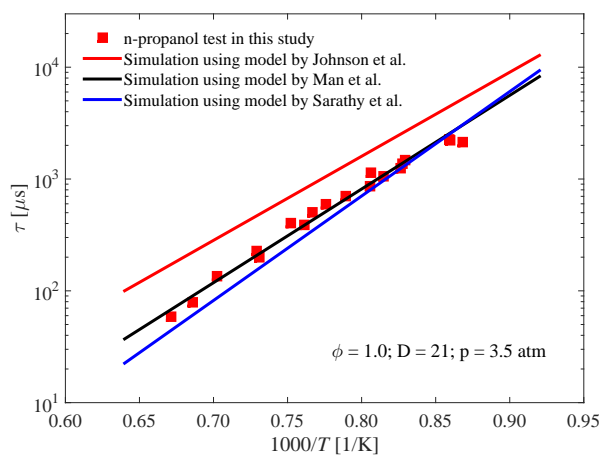


Fig. 3.7.: Comparison of measured *n*-propanol ignition delay times at 3.5 atm with model predictions.

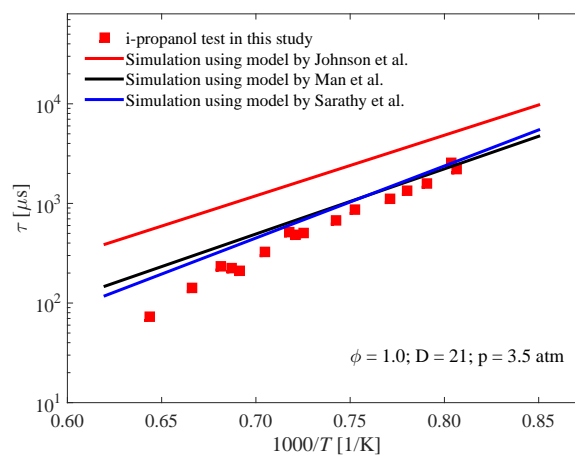


Fig. 3.8.: Comparison of measured *iso*-propanol ignition delay times at 3.5 atm with model predictions.

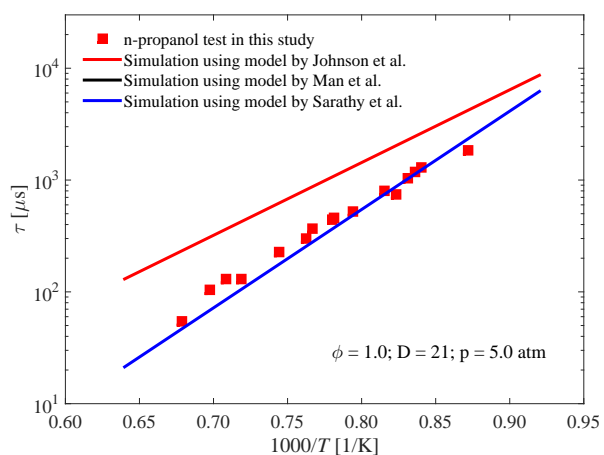


Fig. 3.9.: Comparison of measured *n*-propanol ignition delay times at 5 atm with model predictions.

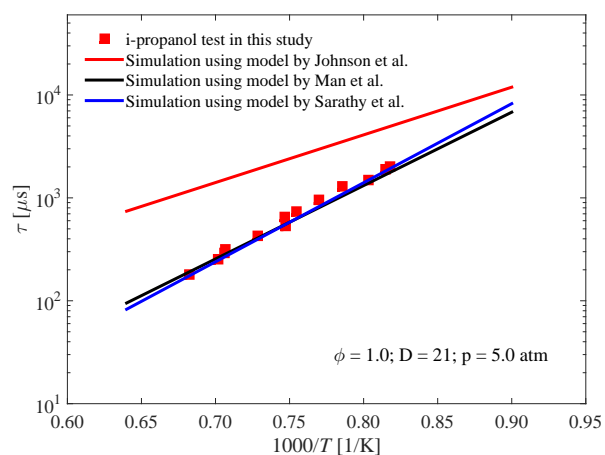


Fig. 3.10.: Comparison of measured *iso*-propanol ignition delay times at 5 atm with model predictions.

decrease with increasing equivalence ratio but are more insensitive to equivalence ratio effects at higher temperatures. This relative behavior is captured by the model even though its predictions are slightly shorter than the measured data.

Figure 3.12 shows the results of equivalence ratio effects for *iso*-propanol. The trend observed for *n*-propanol is seen here at lower temperatures while a reversal occurs around 1300 K, with the rich mixture becoming more reactive. As discussed in one of our publications [155], during the ignition process, there is competition between oxidative processes and purely pyrolysis kinetics, however, pyrolysis kinetics usually has a higher apparent activation energy. The oxidative processes in *iso*-propanol are slower than in *n*-propanol, and so the comparable behavior between pyrolysis and oxidative processes is reached at lower temperatures in *iso*-propanol than in *n*-propanol.

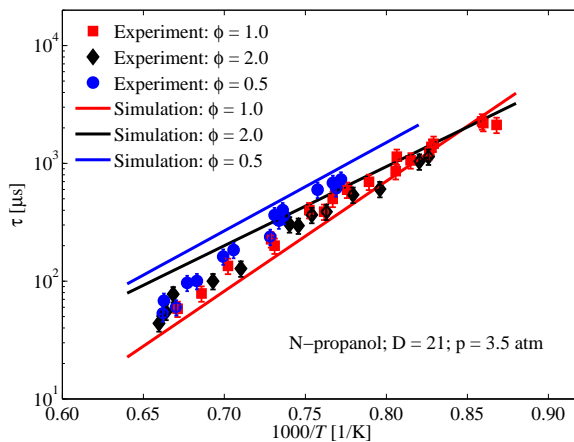


Fig. 3.11.: Comparison of measured *iso*-propanol ignition delay times at three equivalence ratios with predictions of model by Sarathy et al. [56].

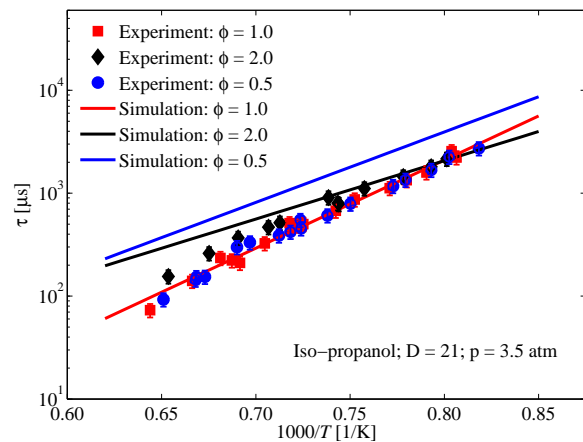


Fig. 3.12.: Comparison of measured *iso*-propanol ignition delay times at three equivalence ratios with predictions of model by Sarathy et al. [56].

The ignition results above have been obtained under very dilute conditions. Figure 3.13 shows that the established isomer effect is consistently realized at the higher average pressure of 12 atm for less dilute mixtures with a ratio of argon to oxygen,  $D$ , of 3.76, reflective of the nitrogen to oxygen ratio in air. The experimental data are compared with predictions of the model by Sarathy et al. [56], showing reasonable agreement.

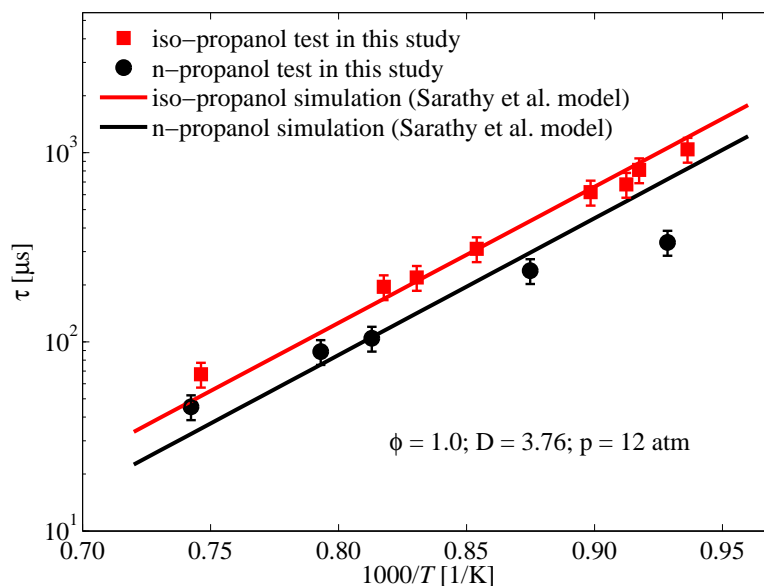


Fig. 3.13.: Isomer effect on ignition of stoichiometric mixtures at a higher average pressure of 12 atm and less dilute condition ( $D = 3.76$ ). Model simulations: Sarathy et al. [56].

Species sensitivity analysis of ignition and reaction pathway analysis are carried out to better understand some of the kinetic reasons for the observed behavior.

The Species sensitivity analysis is done using the Alternate Species Elimination (ASE) approach [115, 156] as introduced in Chapter 2, the essence of which is to determine whether suppression of the sub chemistry of a given species leads to differences in a predicted combustion property such as the ignition delay time. If the delay time increases

upon suppression of a given sub chemistry, it attests to the forward propagating role of the species. A decrease in the ignition delay time indicates that the said species acts as a radical sink or affords a delay channel for fuel oxidation. The effect of the fuel,  $O_2$ ,  $H_2O$ , and  $CO_2$  are not assessed; they are automatically assumed to be indispensable for oxidation.

Figure 3.14 shows the sensitivities of the 20 most important species in the model by Sarathy et al. [56], where sensitivities of corresponding species are also taken from the other two mechanisms. We see that  $CH_2O$ ,  $H_2O_2$ , and  $OH$  are very important for *n*-propanol ignition. It is also observed that suppression of the CO sub chemistry leads to longer delay times, indicating its overall reactivity-promoting role in the mechanism. The stable molecules,  $CH_4$ ,  $H_2$ , and  $C_2H_3OH$ , generally offer ignition-retarding pathways.

In the case of *iso*-propanol as shown in Fig. 3.15, the majority of the important species are those whose removal would slow down the ignition process. On the other hand,  $CO$  and  $C_2H_6$  offer ignition-retarding pathways, since their exclusion leads to faster ignition in all three models. In contrast to the other two models, the Johnson et al. model shows that eliminating the  $CH_2CO$  sub chemistry leads to longer ignition delay times, implying that it offers an ignition promoting channel. The lower rate of  $CO$  formation observed for the Johnson et al. model may be linked to slower reaction channels from  $CH_2CO$  to  $CO$ .

Reaction pathway analysis of representative oxidation processes are carried out using the model by Sarathy et al. [56] on account of its overall better agreement with measurements. All analyses are carried out at the instance where 20% of the initial fuel molar fraction has been consumed.



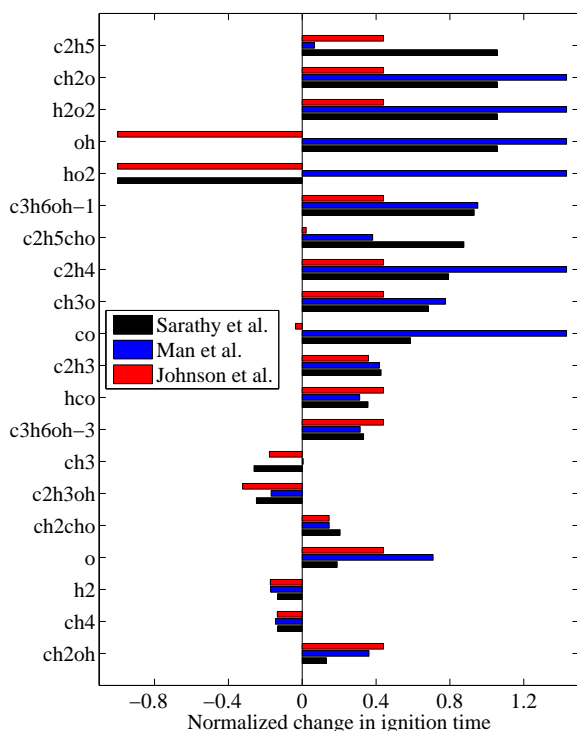


Fig. 3.14.: Species sensitivity analysis of *n*-propanol ignition. Shown are the 20 most important species at the condition  $\phi = 1.0$ ,  $D = 21.0$ ,  $p = 15$  atm, and  $T = 1050$  K.

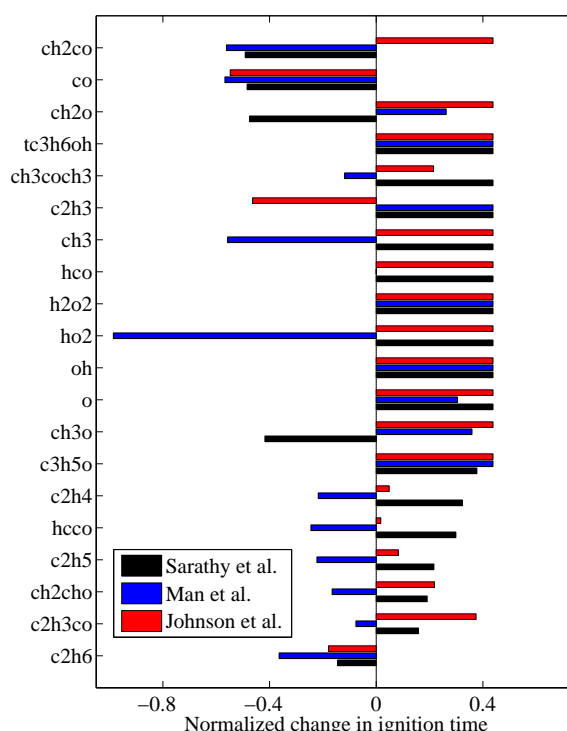


Fig. 3.15.: Species sensitivity analysis of *iso*-propanol ignition. Shown are the 20 most important species at the condition  $\phi = 1.0$ ,  $D = 21.0$ ,  $p = 15$  atm, and  $T = 1050$  K.

Figure 3.16 shows the pathways during ignition of a stoichiometric mixture of 1% *n*-propanol at two temperatures. The conditions are chosen where both isomers have comparable ignition delay times. It is observed that *n*-propanol is primarily consumed through H-abstraction and unimolecular reactions, with the former accounting for more than 70% under both conditions, while the unimolecular decomposition accounts for about 13 % at the lower temperature and increases to about 23 % at the higher temperature. Concerted elimination of H<sub>2</sub>O contributes less than 5 % and is higher at higher temperatures. At higher temperatures, the increasing role of pyrolysis is thus observed. It should also be noted that a proportion of the H-abtracting radicals are derived from

further decomposition of products of the unimolecular decomposition and the fuel radicals obtained from earlier abstractions. The role of unimolecular reactions is stronger at even earlier times than considered in this analysis. A majority of the initial radicals react by  $\beta$ -scission to form smaller radicals and stable molecules.

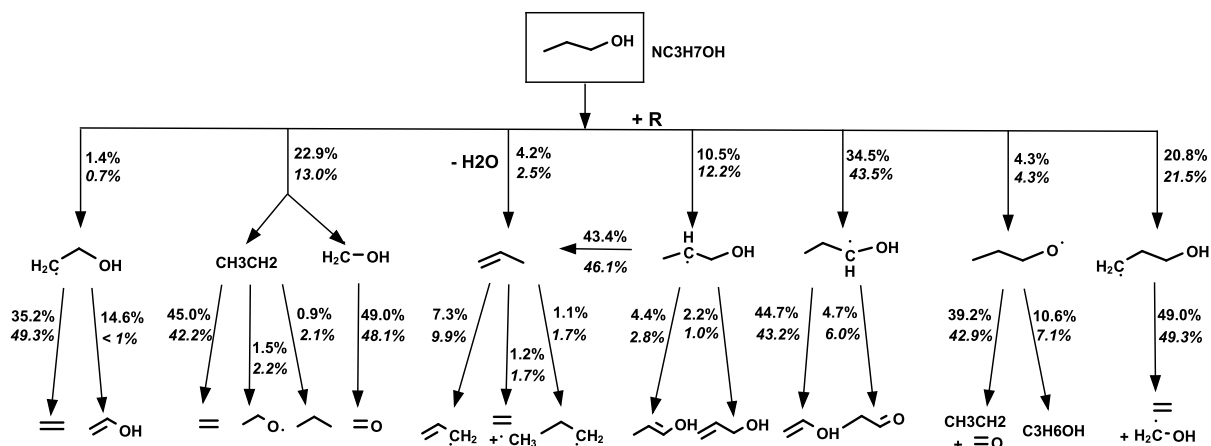


Fig. 3.16.: Reaction pathway for *n*-propanol ignition ( $\phi = 1$ , 1% fuel,  $D = 21$ ,  $p = 3$  atm) using the model by Sarathy et al. [56] at temperatures of 1475 K (top) and 1230 K (bottom).

In the case of *iso*-propanol ignition process (see Fig. 3.17), H-abstraction from methyl C-H sites and the C-H site adjacent to the OH group is dominant at both temperatures (over 80 %). Their further reactions lead to the formation of propenol and acetone, with same carbon number as the fuel and in need of further radical and unimolecular reaction possibilities. Unimolecular reactions include direct C-C bond scission and concerted elimination of H<sub>2</sub>O, with the latter being slightly more important than the direct scission.

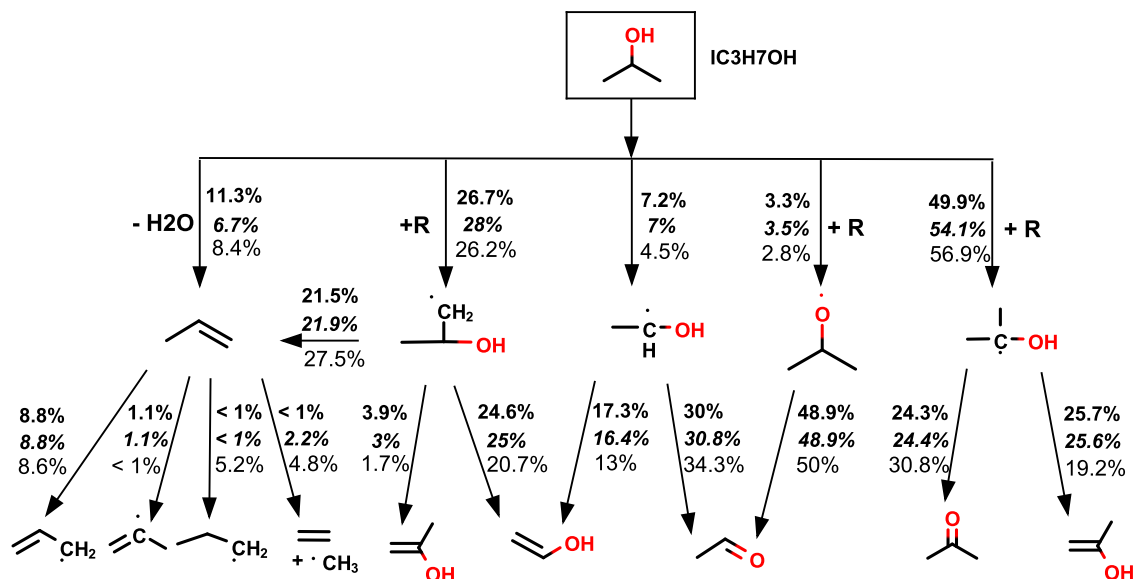


Fig. 3.17.: Reaction pathway for *iso*-propanol ignition ( $\phi = 1$ , 1% fuel,  $D = 21$ ,  $p = 3$  atm) using models by Sarathy et al. [56] with temperatures of 1510 K (top) and 1310 K (bottom).

### 3.1.2 Reduced chemical kinetic model

The aim here is to develop four stand-alone reduced models for binary sets of C1-C4 alcohols using the proven ASE model reduction approach including propanol isomers which we studied in the former section. This work will make available the progress in bioalcohol kinetic modeling for computational analysis of combustion. We anticipate the need for reduced models of those alcohols, herein methanol/ethanol, propanol isomers, and two butanol models each including *n*-butanol and *iso*-butanol or *s*-butanol. To ensure that the essential chemical kinetic performance is preserved, prediction of a number of combustion properties are compared against predictions obtained using the original detailed model.

## Model reduction method

The reduced model for each pair of alcohols is obtained based on ignition simulations and the ASE reduction method. The chemical kinetic solver is CANTERA in its MATLAB platform, chosen for the associated ease of suppressing reactions of a species under consideration. Three equivalence ratios are used ( $\phi = 0.5, 1.0,$  and  $2.0$ ) at a reactor pressure of 15 atm. The temperature is 1050 K for the lean and stoichiometric case and lowered to 1000 K in the case of the rich mixture to get comparable ignition delay times since for fuel/air mixtures, ignition delay times decrease with increasing equivalence ratio in this temperature range.

## Validation of reduced models

The following reduced models are obtained from the detailed model (comprising 600 species and 4100 elementary reactions) using ASE approach: methanol/ethanol: 38 species and 197 reactions; propanol isomers: 68 species and 419 reactions; *n*- and *iso*-butanol: 140 species and 745 reactions ; and *n*- and *s*-butanol: 134 species and 739 reactions. In this part of the work, we are carrying out a series of validation work in order to test the performance of these reduced models and establish that they reproduce the performance of the detailed model.

The purpose of the validation against ignition delay times is to ascertain that the reduced models can accurately predict ignition delay times at conditions different from those used in the reduction process, especially in terms of temperatures and pressures.

Figures 3.18-3.21 show the performance of the models at equivalence ratios of 0.6, 1.0., and 1.5; a reactor pressure of 20 atm; and over a range of temperatures, starting from 950 K. The nitrogen to oxygen ratio,  $D$ , in this case is 3.76, reflecting the composition of air as a technical oxidizer. It is observed that in all four cases the reduced models accurately capture the ignition delay times predicted by the detailed models.

Further comparisons are carried out at conditions with higher nitrogen dilution ( $D = 20$ ) as well as pressures of 20 atm and 40 atm. Similar level of accuracy (less than 3 % at high temperature-end) is observed. Examples of this agreement are shown in Figures 3.22 (reduced model of methanol/ethanol) and 3.23 (reduced model of propanol isomers). This good performance shows that the ignition performance of the detailed kinetic model adequately captured by each of the proposed reduced versions over a representative range of pressures and temperatures. It is now left to verify the assumption that ignition is a sufficiently rigorous combustion problem to capture the essential chemical kinetics needed for most combustion properties.

To examine the ability of the reduced models to predict properties of freely propagating premixed flames, laminar burning velocities obtained from premixed flame simulations using the reduced models are compared with those of the original detailed chemical kinetic models. The laminar burning velocities at various equivalence ratios are obtained from simulations of freely propagating flames using the Premixed solver in CHEMKIN PRO. The unburned temperature is 400 K and the prevailing pressure is 1.0 atm. The fuels considered are binary mixtures of equal molar proportions as in the case of ignition simulations.

Figure 3.24 shows the comparison of detailed and reduced models with respect to prediction of burning velocities. It is observed that the reduced model of propanol isomers

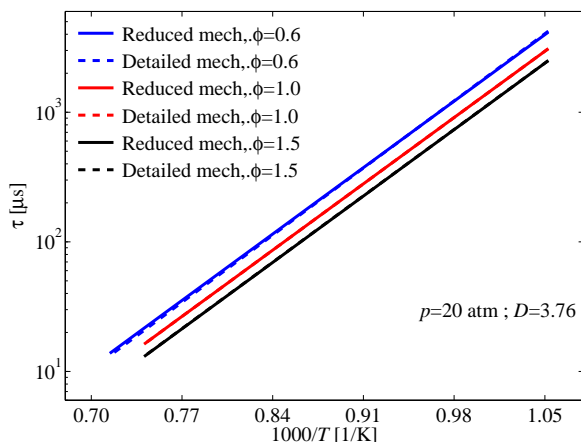


Fig. 3.18.: Methanol and ethanol: comparison of detailed and reduced model with respect to ignition delay time prediction at three equivalence ratios and pressure of 20 atm.

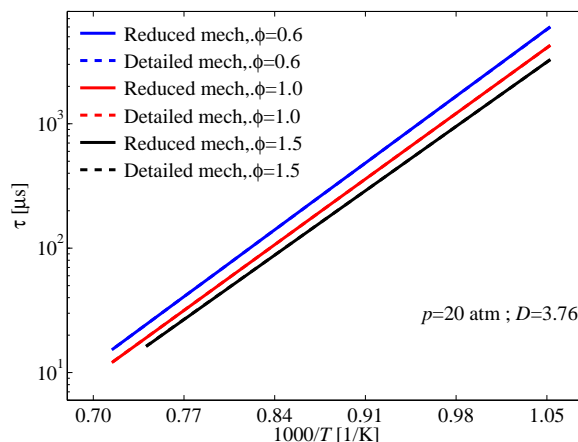


Fig. 3.19.: Propanol isomers: comparison of detailed and reduced model with respect to ignition delay time prediction at three equivalence ratios and pressure of 20 atm.

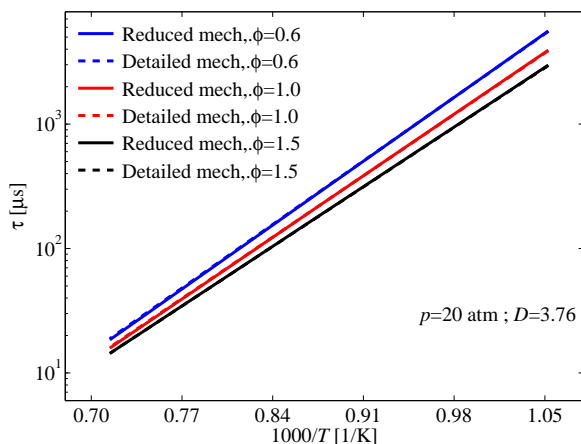


Fig. 3.20.: *n*- And *iso*-butanol isomers: comparison of detailed and reduced model with respect to ignition delay time prediction at three equivalence ratios and pressure of 20 atm.

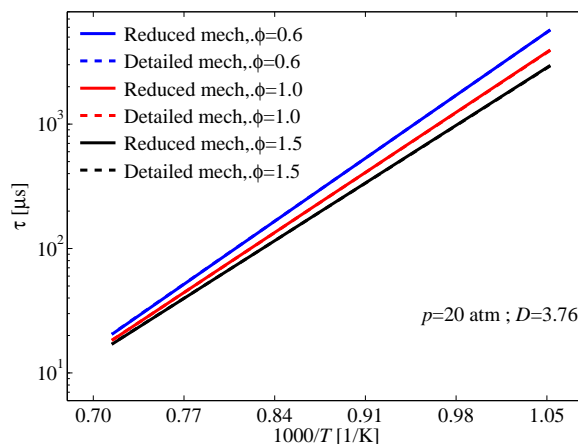


Fig. 3.21.: *n*- And *s*-butanol isomers: comparison of detailed and reduced model with respect to ignition delay time prediction at three equivalence ratios and pressure of 20 atm.

accurately predicts the laminar burning velocities determined using the detailed model. In the case of methanol/ethanol fuel mixture, it is observed that while the lean to

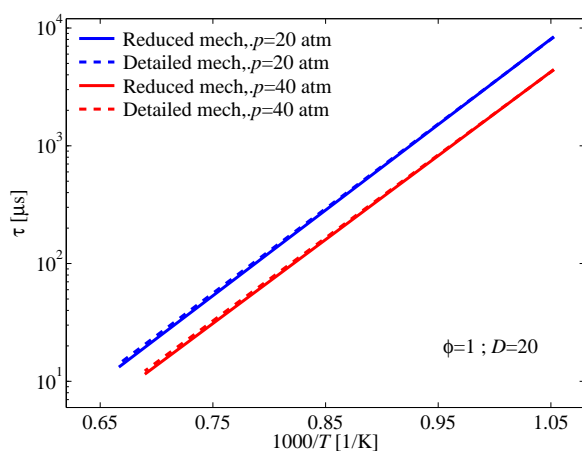


Fig. 3.22.: Methanol and ethanol: comparison of detailed and reduced model with respect to ignition delay time prediction at two different pressures and higher dilution level.

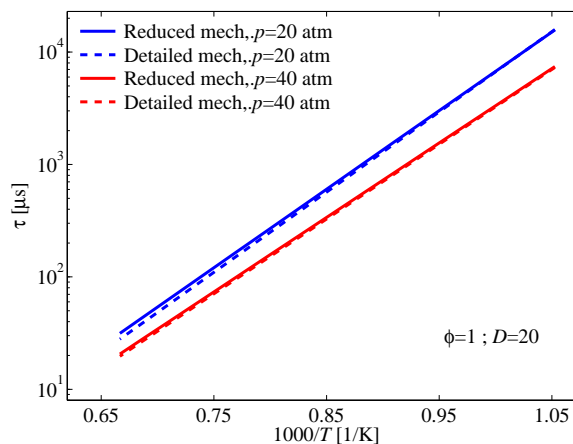


Fig. 3.23.: *n*- and *iso*-propanol isomers: comparison of detailed and reduced model with respect to ignition delay time prediction at two different pressures and higher dilution level.

stoichiometric flames are well predicted by the reduced models, deviations are evident under rich conditions. This case presents the worst possible flame predictions of the reduced models. The simulations show that the reduced models still reproduce the trend in burning velocities, whereby flames of the methanol/ethanol fuel mixture propagate faster than those of equal proportions of propanol isomers.

In the case of butanol isomers, Fig. 3.25 shows that reduced models of *n*-/*s*-butanol and *n*-/*iso*-butanol predict laminar burning velocities that are in good agreement with the simulated results from the original detailed model. The good agreement between reduced and detailed model predictions also imply preservation of the trend whereby flames of *n*-/*s*-butanol are slightly faster than those of *n*-/*iso*-butanol. Although ignition and flame propagation may appear to be completely different combustion events, this validation shows that the connectivity or the reaction network and the heat release mechanisms of the

kinetic model can be properly identified by examining the role of various chemical species in the simulation of homogeneous ignition phenomena. By examining the important species, it is observed that in addition to fuel and immediate fuel radicals, many species in the C0-C2 system feature in the reduced mechanism. These species are responsible for chain propagation reactions and are also essential to the heat release process which typically occur as OH, H, O, CO, and O<sub>2</sub> are converted to the major combustion species, CO<sub>2</sub> and H<sub>2</sub>O.

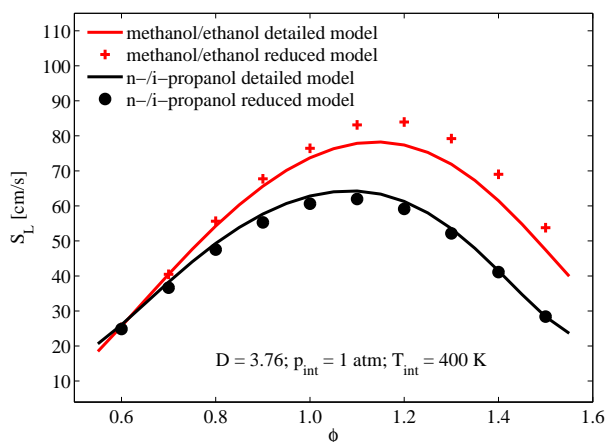


Fig. 3.24.: Methanol and ethanol; propanol isomers: Comparison of detailed and reduced models with respect to burning velocity prediction for fuel/air mixtures at 1.0 atm and 400 K.

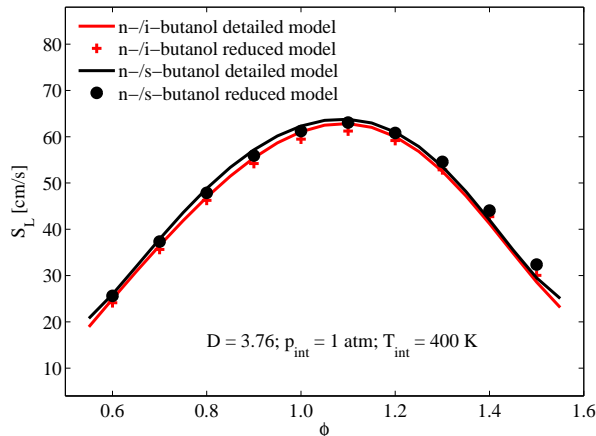


Fig. 3.25.: Binary blends of butanol isomers: Comparison of detailed and reduced models with respect to burning velocity prediction for fuel/air mixtures at 1.0 atm and 400 K.

A further test of the reduced models is carried out to ascertain their ability in capturing the kinetic effects of non-oxidative high-temperature fuel decomposition (pyrolysis). We have recently proposed a method of assessing the global kinetics of pyrolysis through a characteristic chemical time scale obtained from concentration profiles [155].



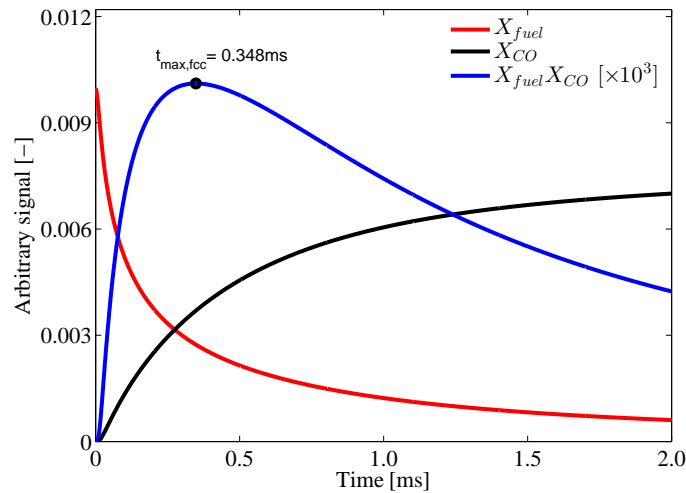


Fig. 3.26.: Concentration correlation function based on fuel and CO concentrations. The time to maximum captures the global chemical kinetics of the pyrolysis process and can be used to investigate effects of temperature, pressure, and fuel concentration.

The method consists in defining a concentration correlation function ( $f_{cc}$ ), such as the product of a species that is consumed during pyrolysis and one that emerges as a product. In the case of oxygenates such as the alcohols considered in this work, this function could be a product of the fuel and CO mole fractions i.e.  $f_{cc} = x_{fuel}x_{CO}$ . This function features a maximum whose associated time can be used as a characteristic property of pyrolysis for the given initial thermodynamic state of the reactor. Figure 3.26 is an example of this correlation function and the pyrolysis time. Using this approach, pyrolysis times can be determined over a range of conditions. The reduced models can then be compared with respect to their prediction of these pyrolysis times and the associated temperature sensitivity (apparent activation energy).

Considered is the pyrolysis of 1% fuel (binary mixture of equal proportions) in argon at a pressure of 3 atm over a range of temperatures. Shown in Fig. 3.27 is a comparison of

the pyrolysis times of a mixture of methanol and ethanol. Similarly, Fig. 3.28 shows pyrolysis times of *n*-/*iso*-butanol fuel mixture. The good agreement between detailed and reduced model predictions indicate that the reduced models, obtained on the basis of ignition simulation, are equally capable of capturing the non-oxidative kinetics of thermal decomposition. Characteristic of the pyrolysis times as defined in this work is the much higher temperature-sensitivity (global activation energy) compared to the activation energy that is typical of ignition processes. Pyrolysis times tend to have activation energies that are closer to the bond dissociation energies of C–C bonds whereas ignition processes have activation energies that are comparable with the activation of energies of elementary kinetic processes, such as decomposition of  $\text{H}_2\text{O}_2$ , H-abstraction by  $\text{O}_2$ , and beta-scission reactions of fuel radicals resulting from initial H-abstraction reactions. The same degree of agreement between pyrolysis times of the reduced and detailed models observed for *n*- and *iso*-butanol is found in the case of methanol/ethanol blends, propanol isomers, and *n*-/*s*-butanol.

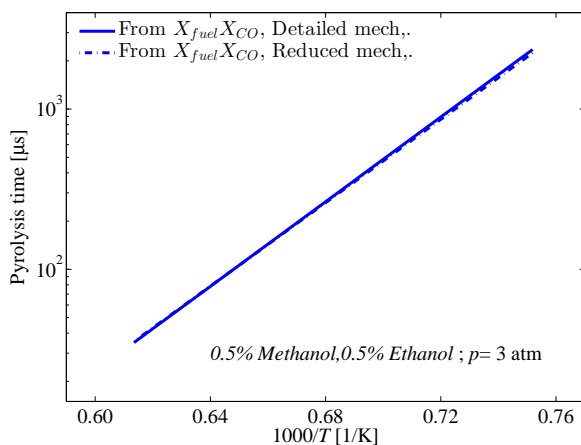


Fig. 3.27.: Comparison of pyrolysis time for 1% fuel (equal proportions of methanol and ethanol) at a pressure of 3.0 atm.

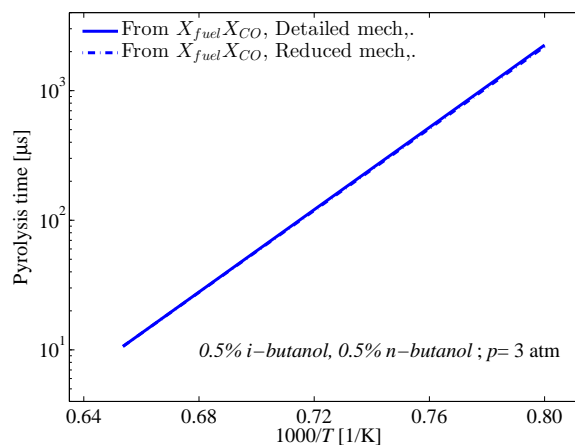


Fig. 3.28.: Comparison of pyrolysis time for 1% fuel (equal proportions of *n*- and *iso*-propanol) at a pressure of 3.0 atm.

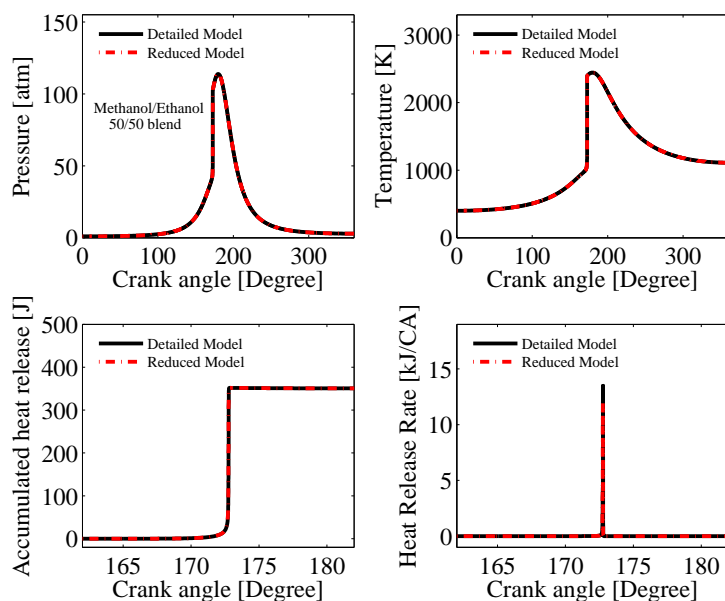


Fig. 3.29.: Simulation of a Homogeneous Charge Compression Ignition cycle at an engine speed of 1000 rpm from an initial state of 400 K and 1.0 atm. The combustible mixture is a stoichiometric fuel/air mixture, with the fuel as equal molar proportions of methanol and ethanol.

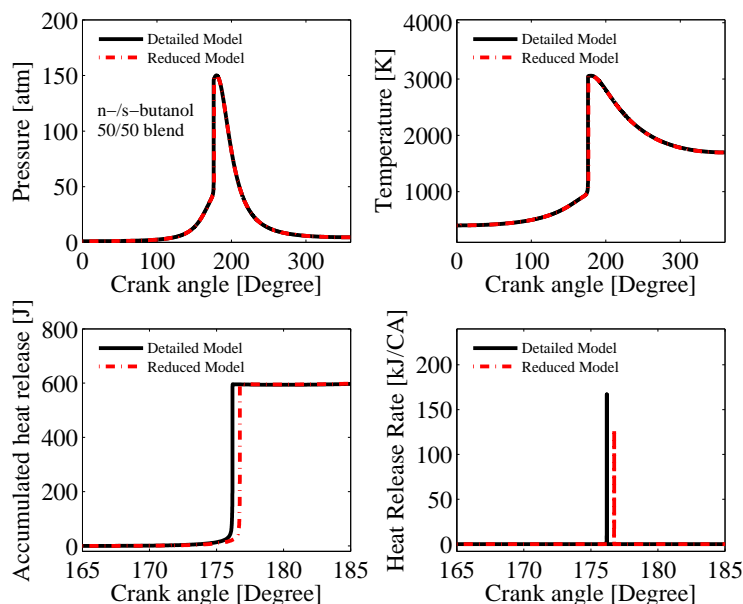


Fig. 3.30.: Simulation of a Homogeneous Charge Compression Ignition cycle at an engine speed of 1000 rpm from an initial state of 400 K and 1.0 atm. The combustible mixture is a stoichiometric fuel/air mixture, with the fuel as equal molar proportions of *n*- and *s*-butanol.

One of the target applications of these reduced models is the simulation of single- or multi-zone engine combustion of alcohols. Unlike the constant initial thermodynamic conditions used in ignition simulation during the reduction phase, SI engine simulations are characterized by time-dependent compressive heating of the combustible mixture. One would like to ascertain that the reduced models can also capture ignition onset and heat release as would be obtained with the detailed model.

For this reason, single-zone adiabatic engine simulations are carried out to compare the engine ignition behavior. The simulations use a compression ratio of 18, initial temperature of 400 K, initial pressure of 1.0 atm, and an engine speed of 1000 rpm with a temporal resolution of 0.03 degree crank angle. These conditions are chosen to ensure autoignition of the fuel/air mixture near the top dead center. For the methanol/ethanol fuel mixture, the simulation using the detailed model took 6 minutes 24 seconds while the reduced model only required 30 seconds using the same settings. This attests to significant reduction in the computational time through use of the reduced model.

Figures 3.29 and 3.30 show the simulations of the methanol/ethanol fuel mixture and the case of propanol isomers, respectively. In the case of methanol/ethanol, good predictions of the pressure, temperature, instantaneous, and cumulative heat release profiles are observed. In the case of the propanol isomers, while the pressure and temperature profiles are well captured, closer analysis shows that a slightly later onset of heat release predicted by using the reduced model instead of the detailed model. This discrepancy, however, is less than one degree crank angle, indicating that the control of combustion is not practically compromised by the reduced model. Similar good behavior is observed for the butanol isomers. These engine simulations show that the reduced models

are capable of capturing the kinetics of the detailed model even in cases of temporally varying pressure and temperature conditions as in combustion engines.

## **3.2 Comparative ignition behavior: MTBE/ETBE**

### **3.2.1 Experimental studies and model validation**

In this part of the work, we investigate reactivity trends between MTBE and ETBE, which are ethers often used as high octane number additives for gasoline fuels. This work seeks to quantify their reactivity similarities and differences based on ignition over a range of temperatures and pressures. The chemical kinetic models available from literature for these fuels are thoroughly studied and evaluated against the test results obtained from the shock tube described before. To the best of our knowledge, this is the first comprehensive work on comparisons and validations of models for MTBE and ETBE. Kinetic analyses including species sensitivity during ignition and reaction pathways are conducted to gain further insight about the observed kinetic behavior. Lastly, a reduced chemical kinetic model for MTBE and ETBE is constructed based on the Alternate Species Elimination method proposed by our group and aimed at establishing the important species needed for ignition predictions. The reduced version is then validated under various conditions against the predictions of the detailed model. This work provides foundation for the next study which focuses on ETBE and gasoline representative blend fuels and the reduced model developed here is later on incorporated into a combined model with the gasoline fuel surrogate to capture the ETBE-gasoline blending effect on combustion behavior.

Mixtures used for the ignition study is presented in Tab. 3.2. The test conditions and mixtures are chosen so that the effects of fuel, pressure, equivalence and dilution ratios on ignition as well as reactivity of the combustible mixtures can be comparatively studied. In the following text, we first present the ignition delay time measurements alongside the validation of different chemical kinetic models. The controlling factors mentioned above are analyzed. Chemical kinetic analyse are then carried out to explain the observed results.

Ignition mixtures	$\phi$	% fuel (MTBE)	% O <sub>2</sub>	% Ar	$D$
1	1	0.0060	0.0450	0.9490	21.088
2	0.5	0.0030	0.0451	0.9519	21.088
3	2	0.0119	0.0447	0.9434	21.088
4	1	0.0273	0.2043	0.7684	3.76
Ignition mixtures	$\phi$	% fuel (ETBE)	% O <sub>2</sub>	% Ar	$D$
1	1	0.0050	0.0450	0.9500	21.088
2	0.5	0.0025	0.0452	0.9523	21.088
3	2	0.0100	0.0448	0.9452	21.088
4	1	0.0228	0.2053	0.7719	3.76

Table 3.2: Composition of ethers mixtures used in this study. In the text, an ignition mixture is identified by the fuel type, its equivalence ratio,  $\phi$ , and its argon/oxygen molar ratio,  $D$ .

The experimental data set obtained from the Syracuse shock tube facility at conditions previously studied by Fieweger et al. [95,96] is first compared with the literature data. Figure 3.31 shows the comparison between our results and the data from [95,96] ignition of stoichiometric MTBE/air mixture study at 13 atm. It shows that our experimental measurements agree well with the previous data. The one difference is that the dilution gas in the test mixtures by Fieweger et al. is nitrogen where our diluent gas is argon. This difference is tolerable since the chemical kinetic effects of the diluent gas are known to be minimal. This is confirmed by the simulation results in Figure 3.31 of paper by the Galway group [83] where two cases differing only in the diluent are shown. As can be seen from

Figure 3.31, there are no significant differences in ignition delay times between these two cases. The figure also presents comparison of measurements with model predictions using three chemical kinetic models for modeling MTBE/ETBE combustion from the Galway [83], the CNRS [87] and the Milano [86] groups respectively. It is observed that the model by the Galway group [83] more accurately captures the temperature sensitivity of the experimental data. However, the simulated ignition delay times are generally longer than the measured values. The other two models show greater deviations in temperature sensitivities but they happen to predict ignition delay times that are in closer agreement in a narrow temperature range from 1100 K to 1250 K while larger differences start to appear at temperatures below 1050 K.

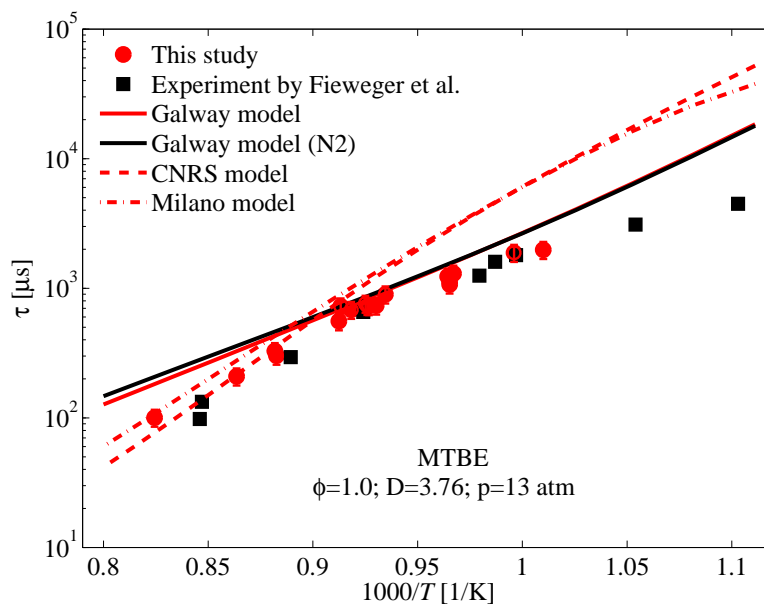


Fig. 3.31.: Validation of MTBE experiment against literature data by Fieweger et al. [95,96] and comparison with model predictions using models by the Galway [83], the CNRS [87] and the Milano [86] groups.

From our discussion before, ETBE has been proposed as one substitute of MTBE for enhancing gasoline octane number due to its superior capability as ignition-resistant fuel with lower ground water pollution tendency. It is thus worth investigating their relative ignition behavior in this work. The comparative study is established by carrying out ignition experiments using mixtures with the same constraints and at similar test conditions. As can be seen from the Figure 3.32, MTBE and ETBE display comparable ignition delay times in the conditions studied at both low and high pressures and two dilution ratios. ETBE does show slightly longer ignition times at high-pressure conditions. These findings are in line with the previous work and further confirm that ETBE can be used as an alternative additive to MTBE for greater ignition resistance of fuel blends.

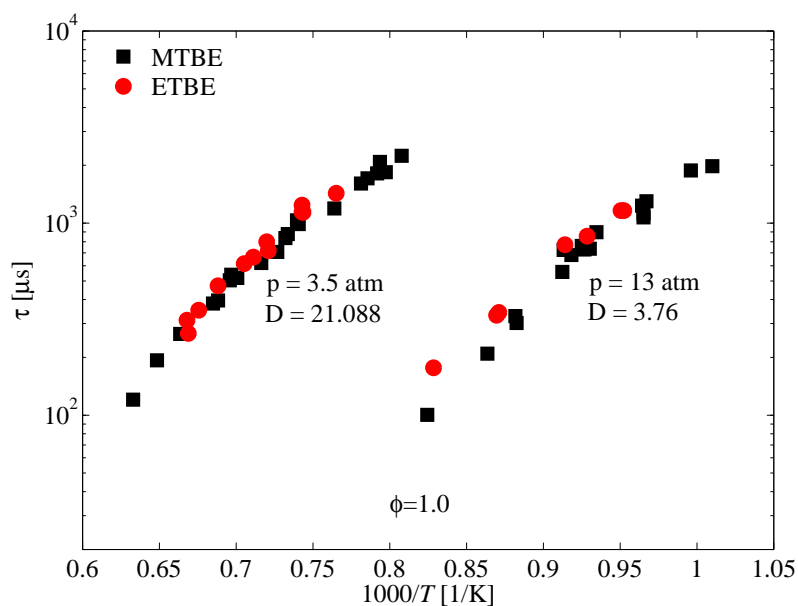


Fig. 3.32.: Relative ignition behaviors of MTBE and ETBE at average pressures of 3.5 atm and 13 atm.



To shed light on the observed reactivity differences between MTBE and ETBE, quantum chemistry calculations are performed at the complete basis set CBS-QB3 level using the Gaussian 09 software package [157]. The Gaussian software package is a computer program developed for electronic structure calculations. The Complete Basis Set (CBS) methods used in this study are a family of composite theoretical methods including approximate self-consistent field methods and corrections. These composite methods are calibrated to accurately predict thermodynamic properties such as enthalpies of formation and atomization energies [157]. In the present study, we used CBS-QB3 methods to calculate the bond dissociation energies (BDEs) of MTBE and ETBE. The results allow us to rationalize the global reactivity as revealed through the ignition delay times. The results of the BDE calculation are shown in Figure 3.33. It confirms the past study that the C-O bond presented in the ether molecules decreases the bond dissociation energy of adjacent C-H bonds from the alkyl group on the counter side of -O- center [90, 158]. This makes these sites the most favored places for reaction initiations. The differences in BDEs lead to differences in the rate constants and affect the selectivity of reaction pathways. This will be further explored in the reaction pathway analysis that follows. This figure also shows that ETBE in general is characterized by slightly stronger bonds compared to the counterpart MTBE, which partly explains the relative ignition behaviors discovered in Figure 3.32, where ignition delay times of ETBE were slightly longer than these of MTBE.

Further reactivity trends could be explored using radical reactions with the various sites. If these are properly accounted for in chemical kinetic models, then the overall effects can be established using reaction pathway analysis. Since there are currently three chemical kinetic models [83, 86, 87] for MTBE and ETBE fuels, the reactivity trends

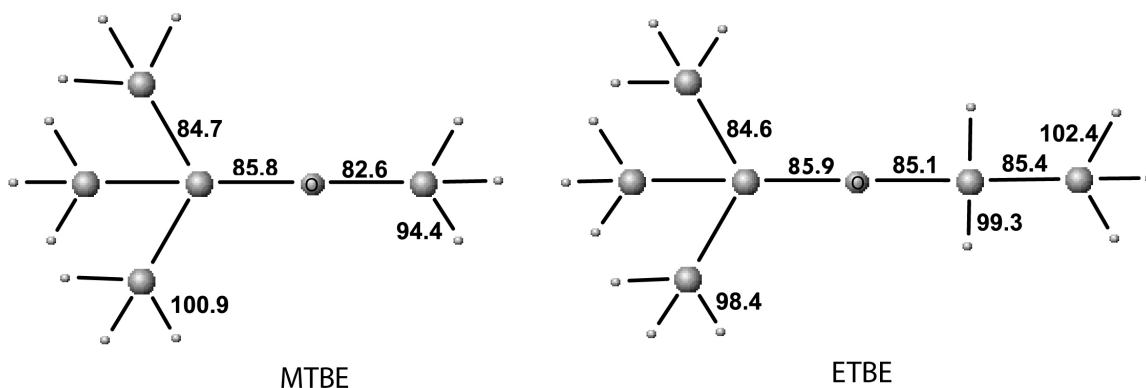


Fig. 3.33.: Bond dissociation energies (BDEs) of MTBE/ETBE calculated by direct atomization (CBS QB3 method) using the Gaussian 09 software package. The values are in units of kcal/mol.

observed in experiments can be verified by comparing the data with model predictions.

Figure 3.34 shows the comparison of model predictions with measured ignition delay times for stoichiometric mixtures of MTBE at 3.5 atm. It is observed that the models by CNRS and Milano groups [86, 87] predict much shorter ignition delay times than measured while the predictions of the model by NUI Galway group [83] are in closer agreement with the experimental observations albeit with some differences at the lower temperature region.

Similar comparisons are conducted for stoichiometric ETBE mixtures as shown in Fig.

3.35. Also added to this is a fourth model for blends of ETBE and other fuels, but without MTBE by the Tokyo group [93]. It can be seen that the predictions by the Galway model has a similar level of agreement with the experimental data while the other three models underpredict the ignition delay times at different levels. The comparison of experimental results with model simulations is also carried out for ETBE ignition at the higher pressure of 13 atm. Fig. 3.36 shows that the trends are consistent with earlier findings at 3.5 atm

while the Galway model predicts longer ignition delay times but the other three models show closer agreements with measurements.

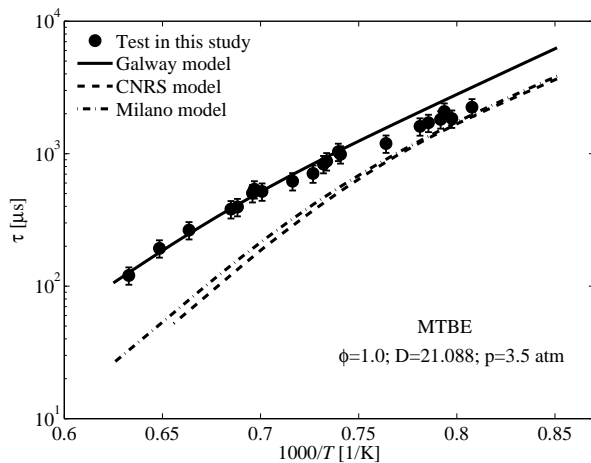


Fig. 3.34.: Comparison of measured MTBE ignition delay times at 3.5 atm with model predictions.

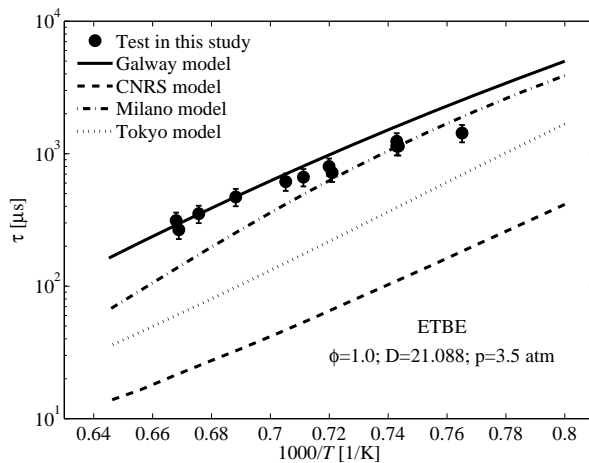


Fig. 3.35.: Comparison of measured ETBE ignition delay times at 3.5 atm with model predictions.

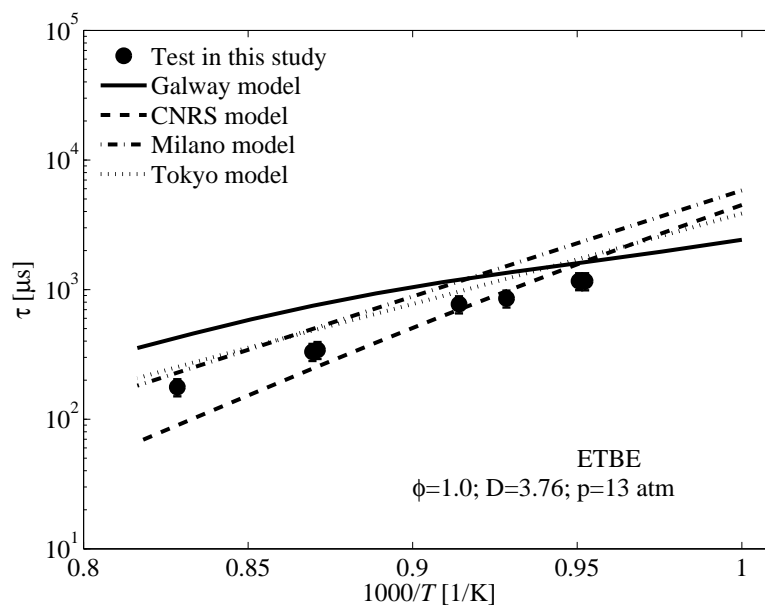


Fig. 3.36.: Comparison of measured ETBE ignition delay times at 13 atm with model predictions.

The equivalence ratio effect on ignition delay times is also examined by measuring ignition delay times under rich, lean, and stoichiometric conditions with a fixed  $D$  of 21.1 at 3.5 atm and the results are compared with predictions of the Galway model [83]. This model is chosen to examine the equivalence ratio effect on account of the close agreement between simulations and measured ignition delay times at stoichiometric conditions, discussed above. In the case of MTBE, Fig. 3.37 shows that under the chosen conditions, there is a weak dependence on equivalence ratio. Ignition delay times increase with increasing equivalence ratio but are less sensitive to equivalence ratio effects at lower temperatures. This relative behavior is captured by the model even though the predictions show deviations in the higher or lower temperature regimes. Figure 3.38 shows the equivalence ratio effects for ETBE. The trends for ETBE are consistent with the previous observations for MTBE with less changes in the ignition delay times shown in the ETBE study among the three different equivalences in the chosen conditions.

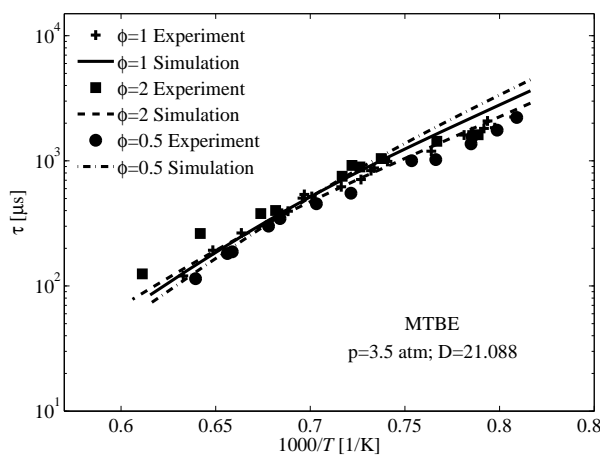


Fig. 3.37.: Comparison of measured MTBE ignition delay times at three equivalence ratios with predictions of Galway model [83].

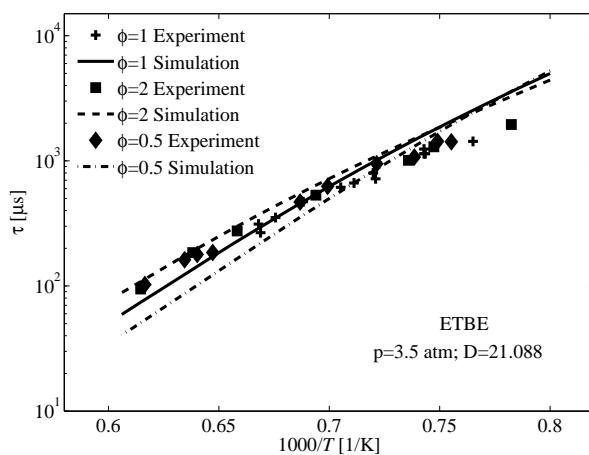


Fig. 3.38.: Comparison of measured ETBE ignition delay times at three equivalence ratios with predictions of Galway model [83].

The oxygen concentration or dilution ratio ( $D$ , argon/oxygen molar ratio) effect on ignition delay times is also investigated by measuring ignition delay times under high and low dilution ratio conditions at 3.5 atm. The results are also compared with predictions of the available models in literature [83,86,87,93]. The ratios correspond to oxygen concentration changes from a lower value of 4.5 percent to as high as over 20 percent in these two test conditions. For stoichiometric MTBE mixtures, Fig. 3.39 shows that the ignition delay times decrease as the dilution ratio decreases reflecting the positive effect of higher oxygen concentration on reactivity. The change in ignition delay times is also accompanied by a discernible difference in the global temperature sensitivities. It can also be found that the Galway model best aligns with the experiment data in both conditions. The other two models, however, predict much shorter ignition delay times, which are consistent with our previous findings. Similar comparison is performed for lean MTBE mixtures as illustrated in Fig. 3.40. In this case, similar trends are observed compared with the aforementioned stoichiometric mixtures. Nonetheless, the model deviations for the case of higher dilution ratio tend to be larger than the low dilution ratio one. These differences have implications on model validation. As discussed in the introduction part, most chemical kinetic model validations experiments are done at a narrow range of dilution or oxygen ratios. This is often quite remote from the conditions in the real combustion with around 20 percent of oxygen concentration. The analysis so far implies that this might be a non-trivial problem for the research community engaged in developing modern combustion models. In Fig. 3.41, results of dilution effect on ETBE ignition are shown, reinforcing the concern that a model which was validated at only low oxygen concentration test conditions

can lead to significant errors or even failures in predicting combustion at technically relevant conditions.

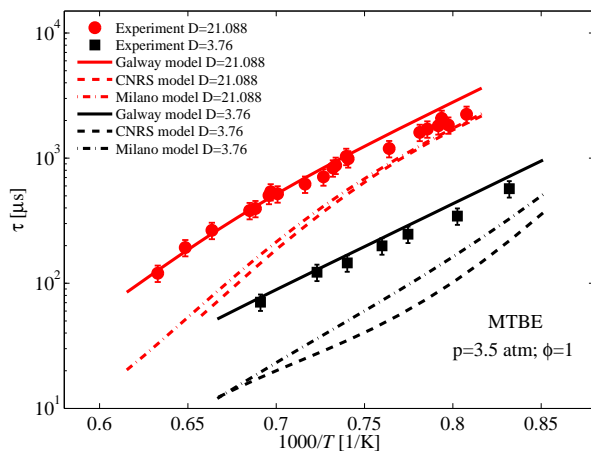


Fig. 3.39.: Comparison of measured ignition delay times for stoichiometric MTBE mixtures at two different dilution ratios with model predictions.

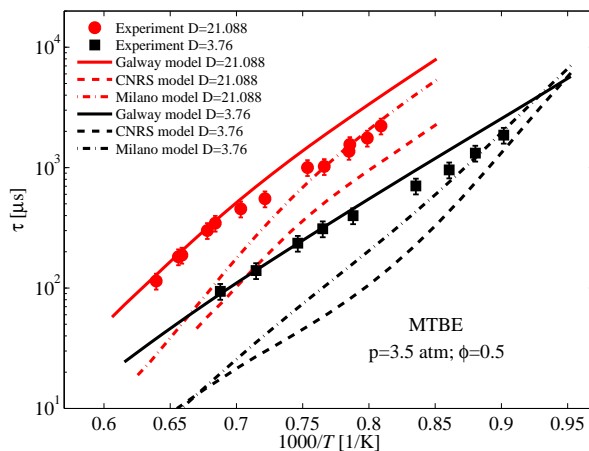


Fig. 3.40.: Comparison of measured ignition delay times for lean MTBE mixtures at two different dilution ratios with model predictions.

Species sensitivity and reaction pathway analyse are carried out to better understand the underlying chemical kinetics of the observed ignition behaviors.

The species sensitivity analysis is executed via the Alternate Species Elimination (ASE) approach [115, 156] as introduced in Chapter 2. It essentially determines the changes that arise from the suppression of the chemical reactions involving a given species and evaluating the effect on a combustion property such as the ignition delay time. In predicting the ignition delay times, the increase of the delay time upon removal of a given sub chemistry indicates that the species promotes ignition while a decrease in the ignition delay time implies the opposite effect when present.

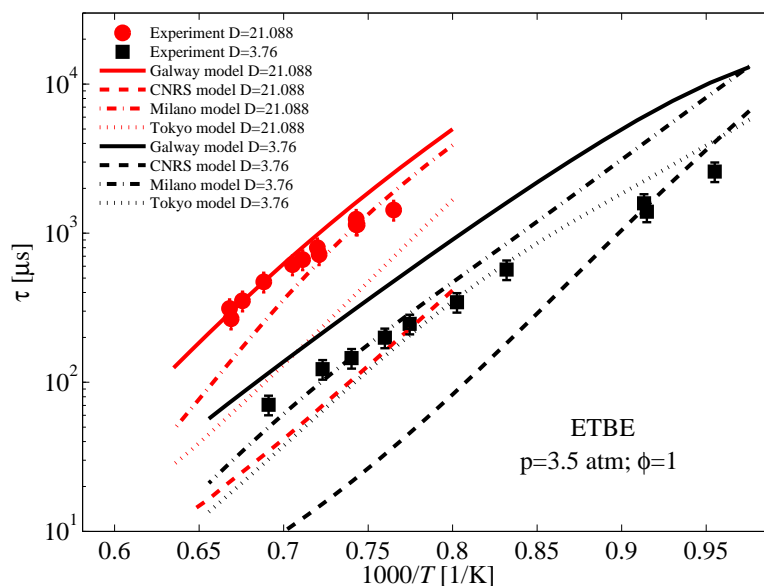


Fig. 3.41.: Comparison of measured ignition delay times for stoichiometric ETBE mixtures at two different dilution ratios with model predictions.

Figure 3.42 shows the sensitivities of the 20 most important species in the model by Galway group [83], during MTBE ignition where sensitivities of corresponding species are also taken from the other two mechanisms [86,87]. We see that  $\text{CH}_2\text{O}$ ,  $\text{CH}_3\text{O}$ ,  $\text{H}_2\text{O}_2$ , and  $\text{OH}$  are very important for MTBE ignition. It is also observed that suppression of the *iso*-butene ( $\text{iC}_4\text{H}_8$ ) chemistry leads to a reduction in predicted delay times in the models except in the case of Galway model, indicating its overall reactivity-retarding role in the former two mechanisms [83,86]. The other radicals,  $\text{HCO}$ ,  $\text{CH}_3\text{OC}_4\text{H}_8\text{i}$ , and  $\text{CH}_3$ , generally offer ignition forward propagating pathways, and their removal reduces ignition propensity.

In the case of ETBE as shown in Fig. 3.43, the majority of the important species are active radicals whose removal would slow down the ignition process. On the other hand, the stable molecules,  $\text{H}_2$  and  $\text{C}_2\text{H}_6$ , offer ignition-retarding pathways, since their exclusion

leads to faster ignition in all four models. The distinctive consequences for the removal of  $iC_4H_8$  sub chemistry still exist. In contrast to the models from Galway and CNRS groups, the other two models show that eliminating the  $iC_4H_8$  sub chemistry leads to shorter ignition delay times, implying that it offers an ignition inhibiting channel when present.

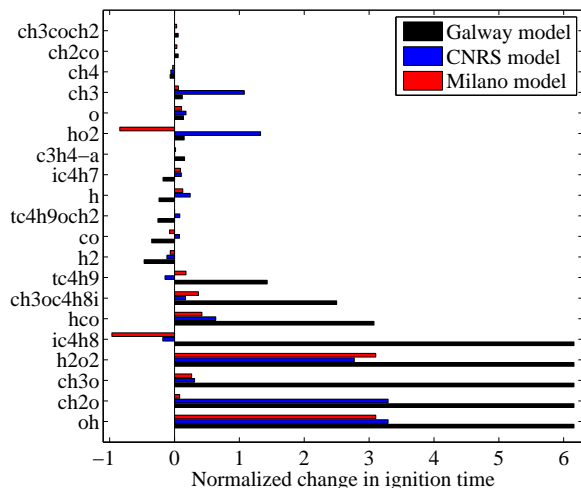


Fig. 3.42.: Species sensitivity analysis of MTBE ignition. Shown are the 20 most important species at the condition  $\phi = 1.0$ ,  $D = 21.0$ ,  $p = 15$  atm, and  $T = 1050$  K.

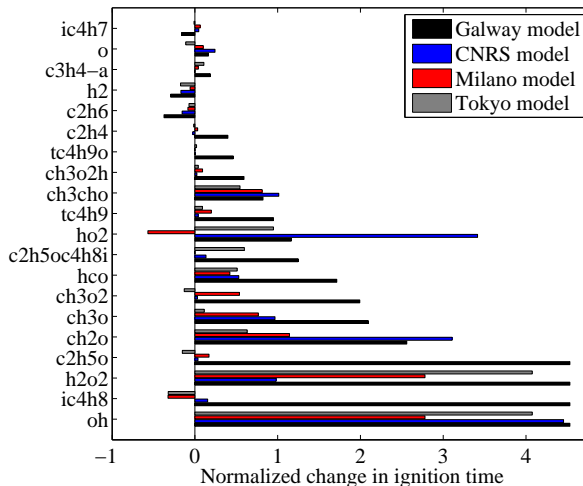


Fig. 3.43.: Species sensitivity analysis of ETBE ignition. Shown are the 20 most important species at the condition  $\phi = 1.0$ ,  $D = 21.0$ ,  $p = 15$  atm, and  $T = 1050$  K.

Reaction pathway analysis of representative oxidation processes are carried out using the model from Galway group [83] on account of its overall better agreement with measurements. All analyse are carried out at the instance where 20% of the initial fuel molar fraction has been consumed.

Figures 3.45 shows the pathways during ignition of a stoichiometric mixture of MTBE at two pressures. It is observed that fuel is primarily consumed through the unimolecular initiation reaction herein a four-membered carbon rings elimination reaction producing *iso*-butene and methanol, as well as H atom abstraction reaction. The molecular



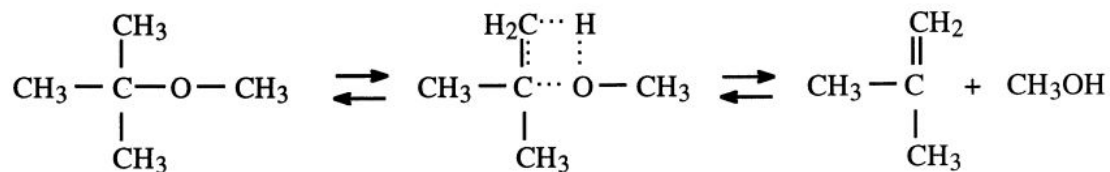


Fig. 3.44.: The four-center elimination reaction for MTBE [87].

four-center elimination reaction for MTBE is shown in Figure 3.44. The H atom abstraction takes place from methyl C-H sites. The decomposition channel accounts for more than 40% at low pressure condition and down to 4.3% at the high pressure condition, while the H abstraction one takes a considerable proportion up to 56.6% at high pressure condition. The other tertiary H-abstraction at the C-H sites in the branched *iso*-butyl group is less than those observed from the methyl C-H sites in both conditions, which is in accordance with the bond dissociation analysis before in Fig. 3.33 where the BDE at methyl C-H sites is 94.4 kcal/mol and thus weaker than the BDE in the other position (100.9 Kcal/mol). The H atom abstraction reaction from methyl C-H sites, followed by  $\beta$ -scission, produces aldehydes and *iso*-butyl radicals while tertiary H-abstraction at the C-H sites in the highly branched tertiary butyl group forms *iso*-butene and  $\text{CH}_3\text{O}$  radicals through  $\beta$ -scission reaction. It can be seen that majority of the reaction channels in the MTBE auto-ignition lead to the formation of stable intermediates of *iso*-butene whose chemistry thus greatly influences the overall reactivity. Because of the resulting *iso*-butene and its strong retarding effect, the high auto-ignition resistance of tert-butyl ethers can therefore be explained [83, 86, 90].

Similar trends are found in the case of ETBE ignition process (see Fig. 3.46). The unimolecular four-membered carbon ring elimination reaction leading to *iso*-butene and

ethanol is important. This is followed by H-abstraction reactions from three different C-H sites dominating at both pressures (over 70 %). The relative proportions of H atom abstraction reactions at the three different C-H sites agree well with the previous BDE calculation results previously shown in Fig. 3.33. The products from H-abstraction reactions at the  $\alpha$ -C sites then undergo  $\beta$ -scission and forms *iso*-butene eventually, which proves again that the intermediate *iso*-butene chemistry plays a central role in MTBE/ETBE combustion.

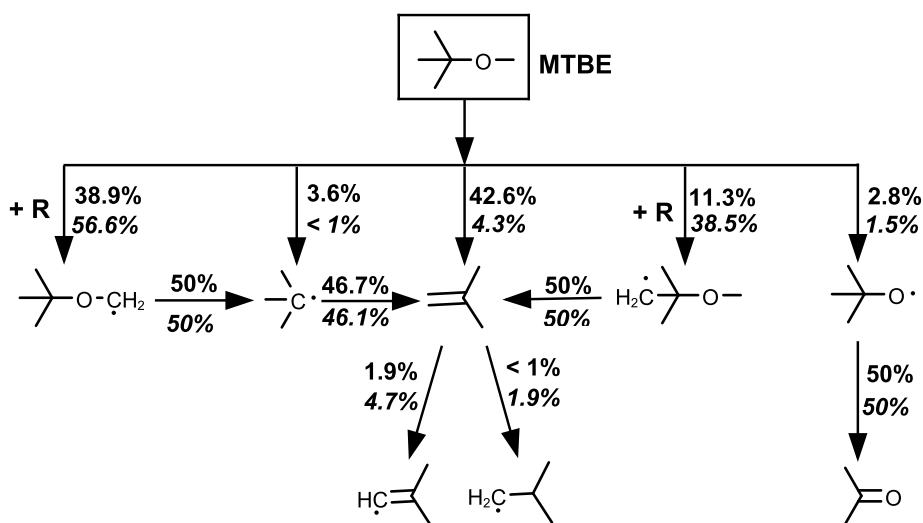


Fig. 3.45.: Reaction pathways for MTBE ignition ( $\phi = 1$ ,  $D = 3.76$ ) using the model by Galway group [83] at pressures of 3.5 atm (top) and 13 atm (bottom).

In the present work, the model from Galway also turned out to be the closest in predicting the ignition delay times for MTBE/ETBE compared to other literature models. To unravel the kinetic differences leading to the different performances among these models, reaction pathways are also examined at the same conditions from one of the models with the least satisfactory performance in capturing the experimental data. Figures 3.47 and 3.48 show the reaction pathways of the model from CNRS group at the instant

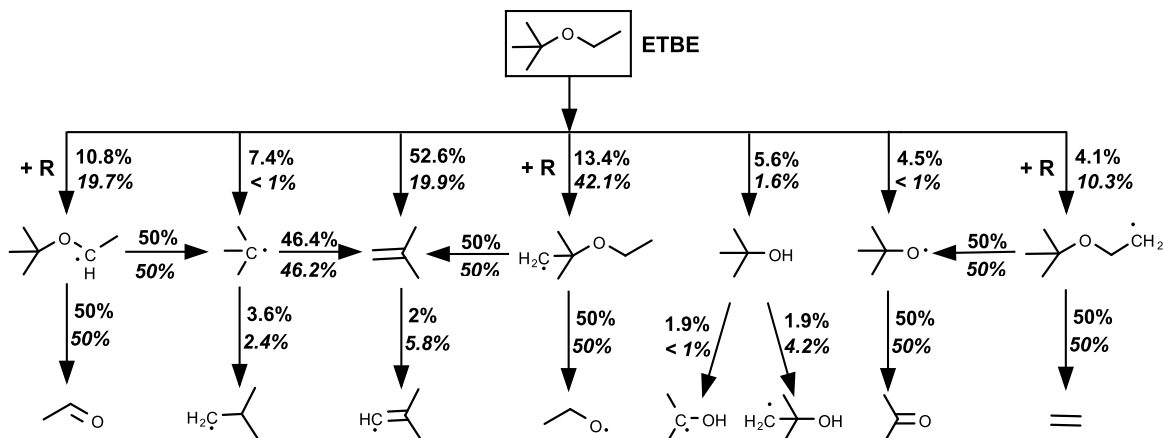


Fig. 3.46.: Reaction pathways for ETBE ignition ( $\phi = 1$ ,  $D = 3.76$ ) using the model by Galway group [83] at pressures of 3.5 atm (top) and 13 atm (bottom).

when 20 % (molar fraction) of fuel is consumed for MTBE and ETBE respectively. With respect to MTBE, it is observed that the four-membered carbon ring elimination reaction into *iso*-butene and methanol plays a dominant role in both conditions while the H-atom abstraction reactions make much less contributions compared with the ones in Galway model. Their relative proportions at the two C-H sites are opposite in trend to the BDE calculations in Fig. 3.33. This suggests that the reaction rates for related reactions in this model need to be adjusted in order to improve the model predictions against experimental data. In terms of ETBE, the largest difference lies in the slow formation of *iso*-butene from initial fuel breakdown which make the H-atom abstraction reactions prevail in both conditions.

### 3.2.2 Reduced chemical kinetic model

The aim here is to develop a reduced model for MTBE and ETBE fuels using the proven ASE model reduction approach which we introduced before. We anticipate the need

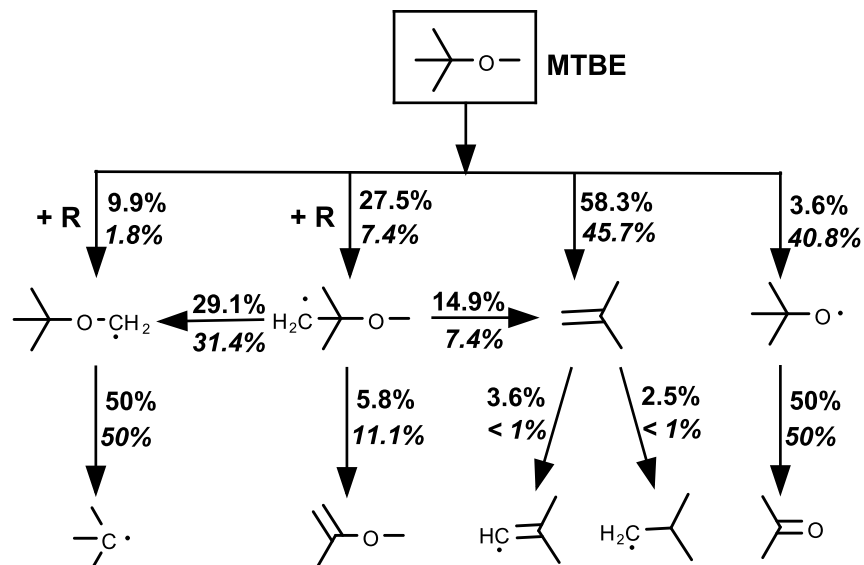


Fig. 3.47.: Reaction pathways for MTBE ignition ( $\phi = 1$ ,  $D = 3.76$ ) using the model by CNRS group [87] at pressures of 3.5 atm (top) and 13 atm (bottom). Contrary to the Galway model, features more reactive channels.

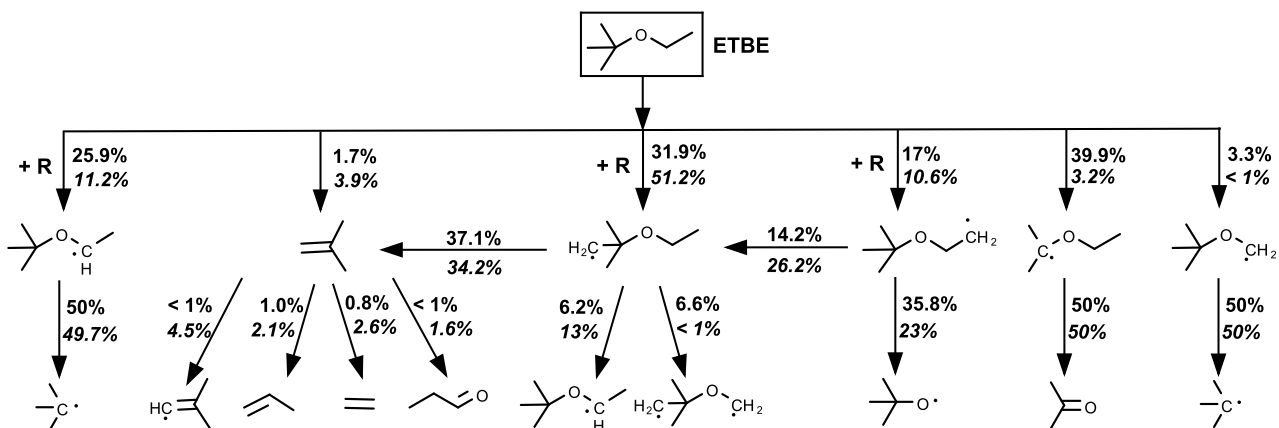


Fig. 3.48.: Reaction pathways for ETBE ignition ( $\phi = 1$ ,  $D = 3.76$ ) using the model by CNRS group [87] at pressures of 3.5 atm (top) and 13 atm (bottom). Contrary to the Galway model, features more reactive channels.

for reduced chemical kinetic models to facilitate the use of ethers fuels, herein

MTBE/ETBE and further development of a combined model with gasoline representatives

in the usage of these additives in gasoline engine combustion. The reduced model is

obtained based on ignition delay time simulations from the detailed model by the Galway group [83] which closely matches the test results in our previous study and consists of 214 species and 1216 reactions. Three equivalence ratios are used ( $\phi = 0.5, 1.0,$  and  $2.0$ ) at a reactor pressure of 15 atm and temperature set at 1050 K. It is expected that the resulting reduced model will capture the kinetics at other conditions.

The final version of the reduced model contains 86 species and 696 reactions. In the following part of this work, its performance in predicting the ignition delay times under various conditions is verified. The purpose of the validation against ignition delay times is to ensure that the reduced models can satisfactorily predict ignition delay times at conditions different from those used in the reduction process, especially in terms of temperatures and pressures.

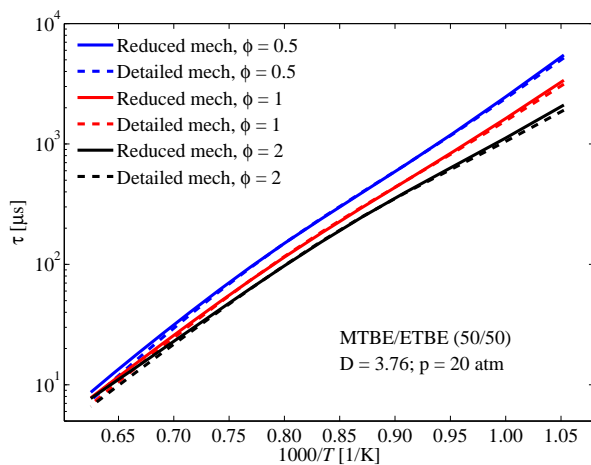


Fig. 3.49.: MTBE and ETBE: comparison of detailed and reduced model with respect to ignition delay time prediction at three equivalence ratios and pressure of 20 atm.

The Ar/O<sub>2</sub>,  $D$ , is 3.76.

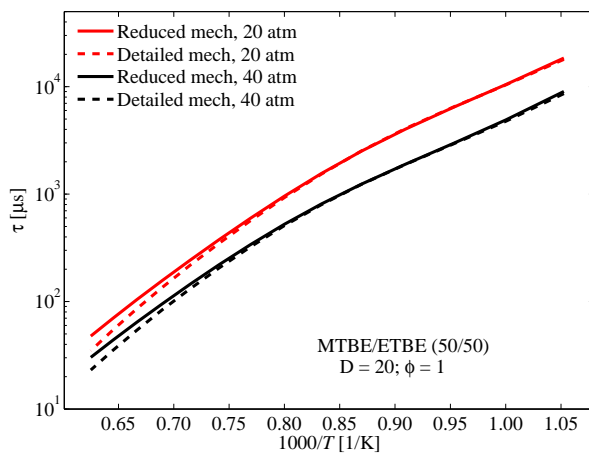


Fig. 3.50.: MTBE and ETBE: comparison of detailed and reduced model with respect to ignition delay time prediction at two different pressures and higher dilution level than used in model reduction.

Figures 3.49 shows the performance of the models at equivalence ratios of 0.5, 1.0., and 2; a reactor pressure of 20 atm; and over a range of temperatures, starting from 950 K. The argon to oxygen ratio,  $D$ , in this case is 3.76, reflecting the composition of air as a technical oxidizer. It is observed that in all three equivalence ratios, the reduced model accurately captures the ignition delay times predicted by the detailed models.

Further comparisons are carried out at conditions with higher argon dilution ( $D = 20$ ) as well as pressures of 20 atm and 40 atm. Similar level of accuracy (less than 3 % for most of the cases) is observed. Examples of this agreement are shown in Figure 3.50. This good performance shows that the ignition performance of the detailed kinetic model is adequately captured by the proposed reduced versions over a representative range of pressures and temperatures.

### 3.3 Ignition behavior of gasoline-biofuel blends

#### 3.3.1 *Iso*-octane - *iso*-propanol blend

##### Ignition Experiments

Due to its superior ignition-resistance capability as discussed before, *iso*-propanol can be used to improve the octane rating of gasoline. In this part of the work, comparative ignition behavior of *iso*-propanol and *iso*-octane, a representative of gasoline fuels, is determined. The effect of adding *iso*-propanol to *iso*-octane is then investigated to establish the effect of using *iso*-propanol as an octane improver in blends with conventional gasoline. A combined chemical kinetic model is assembled to simulate the *iso*-octane and

*iso*-propanol blend combustion. The model is assembled by combining the sub-mechanism of the previously derived reduced model for propanol into a reduced version of the *iso*-octane model by Mehl et al [107]. The performance of the new model is assessed and validated against the experimental data. It is also compared with other models available in the literature. Subsequently, chemical kinetic analyses are carried out to explain the experimental findings. The mixtures used for the fuel blends are presented in Tab. 3.3.

iso-propanol mixtures	$\phi$	% iso-octane	% iso-propanol	% O <sub>2</sub>	% Ar	$D$
50/50 blend	1	0.0092	0.0198	0.2040	0.7670	3.76
75/25 blend	1	0.0130	0.0094	0.2054	0.7722	3.76
75/25 blend	2	0.0255	0.0184	0.2009	0.7552	3.76
75/25 blend	0.5	0.0066	0.0047	0.2077	0.7810	3.76
ETBE mixtures	$\phi$	% iso-octane	% ETBE	% O <sub>2</sub>	% Ar	$D$
50/50 blend	1	0.0089	0.0106	0.2060	0.7745	3.76
75/25 blend	1	0.0128	0.0051	0.2063	0.7758	3.76

Table 3.3: Composition of mixtures used for blend fuels study. In the text, an ignition mixture is characterized by the fuel type, its equivalence ratio,  $\phi$ , and its argon/oxygen molar ratio,  $D$ .

Figure 3.51 shows ignition delay times of stoichiometric mixtures at a pressure of 12 atm. Ignition delay times of *iso*-octane at various conditions are those previously measured by our group [138,139]. Those data are used in this study to compare with the blend fuel ignition delay times. New experimental data set obtained in our shock tube facility at conditions studied before were used to verify the method [138,139]. Figure 3.51 shows the comparison between the new test data and previous ignition measurements of stoichiometric *iso*-octane/O<sub>2</sub>/Ar mixture at 12 atm. It shows that the experimental measurements agree well with the previous data. At this condition, it is observed that there is no significant difference in the reactivities of *iso*-propanol and *iso*-octane even though *iso*-octane exhibits slightly stronger ignition-resistance in the lower temperature

region below 1100 K. It should be noted that although *iso*-octane is used to represent gasoline for simplicity, its octane number is higher than that of gasoline. Also reactivity difference are more important at lower temperatures. This similarity between these high-temperature ignition of *iso*-propanol and *iso*-octane suggests that the blend effect might not show significant differences under these conditions.

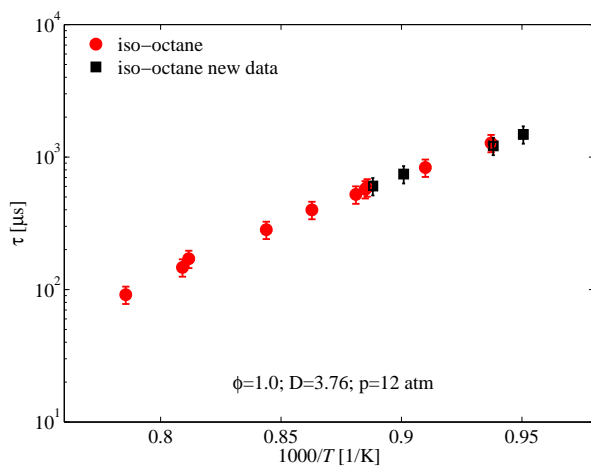


Fig. 3.51.: Validation of *iso*-octane experiment against data previously measured by our group [138, 139].

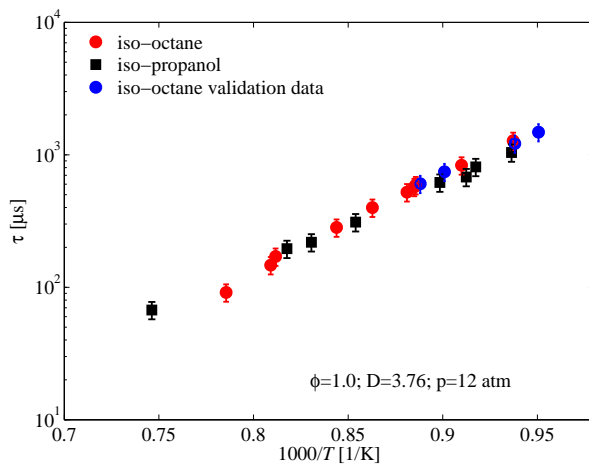


Fig. 3.52.: Relative ignition behavior of stoichiometric fuel/ $O_2$ /Ar mixtures of *iso*-propanol and *iso*-octane at a pressure of 12 atm.

This is verified by measuring ignition delay time of blends of different proportions by liquid volume of both fuels as described in Tab. 3.3. The resulting ignition delay times of the blends are then compared to ignition measurements of the pure fuels at the same conditions to establish relative reactivity trends. Figure 3.53 is a comparison between the ignition delay times of the *iso*-octane/*iso*-propanol blend and of the two pure fuels at stoichiometric conditions and a pressure of 12.0 atm, under a constrained Ar/ $O_2$  ratio  $D$  of 3.76. The main observation is that whereas the ignition delay times of the pure fuels are



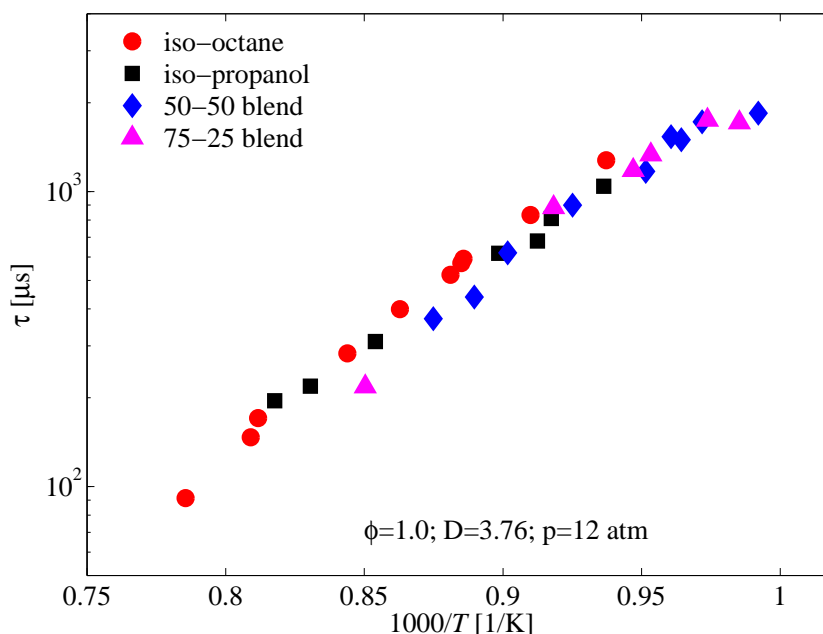


Fig. 3.53.: Relative ignition behavior of *iso*-octane, *iso*-propanol, 50/50 and 75/25 blends of both (by liquid volume) at a pressure of 12.0 atm. The experimental data has same level of uncertainty as shown before.

largely similar, the addition of *iso*-propanol to *iso*-octane does seem to alter the ignition behavior. The change seem to show that the blend becomes slightly easier to ignite, contrary to our anticipations. The reason for this seems to be a chain reaction promotion effect from the *iso*-propanol on the *iso*-octane. These results are valid for stoichiometric fuel/O<sub>2</sub>/Ar mixtures.

The equivalence ratio effect on ignition delay times of the blends is also explored by measuring ignition delay times under rich, lean, and stoichiometric conditions with a fixed  $D$  of 3.76 at 12 atm. The fuel blend chosen for this investigation is that with 75% *iso*-octane + 25% *iso*-propanol by their volumes. Fig. 3.54 shows that under the chosen conditions, ignition delay times generally decrease with increased equivalence ratio but

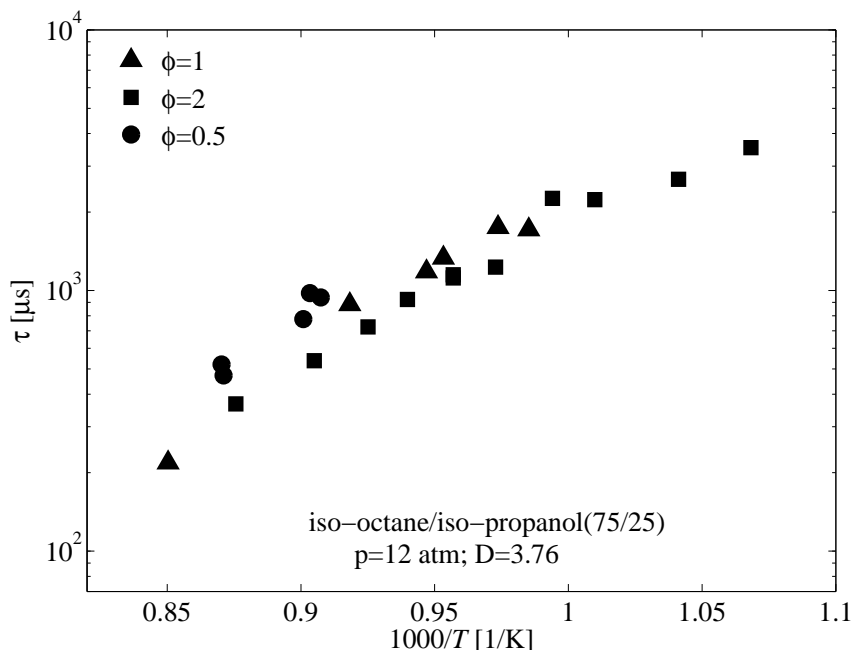


Fig. 3.54.: Relative ignition behavior of *iso*-octane/*iso*-propanol (75/25 by liquid volume) blends at three equivalence ratios.

have a weaker dependence on equivalence ratios at higher temperatures. This behavior is in accordance with observed trends for other hydrocarbons. Although substantial blending effects are seen in this temperature window, further investigations at lower temperatures are recommended.

### Chemical kinetic modeling

It is necessary to construct a chemical kinetic model to carry out detailed analysis of the fuel blends ignition behavior to understand the interaction chemistry. The combined model is developed based on the models previously published for each of the blend components. For *iso*-propanol, the reduced model from the previous section derived from

the C1-C5 alcohols model by Sarathy et al. [159] is used. The model contains 68 species and 419 reactions after the reduction from the detailed model comprising 600 species and 4100 elementary reactions. The performance of this reduced model is comprehensively assessed and validated for key combustion properties and HCCI engine analysis in the previous discussions against the predictions from the detailed model. In terms of *iso*-octane, a model from Lawrence Livermore National Laboratory by Mehl et al. [107] is adopted. The *iso*-octane model by Mehl et al. [107] contains 7522 reactions among 874 species. The large size of the detailed model for *iso*-octane makes it necessary to deduce a reduced version of the original model before the combined model is developed. Here the species sensitivity approach shown in [115, 156] as the Alternate Species Elimination (ASE) is used to identify species essential to the ignition prediction. To develop the skeletal model, the initial temperature is set at 950 K to consider both the low and high temperature ignition chemistry. Three mixtures with different equivalence ratios including lean ( $\phi = 0.5$ ), stoichiometric, and rich ( $\phi = 2.0$ ) ignition and a reactor pressure of 30 atm are used. The NC threshold for species elimination is  $1.0 \times 10^{-4}$ .

The resulting skeletal model for *iso*-octane is made of 269 species and 1248 reactions. Its performance in predicting the ignition delay times under various conditions is verified. Figures 3.55 shows the performance of the models at equivalence ratios of 0.5, 1.0., and 2; a reactor pressure of 15 atm; and over a range of temperatures, starting from 950 K. The dilution ratio/factor,  $D$ , in this case is 3.76, reflecting the composition of air as a technical oxidizer. It is observed that under all three equivalence ratios, the reduced model accurately captures the ignition delay times predicted by the detailed models.

Further comparisons are carried out at conditions with higher argon dilution ( $D = 20$ ) as well as pressures of 15 atm and 45 atm. Similar level of accuracy (less than 3 % for almost all of the cases) is observed. Example of this agreement is shown in Figure 3.56. This good performance shows that the ignition performance of the detailed kinetic model is adequately captured by the proposed reduced version over a representative range of pressures and temperatures.

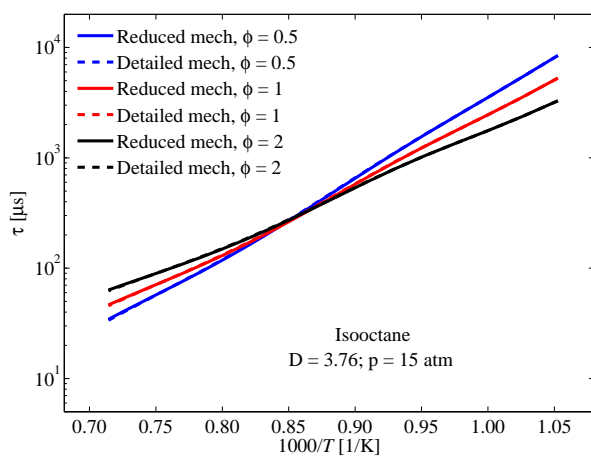


Fig. 3.55.: Isooctane: comparison of detailed and reduced model with respect to ignition delay time prediction at three equivalence ratios and pressure of 15 atm.

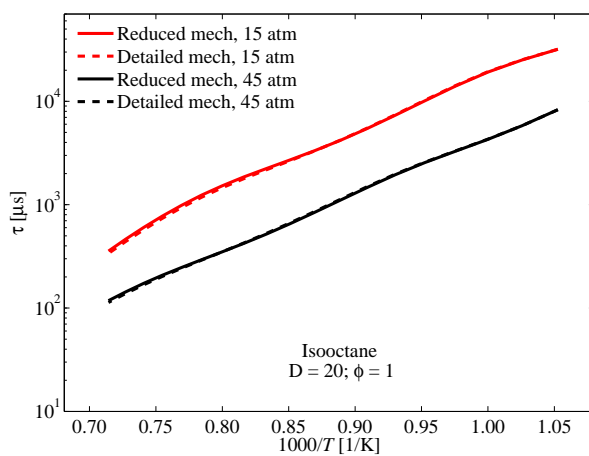


Fig. 3.56.: Isooctane: comparison of detailed and reduced model with respect to ignition delay time prediction at two different pressures and higher dilution level.

To develop the combined model for fuel blends, the reduced model for *iso*-propanol is then incorporated into the skeletal model for *iso*-octane. The species and reactions specific to the *iso*-propanol model are identified and integrated into in the *iso*-octane model while excluding the reactions that are common to both models. The new blend model includes 287 species and 1406 reactions. For the blend model, the inter-reactions or cross-reactions between individual fuel components are considered to be limited to the reactions among

small radicals such as H, OH and O [160, 161]. Those small radicals bridge the reactions between the fuel components. Consequently, cross-reactions are not included in the combined model as their effects are of less importance for smaller alcohols like ethanol and propanol mixed with *iso*-octane compared to more complex gasoline surrogate fuels such as the *iso*-octane [162–164].

The combined model should be able to make good predictions of properties of both the mixture and pure fuels. In this part of the work, the new blend model is validated against ignition delay times measurements and the predictions from detailed models for both pure *iso*-octane and *iso*-propanol, as shown in Figs. 3.57 and 3.58. Two pressures of 5 atm and 12 atm are included in this discussion. In the next section, a combined model for ETBE and *iso*-octane will be described. But for comparison, it is also added to Fig. 3.57. Both combined models are still in good agreement with the *iso*-octane detailed model by Mehl et al. [107]. The model predictions from all models are well in line with the experimental data, albeit with slightly longer ignition delay times predicted at lower pressure condition. With respect to propanol, reasonable agreement is achieved by using the combined model although it predicts shorter ignition delay times than the detailed model by Sarathy et al. [159] in both cases. The differences can be partly explained by the fact that the combined model for *iso*-octane/*iso*-propanol is developed based on the highly reduced *iso*-propanol model from the detailed model by Sarathy et al. [159] as discussed before. Also the chemistry of the small chemical species is taken from the *iso*-octane model.

In Figures 3.59 and 3.60, the blend model is compared with the ignition delay times for the stoichiometric fuel blends of *iso*-octane/*iso*-propanol at two blending ratios, a pressure of 12.0 atm, and  $D$  of 3.76. The blend model is also compared with predictions of a model

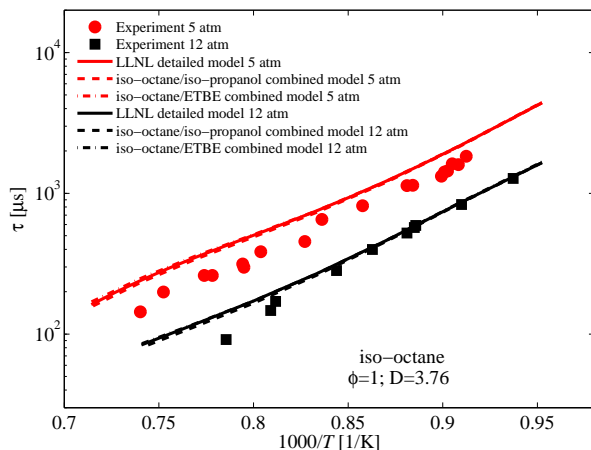


Fig. 3.57.: Comparison of *iso*-octane test data with the model predictions from the blend models in this work and detailed model by Mehl et al. [107].

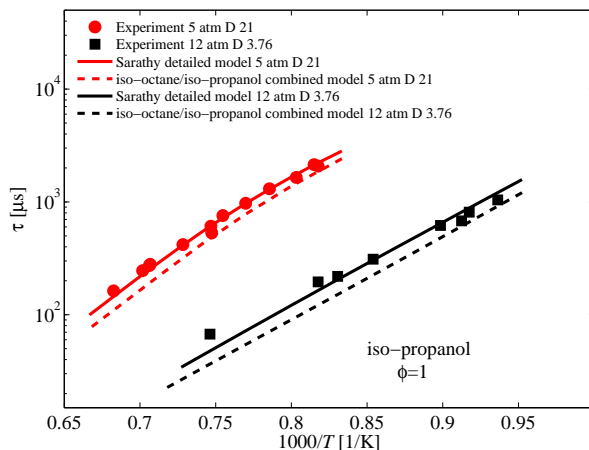


Fig. 3.58.: Comparison of *iso*-propanol test data with the model predictions from the blend model in this work and detailed model by Sarathy et al. [159].

from the Milano group [24], which includes mechanisms for blends of Primary Reference fuels, with alcohols (ethanol, propanol and butanol isomers) and ethers (DME, MTBE, ETBE, DIPE, TAME). It is observed that the predictions of combined model developed in this study are in overall better agreement with the experimental data than those of the Milano group model [24]. Similar performance of the blend model is observed at rich conditions of  $\phi = 2.0$  in Fig. 3.61.

To gain further insight into the fuels blend chemistry, reaction pathway analysis are carried out using the CHEMKIN software package [165] for an ignition process of stoichiometric fuel/ $O_2$ /Ar mixtures with  $D$  of 3.76 at a temperature of 1150 K and a pressure of 12.0 atm, where the fuels are *iso*-octane, *iso*-propanol, and a blend of equal liquid volume proportions. The results are shown in Fig. 3.62 - Fig. 3.64.

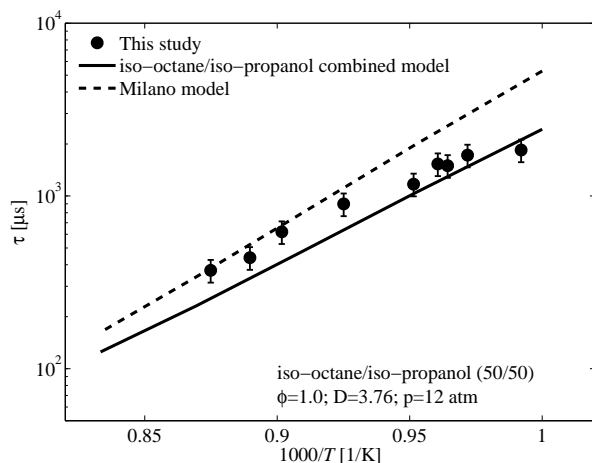


Fig. 3.59.: Comparison of test for stoichiometric *iso*-octane/*iso*-propanol (50/50) mixture with the model predictions from the blend model in this work and model by Milano group [24].

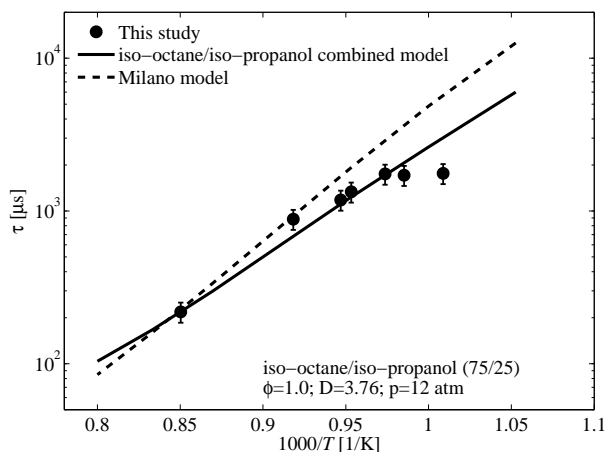


Fig. 3.60.: Comparison of test for stoichiometric *iso*-octane/*iso*-propanol (75/25) mixture with the model predictions from the blend model in this work and model by Milano group [24].

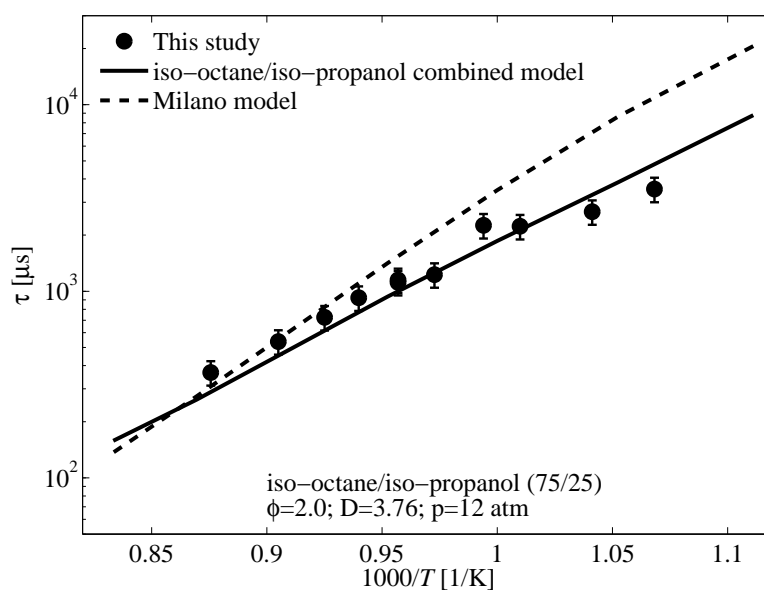


Fig. 3.61.: Comparison of test for rich *iso*-octane/*iso*-propanol (75/25) mixture with the model predictions from the blend model in this work and model by Milano group [24].

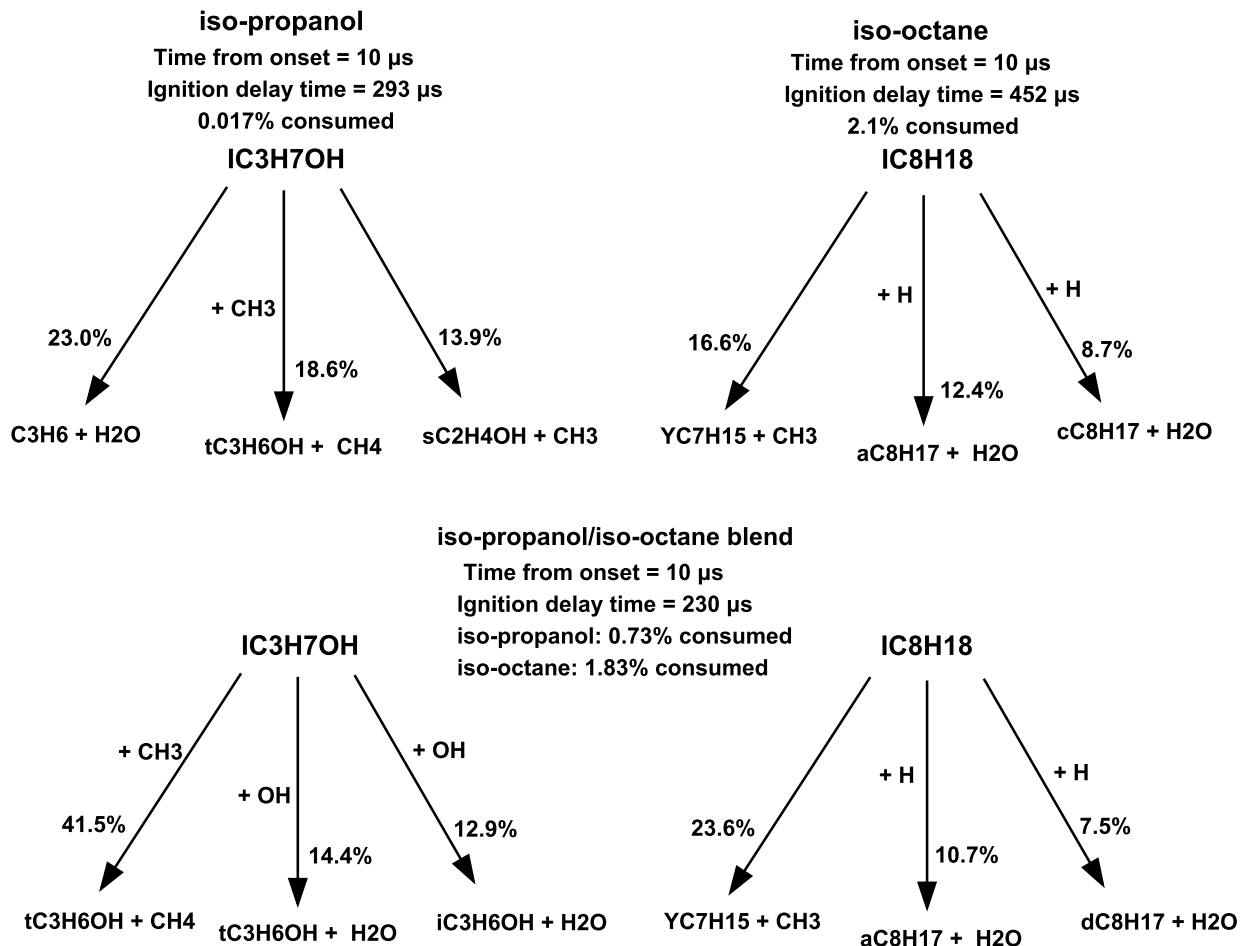


Fig. 3.62.: Reaction pathways for *iso*-octane, *iso*-propanol, and a blend of equal liquid volume proportions during ignition process ( $\phi = 1$ ,  $D = 3.76$ ) using the combined model at a pressure of 12 atm. Shown are the results close to the onset of the reactor.

The reaction pathway analysis for *iso*-propanol is performed at the times 10, 156, and 249  $\mu$ s close to the ignition delay time of 293  $\mu$ s. It was observed that at 10  $\mu$ s, *iso*-propanol is consumed through the channels of H<sub>2</sub>O elimination reactions forming C<sub>3</sub>H<sub>6</sub>, H-abstraction reactions and C-C bond scission all with significant contributions while at later times, H-abstraction by OH and HO<sub>2</sub> radicals become more significant. In the case of *iso*-octane, the ignition delay time is 452  $\mu$ s, and the pathway analysis is performed at the



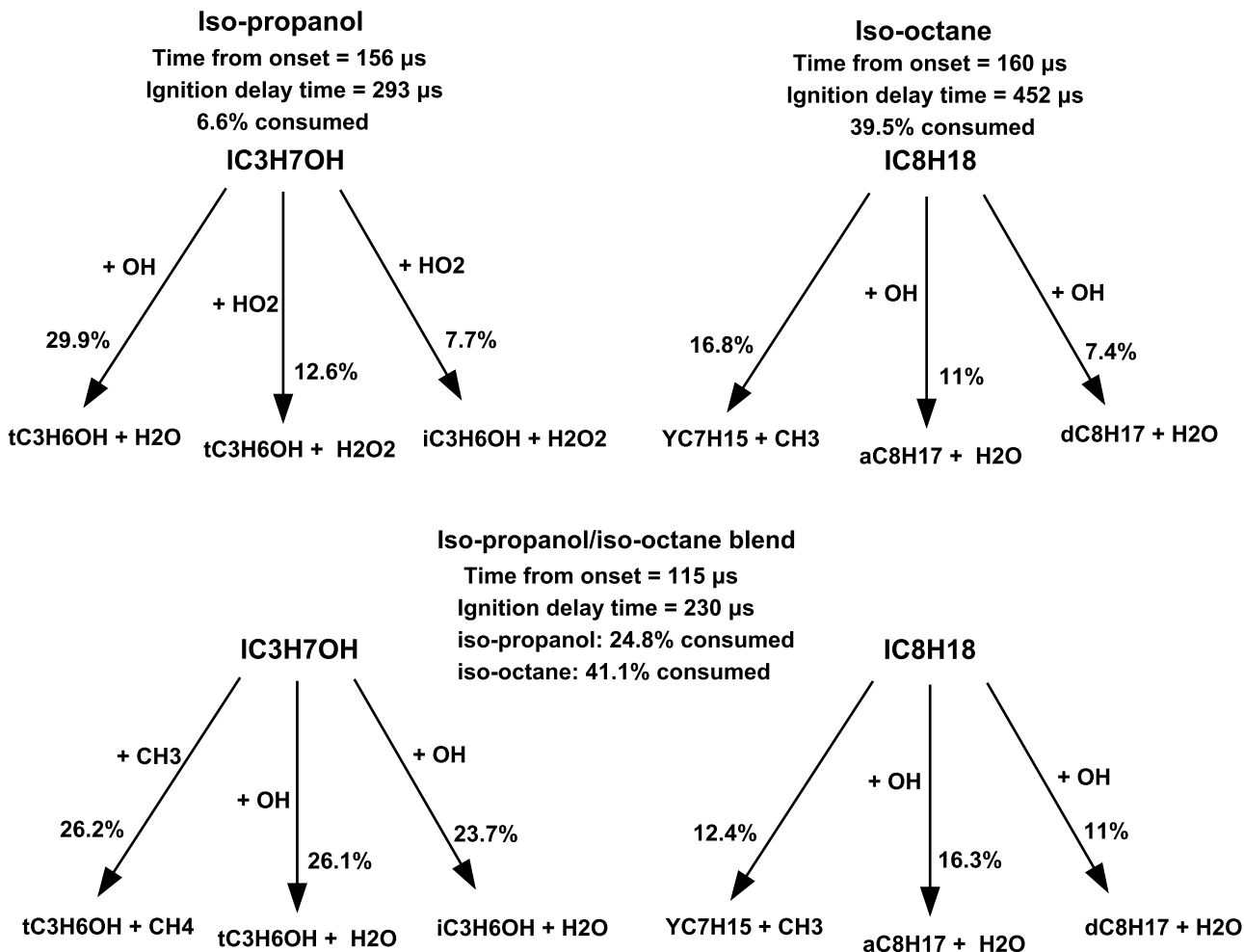


Fig. 3.63.: Reaction pathways for *iso*-octane, *iso*-propanol, and a blend of equal liquid volume proportions during ignition process ( $\phi = 1$ ,  $D = 3.76$ ) using the combined model at a pressure of 12 atm. Shown are the results of the reactor midway to the ignition instance.

times 10, 160, and 400  $\mu\text{s}$ . The main reaction pathway of *iso*-octane at the beginning is unimolecular decomposition to heptyl and methyl radicals, which accounts for 16.6% of the *iso*-octane consumption at 10  $\mu\text{s}$ . H-abstraction through CH<sub>3</sub>, H, and OH radicals are other active pathways at 10  $\mu\text{s}$ . Later on, unimolecular decomposition increases to 45.7% close to ignition. The significance of H-abstraction reactions declines as ignition is approached.

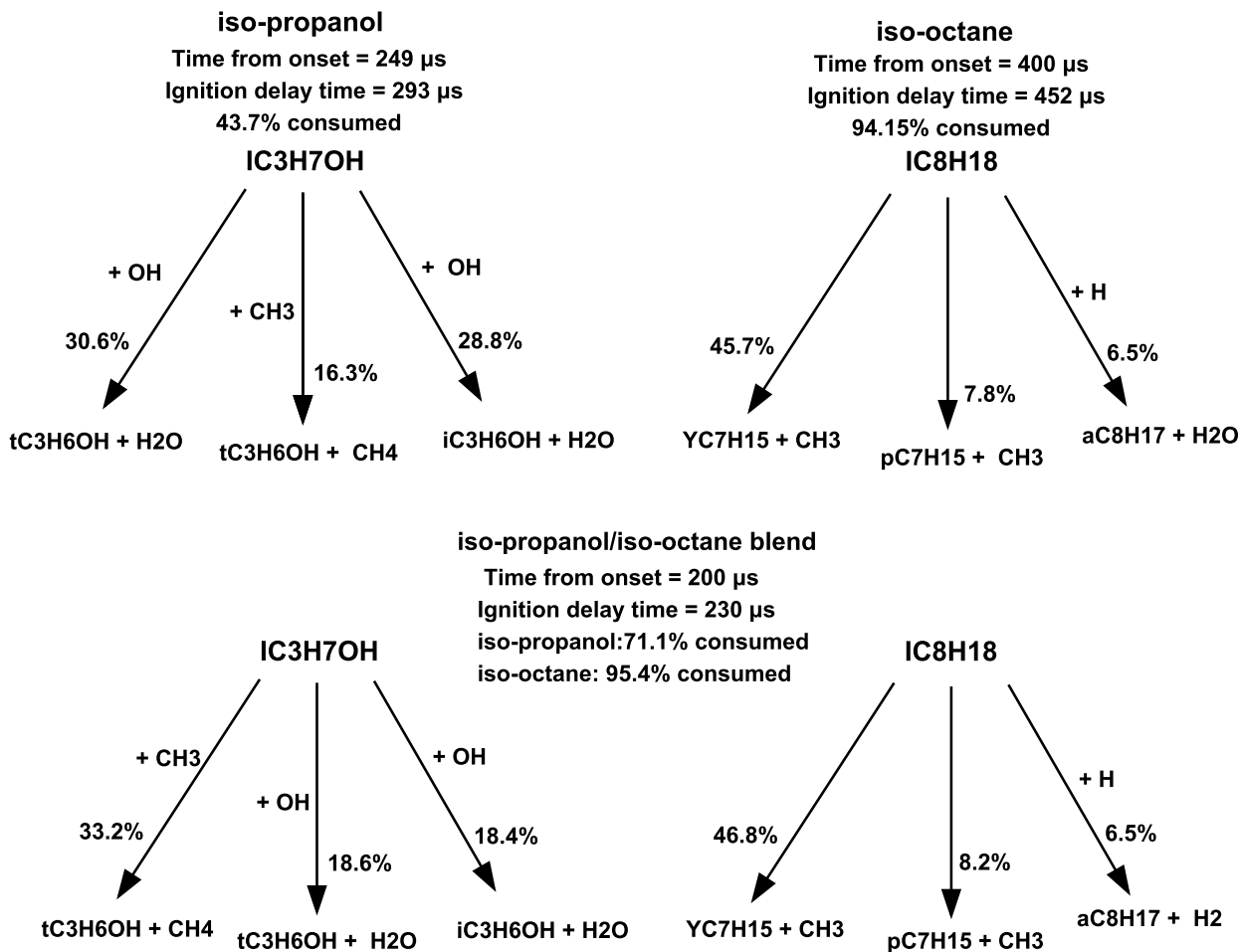


Fig. 3.64.: Reaction pathways for *iso*-octane, *iso*-propanol, and a blend of equal liquid volume proportions during ignition process ( $\phi = 1$ ,  $D = 3.76$ ) using the combined model at a pressure of 12 atm. Shown are the results very close to ignition onset.

For the fuel blend, the ignition delay time is 230  $\mu$ s, and the pathway analysis is performed at 10, 115, and 200  $\mu$ s. Initially, *iso*-octane preserves the main reaction pathway observed in the case of pure fuel, where 23.6% of the *iso*-octane is consumed through unimolecular decomposition to heptyl and methyl radicals. However, the main initial pathway of *iso*-propanol consumption becomes H-abstraction through CH<sub>3</sub>, which accounts for 41.5% of the DMF consumption. This is in contrast to the preferred initial pathway in

the case of pure *iso*-propanol. Later on, H-abstraction reactions by OH and H radicals become more significant in *iso*-propanol consumption, while the H-abstraction by CH<sub>3</sub> channel remains an active pathway. The main consumption pathway of *iso*-octane is similar to the pure fuel. The main result of these analyses is the difference in initial reaction pathway for *iso*-propanol in the pure fuel and blend cases. *Iso*-Propanol favors H<sub>2</sub>O elimination reactions in the case of the pure fuel, while it prefers H-abstraction by radicals in the case of blends. At play in this scenario is the CH<sub>3</sub> radical formation by *iso*-octane decomposition, which attacks *iso*-propanol molecules to abstract atomic hydrogen, resulting in a faster consumption of *iso*-propanol compared to the pure *iso*-propanol case, with approximately 95% of the *iso*-propanol consumed close to ignition in the blend case, compared to 43.7% consumption of *iso*-propanol close to ignition in the pure fuel case.

### 3.3.2 *Iso*-octane - ETBE blend

Having established ETBE having comparable ignition behavior as the undesirable octane number enhancer, MTBE, ETBE's effect on gasoline ignition is now explored. In this section, the ignition delay times of blends of ETBE and *iso*-octane as a gasoline surrogate are experimentally measured and a combined chemical kinetic model is assembled for simulating fuel blends combustion. The model is constructed via the same approach utilized as before in *iso*-octane/*iso*-propanol study and based on the reduced model for ethers from Galway group [83] and skeletal *iso*-octane model deduced from detailed model by Mehl et al. [107]. The details about these models are described in the former sections. The performance of the new model is assessed and validated against the

measured data and compared with other models available in the literature. Subsequently, chemical kinetic analyses are carried out to explain the experimental findings. The mixtures used for the blend fuels study are also shown in Tab. 3.3.

Figure 3.65 shows ignition delay times of stoichiometric mixtures at a pressure of 12 atm. At both conditions, it is observed that the ignition delay times of ETBE are shorter than *iso*-octane thus implies that ETBE has a weaker reactivity compared with *iso*-octane.

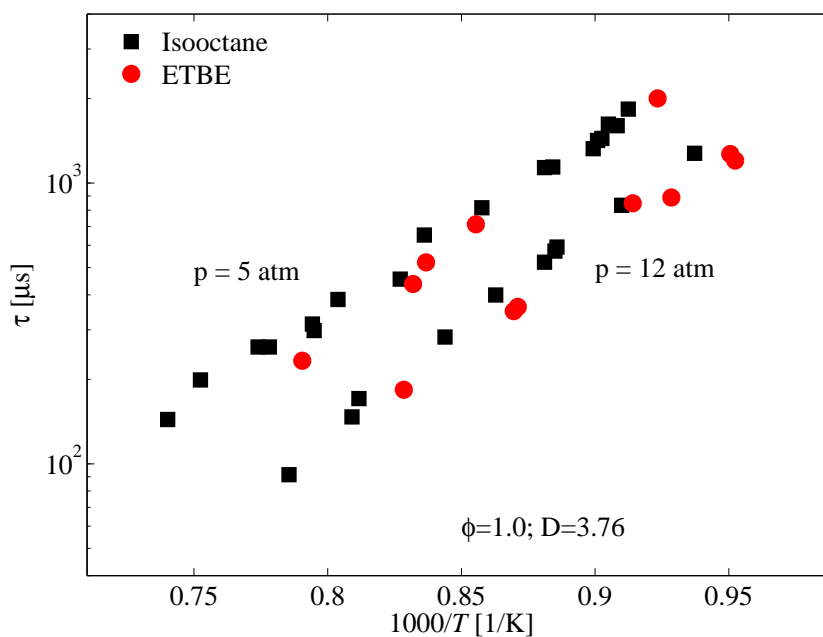


Fig. 3.65.: Relative ignition behavior of stoichiometric fuel/O<sub>2</sub>/Ar mixtures of ETBE and *iso*-octane at two pressures of 5 and 12 atm. The experimental data has same level of uncertainty as shown before.

Effects of blending ETBE into *iso*-octane are investigated by measuring ignition delay time of blends of different proportions by liquid volume of both fuels in this study as in Tab. 3.3. The ignition delay times of the blends are compared to ignition measurements of the pure fuels at the same conditions to establish relative reactivity trends. Figure 3.66 is a

comparison between the ignition delay times of the ETBE/*iso*-octane blends and of the pure fuels at stoichiometric conditions and a pressure of 12.0 atm, under a constrained Ar/O<sub>2</sub> ratio  $D$  of 3.76. It shows that in the lower temperature test range, ignition delay times follow the order of *iso*-octane, *iso*-octane/ ETBE 75/25 blend, *iso*-octane/ ETBE 50/50 blend, and ETBE from the longest to the shortest. This trend is expected from the previous comparative reactivities study between ETBE and *iso*-octane. But it is noted that the differences at these high temperatures are not pronounced. Fig. 3.67 shows similar ignition trends among the neat fuels and their blends at a lower pressure of 5 atm.

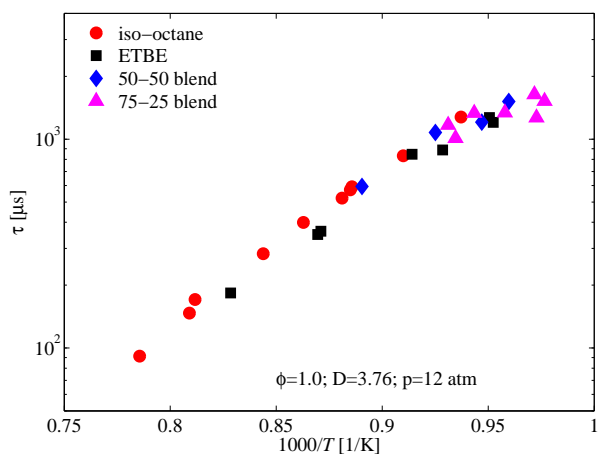


Fig. 3.66.: Relative ignition behavior of *iso*-octane, ETBE, 50/50 and 75/25 blends of both (by liquid volume) at a pressure of 12.0 atm.

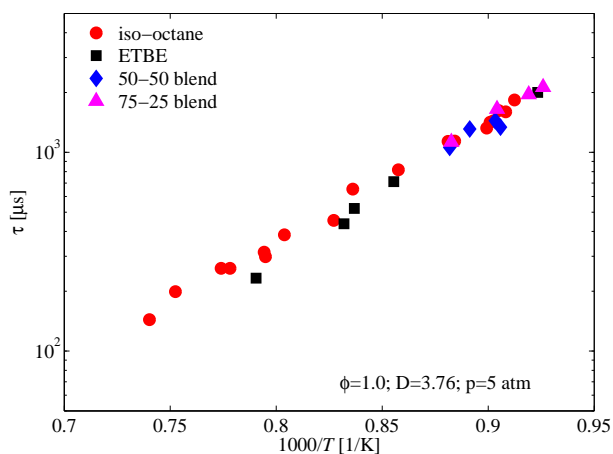


Fig. 3.67.: Relative ignition behavior of *iso*-octane, ETBE, 50/50 blend of both (by liquid volume) at a pressure of 5.0 atm.

The new blend model involves 334 species and 1405 reactions. It is validated against ignition delay times measurements and the predictions from detailed models for both pure *iso*-octane and ETBE, as shown in Figs. 3.57 and 3.68. For *iso*-octane, the combined model shows good agreement with both the detailed model and experimental measurements as discussed in the previous subsection. In terms of ETBE, two pressures of

5 atm and 12 atm are included in Fig. 3.68 for the comparison. It shows the combined model has reasonable agreements with predictions from the detailed model by Galway group [83] while both models predict longer ignition delay times than the measured data.

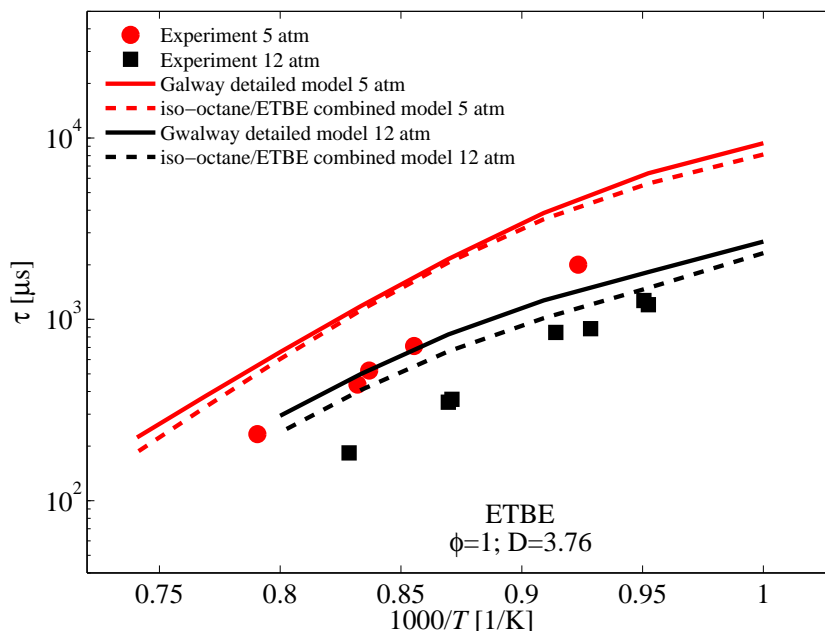


Fig. 3.68.: Comparison of ETBE test with the model predictions from the blend model in this work and detailed model by Galway group [83].

In Figures 3.69 and 3.70, the blend model is compared with the ignition delay times for the stoichiometric fuel blends of *iso*-octane/*iso*-propanol at two blending ratios, a pressure of 12.0 atm, and  $D$  of 3.76. The blend model is also compared with predictions of two models from Milano [86] and Tokyo groups [93]. The mechanism from Milano group was introduced before and the model from Tokyo group was developed to model the oxidation processes of Primary Reference Fuel in the presence of ethyl tert-butyl ether and ethanol as oxygenated octane improvers. It is observed that the combined model developed in this study is in closest agreement with the measurements while models from Milano and Tokyo

groups present larger deviations but all models predictions are in general longer than measured delay times.

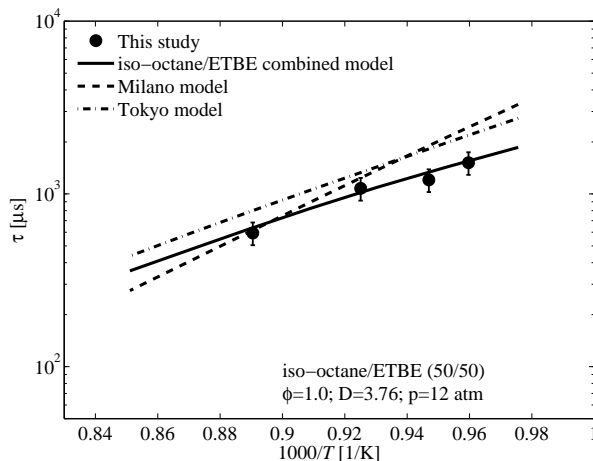


Fig. 3.69.: Comparison of test for stoichiometric *iso*-octane/ETBE (50/50) mixture with the model predictions from the blend model in this work, and models by Milano [86] and Tokyo [93] groups.

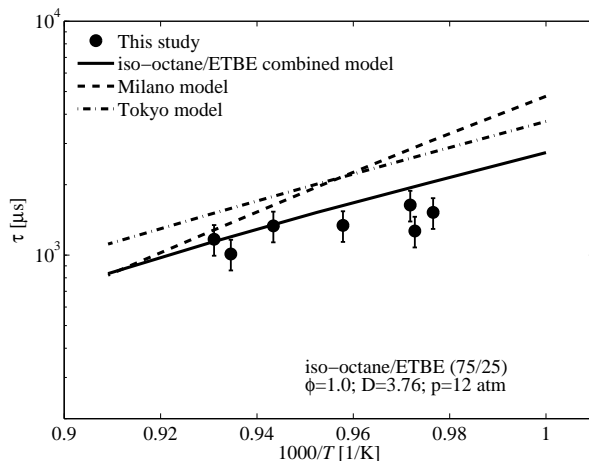


Fig. 3.70.: Comparison of test for stoichiometric *iso*-octane/ETBE (75/25) mixture with the model predictions from the blend model in this work, and models by Milano [86] and Tokyo [93] groups.

To gain further insight into the fuels blend behavior, reaction pathway analyses are carried out using the CHEMKIN software package [165] for an ignition process of stoichiometric fuel/O<sub>2</sub>/Ar mixtures with  $D$  of 3.76 at a temperature of 1150 K and a pressure of 12.0 atm, for the fuels *iso*-octane, ETBE, and a blend of equal liquid volume proportions. The results are shown in Fig. 3.71 - 3.73.

The reaction pathway analysis for ETBE is performed at the times 10, 314, and 597  $\mu$ s close to the ignition delay time of 666  $\mu$ s. It was observed that at 10  $\mu$ s, ETBE is mainly consumed through the four-center elimination reactions forming *iso*-butene and ethanol, with 67.9% of ETBE consumption proceeding through this channel. Contributions of H-abstraction reactions by free radicals are secondary to the former reaction. At later

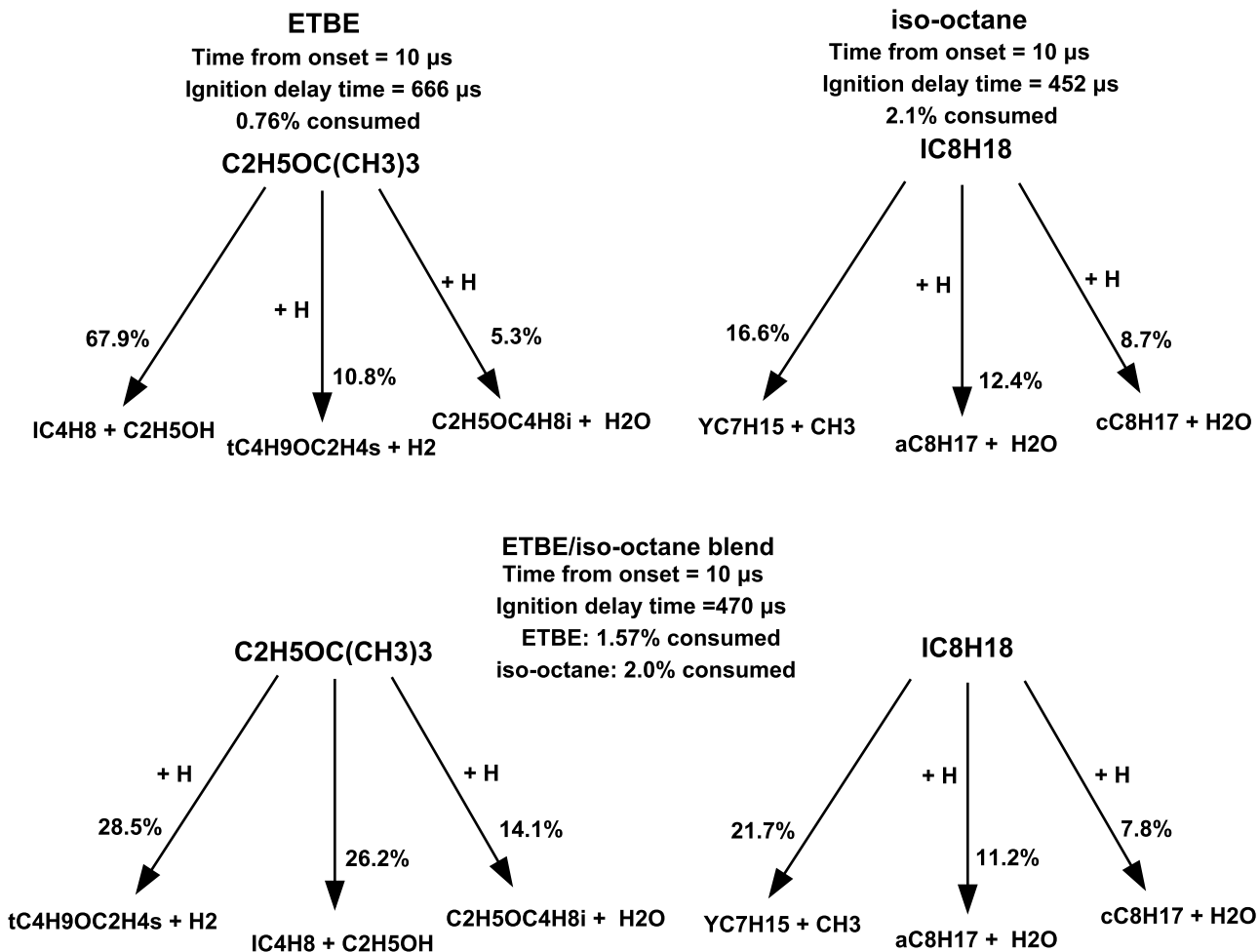


Fig. 3.71.: Reaction pathways for *iso*-octane, ETBE, and a blend of equal liquid volume proportions during ignition process ( $\phi = 1$ ,  $D = 3.76$ ) using the combined model at a pressure of 12 atm. Shown are the results close to the onset of the reactor.

times, H-abstraction by free radicals becomes more significant. In the case of *iso*-octane, as discussed before, the main reaction pathway of *iso*-octane at the beginning is unimolecular decomposition to heptyl and methyl radicals. Later on, unimolecular decomposition increases to 45.7% close to ignition. The significance of H-abstraction reactions declines as ignition is approached.



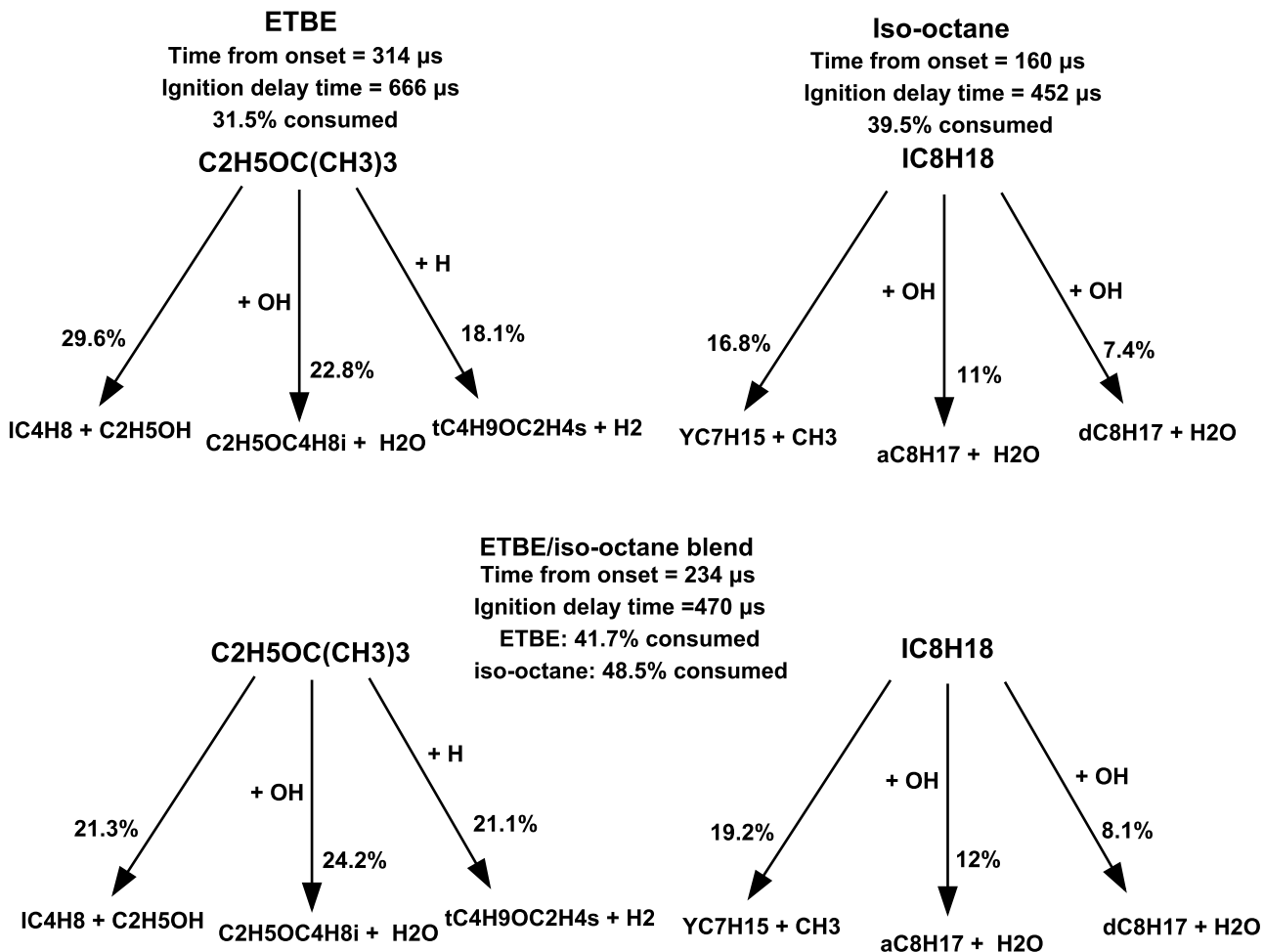


Fig. 3.72.: Reaction pathways for *iso*-octane, ETBE, and a blend of equal liquid volume proportions during ignition process ( $\phi = 1$ ,  $D = 3.76$ ) using the combined model at a pressure of 12 atm. Shown are the results of the reactor midway to the ignition instance.

For the fuel blend, the ignition delay time is 470  $\mu$ s, and the pathway analysis is performed at 10, 234, and 415  $\mu$ s. Initially, *iso*-octane preserves the main reaction pathway observed in the case of pure fuel, where 21.7% of the *iso*-octane is consumed through unimolecular decomposition to heptyl and methyl radicals. However, the main initial pathway of ETBE consumption becomes H-abstraction through H, which accounts for 28.5% of the ETBE consumption while the contribution from four-center elimination

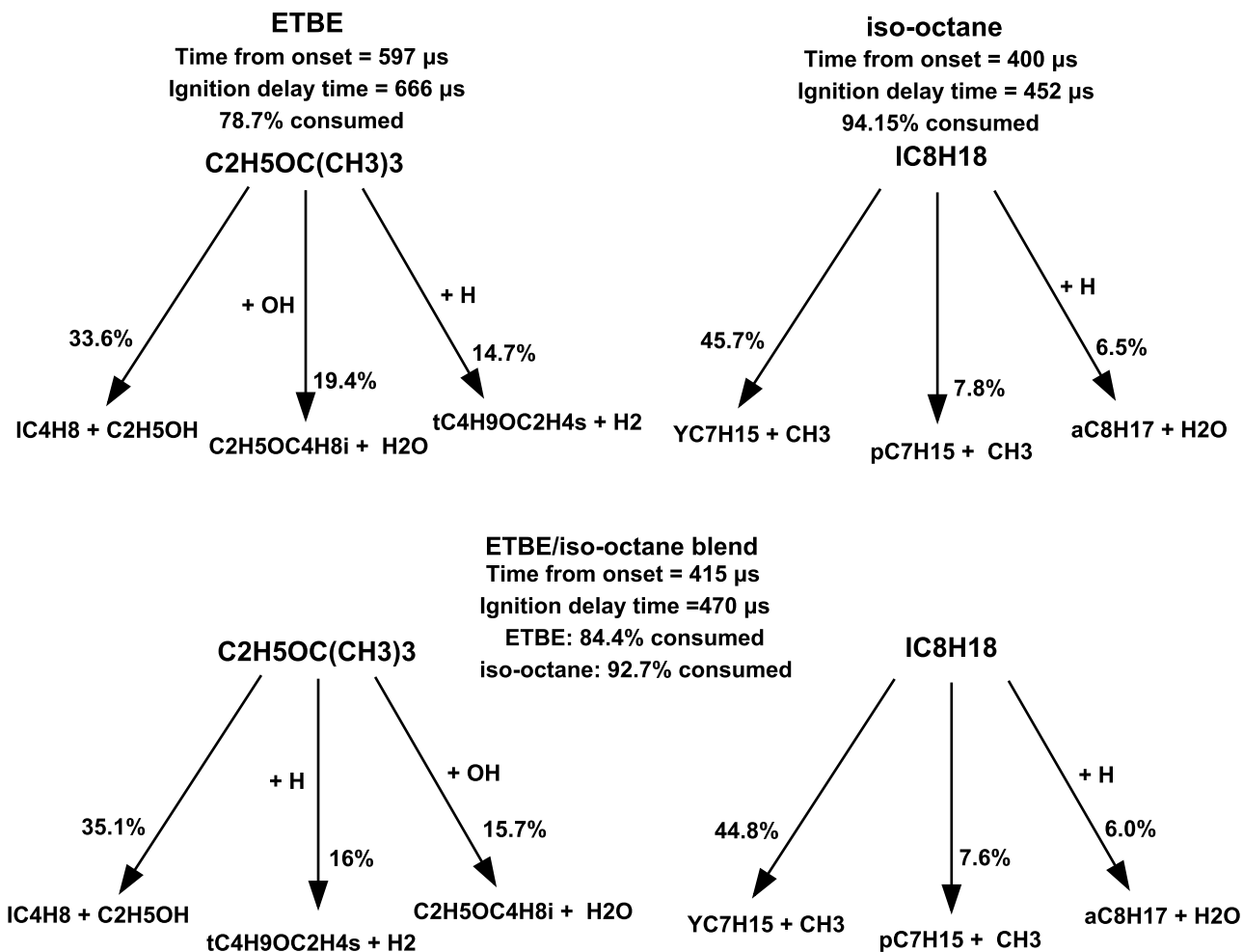


Fig. 3.73.: Reaction pathways for *iso*-octane, ETBE, and a blend of equal liquid volume proportions during ignition process ( $\phi = 1$ ,  $D = 3.76$ ) using the combined model at a pressure of 12 atm. Shown are the results very close to ignition onset.

reactions goes down to 26.2%. This is in contrast to the preferred initial pathway in the case of pure ETBE. Later on, H-abstraction reactions by OH and H radicals become more significant in ETBE consumption, while the four-center elimination reaction channel remains an active pathway. The main consumption pathway of *iso*-octane is similar to the pure fuel. The main result of these analyses is the difference in initial reaction pathway difference for ETBE in the pure fuel and blend cases. ETBE favors four-center elimination

reactions in the case of the pure fuel, while it prefers H-abstraction by radicals in the case of blends. The combined model will be further optimized to accord with the measured data. This can be done by revising the reaction rate parameters assigned for the key reactions and replacing with faster reaction rates to bring the overall chemical times into accord with the measurements.

## 4. GENERALIZED IGNITION CORRELATION

### 4.1 Demonstration

Figure 4.1 shows simulated ignition delay times of the biodiesel surrogate, methyl decanoate, at various pressures, demonstrating its NTC behavior. It is observed that the pressure dependence of the low-temperature region is weaker than that observed for the high-temperature and NTC regions. The NTC behavior is such that its onset and end temperatures shift to higher temperatures as the pressure increases. In the current correlation approach, a relation is sought between the cross-over temperature and the pressure of the reactor,  $T \propto p^k$ , where the pressure,  $p$ , is in atm and  $k$  is an exponent. The proportionality constant and the exponent are obtained through linear regression of a set of turning points at various pressures obtained from the simulations presented in Figure 4.1. The regression results for methyl decanoate are shown in Figure 4.2.

There is a stronger pressure dependence of the low-temperature cross-over than observed for the high-temperature cross-over. At a pressure of 1 atm, the relation obtained shows that the NTC region is embedded between 656.0 and 826.4 K, while for the gasoline surrogate model, the cross-over temperatures at 1 atm are found to be 610.5 K and 785.8 K.

This cross-over behavior can be linked to elementary chemical kinetics that determines the transition from high-temperature reactions, controlled by beta-scission of primary

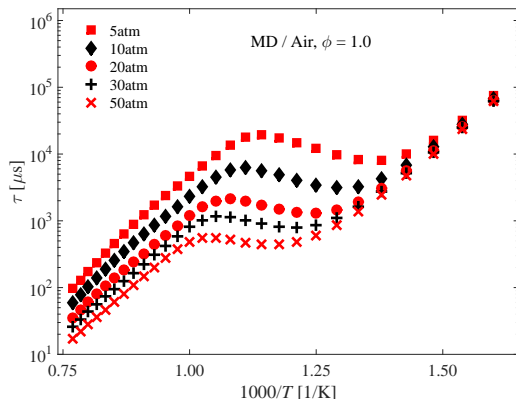


Fig. 4.1.: Representative ignition simulations for methyl decanoate (MD) correlation development based on model by Herbinet et al. [149].

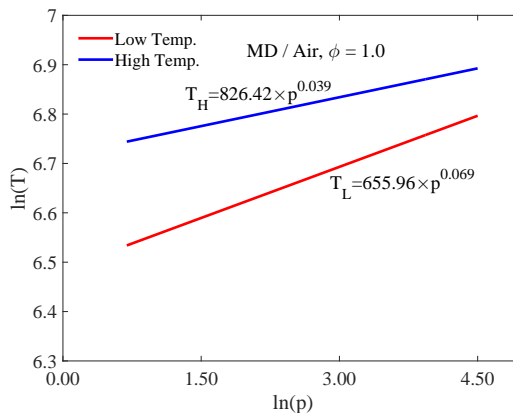
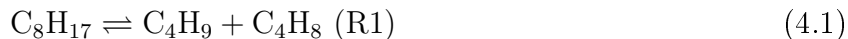


Fig. 4.2.: Dependence of cross-over temperatures on reactor pressures.

radicals to the low-temperature peroxy chemistry, characterized by molecular oxidation addition to the primary radical, followed by intramolecular hydrogen transfer reactions.

If one considers further reactions by a primary radical of iso-octane oxidation,  $C_8H_{17}$ , these two competing reactions are possible:



The forward rate constant of  $R1$  is  $k_{1f}$  and since the concentration of  $O_2$  is generally much higher than that of the radical,  $C_8H_{17}$ , the forward reaction of  $R2$  can be made pseudo-first order with a modified reaction rate constant  $k'_2 = k_{2f}[O_2]$ . Typically,  $R1$  is characterized by an activation energy in the range of 30-45 kcal/mol while  $R2$  has almost

zero activation energy. This means that the rate of  $R1$  decreases as the temperature reduces until a point is reached when the rate of  $R2$  predominates. The dependence of  $k'_2$  on  $[O_2]$  means that the rate increases as the reactor pressure increases, with the implication that the cross-over occurs at higher temperatures as the reactor pressure increases. This means that as rightly depicted in Fig. 4.2, the onset of low-temperature chemistry is not aligned with a fixed temperature. The cross-over of the two reaction rate constants above have been found to have comparable pressure exponent as established through correlation of cross-over temperatures and pressures.

By linearly regressing the data using a postulated ignition dependence, three separate correlations are obtained. For each region, correlations of the form are assumed:

$$\tau = cp^\alpha \left( \frac{T}{T_{ref}} \right)^\beta \exp \left( \frac{\theta_a}{T} \right), \text{ with } T_{ref} = 298 \text{ K here.}$$

The correlation parameters are obtained by inverse matrix division using the MATLAB software package. The format is motivated by the the Arrhenius rate constant, interpreting ignition delay time as the reciprocal of a first order global reaction rate. For the constants have usual physical meaning linked to Arrhenius form, the delay time would have to be regressed in the format:  $\tau \propto \exp \left( \frac{E_a}{RT} \right)$ . For a pressure of 20 atm, these correlations are plotted alongside the original data in Fig. 4.3a. It is observed that the correlations accurately reproduce the simulations in each region, while deviations are shown around the cross-over temperatures, as expected.

In the current approach, we combine the sub-correlations by introducing the hyperbolic tangent as a switch function with parameters consisting of cross-over temperatures and a temperature difference over which the function transitions. Hyperbolic tangents or their associated logistic functions are known to be good switch functions for smooth connection of two separate functions. The hyperbolic tangent function is defined as the ratio of the

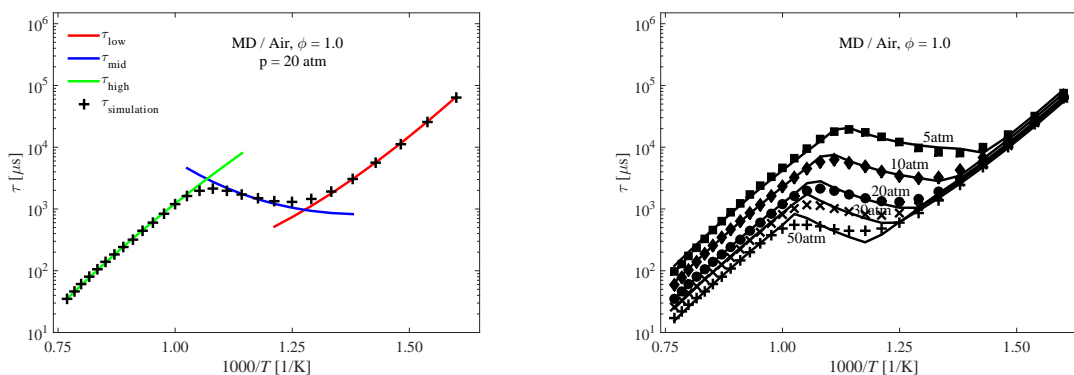


Fig. 4.3.: a. Simulated methyl decanoate (MD) ignition delay times and correlation predictions in the three regions. b. Comparison of MD ignition correlation predictions with simulated delay times using two switches at cross-over temperatures.

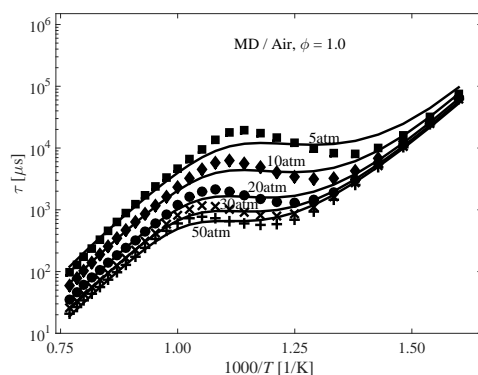


Fig. 4.4.: Comparison of simulated MD ignition delay times with ignition predictions using the empirical correlation proposed by Vandersickel et al. [121, 122].

hyperbolic sine to the cosine functions, or in the expanded form shown in eqn. 4.3 as the ratio of the difference to sum of  $e^x$  and  $e^{-x}$ . This function acts as an analytic switch from one regime to the other. Fig. 4.6 is a graphical representation of this hyperbolic tangent function for real values of its argument,  $x$ .

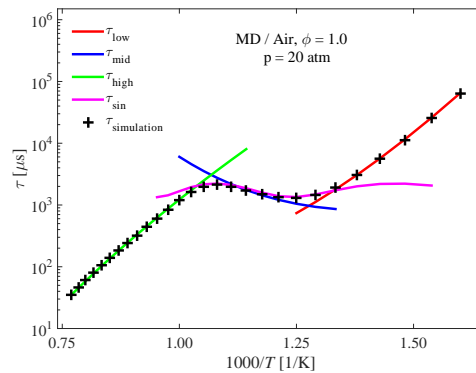


Fig. 4.5.: Merging of MD ignition correlations of the three sub-regions using the sine function.

$$\tanh(x) = \frac{\sinh(x)}{\cosh(x)} = \frac{e^x - e^{-x}}{e^x + e^{-x}} \quad (4.3)$$

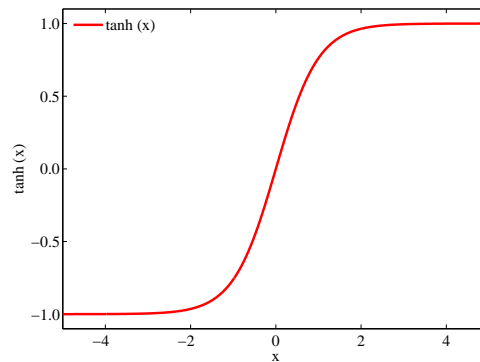


Fig. 4.6.: Graphic description of hyperbolic tangent function.

With two switches at the cross-over temperatures, we evaluate the performance of the proposed correlation with respect to reproducing the original simulation data. In this work, our switches have the form  $\eta_1 = \frac{1}{2}(1 - \tanh[\frac{T-(T_L-10)}{10}])$ ,  $\eta_2 = \frac{1}{2}(1 - \tanh[\frac{T-(T_H+10)}{10}])$  and the correlation has the form  $\tau = \tau_{low}\eta_1 + \tau_{mid}(1 - \eta_1)\eta_2 + \tau_{high}(1 - \eta_2)$ , capturing the whole



temperature region. However, deviations are observed at the cross-over points as shown in Fig. 4.3b.

It is interesting to compare the current approach with that proposed by [121,122] in eqn. 1.3, focusing on methyl decanoate. The three sub correlations for methyl decanoate obtained in this work are fused into a generalized correlation using eqn. 1.3. The performance is shown in Figure 4.4. Significant deviations are observed at the cross-over temperatures while good agreement is observed at the center of the NTC region and toward the extremes of the high- and low-temperature regions. The deviations are in line with our previous discussion of eqn. 1.3 and also found for the other fuels in this study. There is need, therefore, for a transition function and an understanding of its pressure-temperature dependence such that more insight is added to global ignition modeling and prediction.

While our suggested switch function is an improvement over the previous correlation approach, its performance in the vicinity of the critical cross-over points still needs further improvement. This is achieved here by means of a sine function around the transition points as shown in Fig. 4.5 and four switches are effectively used to control the smooth change. The cross-over temperatures can be used to center the sine wave around the point of interest but an amplitude function is necessary to capture the departure of the ignition dependence at various pressures. For the biodiesel surrogate model, these amplitudes,  $t_L$  and  $t_H$ , are found by further regression analysis of the form  $t \propto p^k$ . The final sine function,  $\tau_{sin}$ , takes the form as shown in the eqn. 4.4 and 4.5.

$$T_{cross} = ap^m; \quad t_{cross} = bp^n \quad (4.4)$$

$$\tau_{sin} = \frac{t_H - t_L}{2} \sin\left(\frac{\pi}{T_H - T_L}\left(T - \frac{T_H + T_L}{2}\right)\right) + \frac{t_H + t_L}{2} \quad (4.5)$$

The switch functions have the form  $\eta = \frac{1}{2}(1 - \tanh(\frac{T - (T_{cross} + k)}{5}))$ , where  $T_{cross}$  corresponds to  $T_L$  and  $T_H$  for the first two and last two switches,  $k$  equals to -50, 25, -25, and 50 for  $\eta_1$  to  $\eta_4$ , respectively.

The generalized ignition delay correlation now has the form:

$$\tau = \tau_{low}\eta_1 + \tau_{sin}(1 - \eta_1)\eta_2 + \tau_{mid}(1 - \eta_2)\eta_3 + \tau_{sin}(1 - \eta_3)\eta_4 + \tau_{high}(1 - \eta_4) \quad (4.6)$$

With the sine wave modification, parameters for the generalized correlation form in the eqn. 4.6 are shown in Tab. 4.1. The correlation shown in Fig. 4.7a is now in better agreement with the original simulation data over the whole temperature and pressure ranges. The correlations are further tested by comparing their predictions to simulation at conditions not used in their development. Fig. 4.7b confirms that the correlations accurately predict model simulations over a wide range of pressure conditions.

	c	$\alpha$	$\beta$	$\theta_a$	
$\tau_{low}$	$1.22 \times 10^{-30}$	-0.19	32.13	35460	
$\tau_{mid}$	$1.44 \times 10^{-27}$	-1.76	39.36	28130	
$\tau_{high}$	$7.59 \times 10^8$	-0.89	-11.11	2780	
	a	m		b	n
$T_L$	655.96	0.069	$t_L$	$5.66 \times 10^4$	-1.25
$T_H$	826.42	0.039	$t_H$	$2.18 \times 10^5$	-1.53

Table 4.1: MD ignition correlation parameters (four switches) based on model by Herbinet et al. [149].

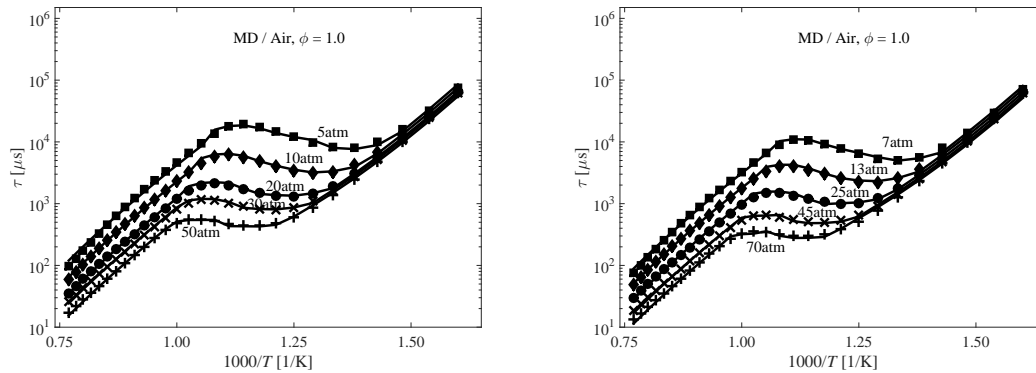


Fig. 4.7.: a. Comparison of correlation predictions with simulated ignition delay times (four switches). b. Test of the correlation at pressures not used in its development.

Following the same approach for MD above, similar correlations are developed for for jet fuel surrogates using the models by Dooley et al. [109] and Honnet et al. [150], for gasoline surrogates using the model by Mehl et al. [166], for *n*-octanol using the model by Cai et al. [151] and ethanol/gasoline blend using the model by Cai et al. [27]. The correlation parameters obtained in this case are summarized in Tabs 4.2-4.6.

	$c$	$\alpha$	$\beta$	$\theta_a$	
$\tau_{low}$	$7.93 \times 10^{-29}$	-0.23	30.16	34070	
$\tau_{mid}$	$4.68 \times 10^{-11}$	-1.76	20.53	13070	
$\tau_{high}$	$6.95 \times 10^7$	-0.82	-10.37	4740	
	a	m		b	n
$T_L$	649.24	0.072	$t_L$	$1.26 \times 10^5$	-1.34
$T_H$	828.07	0.040	$t_H$	$4.35 \times 10^5$	-1.59

Table 4.2: Princeton jet fuel surrogate ignition correlation parameters (four switches) based on model by Dooley et al. [109].

	c	$\alpha$	$\beta$	$\theta_a$	
$\tau_{low}$	$2.96 \times 10^{-29}$	-0.47	31.06	33940	
$\tau_{mid}$	$1.38 \times 10^{-6}$	-2.19	16.50	8330	
$\tau_{high}$	$5.90 \times 10^{-17}$	-0.73	13.17	30660	
	a	m		b	n
$T_L$	641.49	0.073	$t_L$	$1.38 \times 10^5$	-1.66
$T_H$	785.80	0.059	$t_H$	$5.41 \times 10^5$	-1.85

Table 4.3: Aachen jet fuel surrogate ignition correlation parameters (four switches) based on model by Honnet et al. [150].

	c	$\alpha$	$\beta$	$\theta_a$	
$\tau_{low}$	$6.62 \times 10^{-43}$	-0.26	49.24	45640	
$\tau_{mid}$	$1.12 \times 10^{10}$	-1.86	-1.87	-5350	
$\tau_{high}$	$6.57 \times 10^9$	-1.11	-10.98	1520	
	a	m		b	n
$T_L$	610.51	0.075	$t_L$	$5.26 \times 10^5$	-1.43
$T_H$	753.63	0.035	$t_H$	$1.64 \times 10^6$	-1.73

Table 4.4: Gasoline ignition correlation parameters (four switches) based on model by Mehl et al. [107].

	c	$\alpha$	$\beta$	$\theta_a$	
$\tau_{low}$	$2.31 \times 10^{-35}$	-0.27	38.3	39570	
$\tau_{mid}$	$2.32 \times 10^7$	-2.03	-1.94	-4640	
$\tau_{high}$	$1.91 \times 10^{15}$	-0.94	-17.48	-3920	
	a	m		b	n
$T_L$	638.81	0.079	$t_L$	$8.83 \times 10^4$	-1.37
$T_H$	803.92	0.044	$t_H$	$5.80 \times 10^5$	-1.81

Table 4.5: *n*-Octanol correlation parameters (four switches) based on model by Cai et al. [151].

## 4.2 Validation

Results show that the generalized correlations for each fuel type are able to accurately predict ignition delay times that would be obtained using the original detailed chemical kinetic models. These simplified ignition models are therefore recommended for ignition

	$c$	$\alpha$	$\beta$	$\theta_a$	
$\tau_{low}$	$9.43 \times 10^{-37}$	-0.58	42.97	40196	
$\tau_{mid}$	$5.11 \times 10^{24}$	-1.44	22.80	-16985	
$\tau_{high}$	$4.82 \times 10^8$	-0.94	-11.00	-3487	
	a	m		b	n
$T_L$	633.34	0.075	$t_L$	$5.41 \times 10^5$	-1.49
$T_H$	703.87	0.085	$t_H$	$1.20 \times 10^6$	-1.88

Table 4.6: Ethanol/gasoline blend correlation parameters (four switches) based on model by Cai et al. [27].

predictions without the specialized chemical kinetic solver that is needed to integrate detailed chemical kinetic models.

The correlation approach presented here can also be applied to simulation data as well as experimentally determined ignition delay times as far as the temperature range is well resolved and the number of data points is such that uncertainties are minimized. The delineation of the three ignition regions also makes it possible to compare model predictions and experimental determination of the cross-over temperatures and their pressure dependence. In the case where detailed models have been simplified to correlations, the correlations can also be used to compare with experiments. In Figure 4.8a, experimentally determined ignition delay times of methyl decanoate presented by Wang et al. [167] and Li et al. [168] are compared to predictions of the chemical kinetic model by Herbinet et al. [149]. Here the model predictions are both detailed simulations and correlation calculations. It is observed that the temperature sensitivities of the experimental data set and the model correlation prediction are similar. The cross-over temperature between the NTC and high-temperature region at 15 atm is predicted by the model to be 919 K whereas the experimental data at 15 - 18 atm suggest that it is around

900 K. For the NTC and low-temperature regions, the model predicts that the cross-over occurs at 791 K in close agreement with the experimental value of 783 K.

The gasoline correlation is compared to detailed model predictions and available experimentally determined ignition delay times in Fig. 4.8b. The correlation delay times are in good agreement with those predicted by the detailed model and these generally agree with the experimental measurements.

In Figure 4.9a the ignition correlation obtained for *n*-octanol is compared to the detailed model predictions and experimental data set that was used in the model development. Here again, the correlation is in line with the detailed model simulations and agrees generally well with the experimental data. Similar results are also found for the ethanol/gasoline blend fuel as shown in Figure 4.9b.

In Fig. 4.10, ignition delay times of a jet fuel surrogate are compared to predictions of the chemical kinetic model by Dooley et al. [109]. It is observed that the temperature sensitivities of the experimental data set and the model prediction are similar, while the model shows longer ignition delay times and predicts higher cross-over temperatures. Taking these into account, some constants of the generalized correlation developed in this work are modified in accordance with the quantitative differences between the model correlation and using the experimentally observed cross-over temperatures. The model predicts longer ignition delay times than experimentally observed by a factor of approximately 2.0 for the low- and high-temperature regions and a factor of 1.3 for the NTC region (within experimental uncertainties). The cross-over temperature between the NTC and high-temperature region at 20 atm is predicted by the model to be 933.5 K whereas the experiment suggests that it is 886.8 K. For the NTC and low-temperature

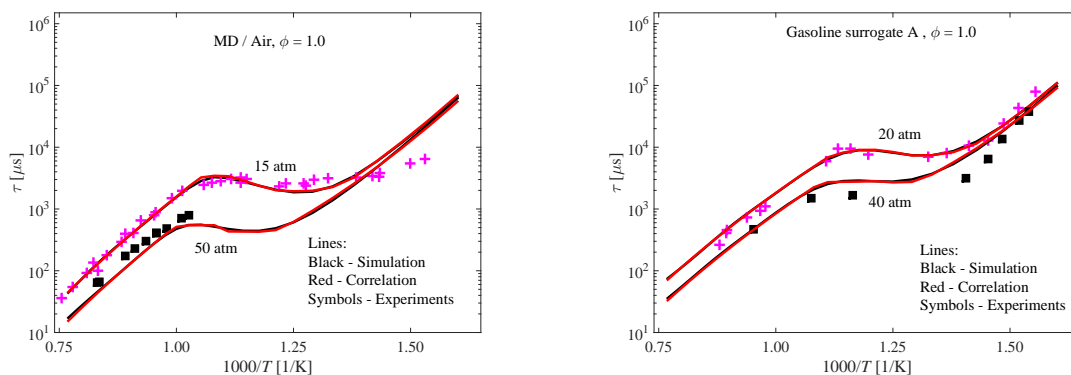


Fig. 4.8.: Comparison of the model-based correlations with experimental data. a). Methyl decanoate shock tube ignition data by Wang et al. [167] and Li et al. [168]. b). Gasoline surrogate RCM data by Kukkadapu et al. [169] and shock tube data by Gauthier et al. [152].

regions, the model predicts that the cross-over occurs at 805.5 K in close agreement with the experimental value of 797 K needed to bring the correlation in better agreement with the experiment. These changes applied to the model correlations are sufficient to yield a new representation of the data by a correlation as shown before.

### Reactors with temporally varying pressure and temperature

The ignition delay times above are obtained for homogeneous gas phase reactors where ignition is induced by instantaneously subjecting the system to high-temperature and pressure conditions. In most combustion systems, the heating process is achieved in finite time, whereby compressive heating is carried out or a temperature profile is applied. In automotive engineering, the simplest model of this gradual process is the adiabatic compressive heating during the compression stroke. The temporal profiles of pressure and

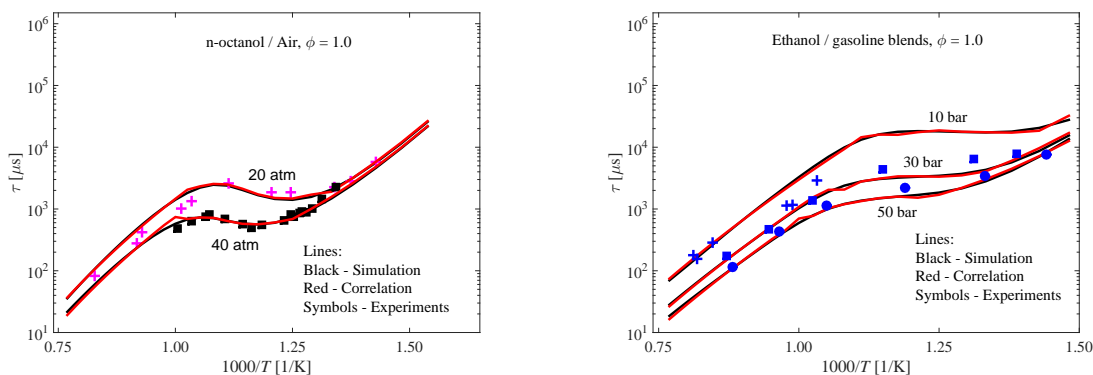


Fig. 4.9.: Comparison of the model-based correlations with experimental data. a. *n*-Octanol shock tube data taken by Cai et al. [151]. b. Ethanol/Gasoline surrogate shock tube data by Fikri et al. [153].

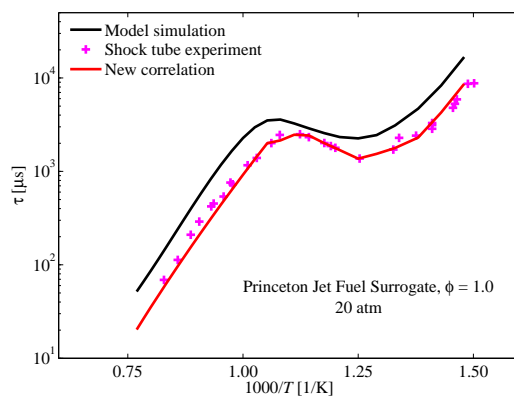


Fig. 4.10.: By modifying correlation parameters, the model-based correlation for Princeton Jet Fuel Surrogate can be brought to better agreement with experimental data. Experimental data taken from Dooley et al. [109]

temperature are related to the rotational speed of the crankshaft. The Livengood-Wu integral is often used in combination with ignition correlations developed on the basis of reactors with prescribed constant temperatures and pressures. Assuming that combustion takes place in one single reaction and that the reaction rate does not change with time for



a fixed process, Livengood and Wu established that ignition takes place the value of the integral obtained in their analysis attains the value of one [170].

Compression Ratios	12, 14, 18
Clearance Volume (cm <sup>3</sup> )	15
Engine Connecting Rod to Crank Radius Ratio	3.33
Engine Speed (rpm)	1000, 2000, 3000
Inlet temperature (K)	300, 400
Inlet pressure (atm)	1

Table 4.7: HCCI Engine Simulation Parameters.

Using a homogeneous reactor, such as the Homogeneous Charge Compression Ignition engine model in CHEMKIN, we evaluate the performance of the correlation for gasoline surrogates. Ignition occurs when the definite integral is unity. In this case the detailed model is used for the time-dependent simulation of the reactive adiabatic compression. Engine simulations are carried out at various compression ratios, inlet temperatures and a range of rotation speeds from 1000 to 3000 rpm as shown in Table 4.7. Figure 4.11 shows two cases where the pressure traces and the Livengood-Wu integral plotted against engine crank angles are compared. In these examples, as in Fig. 4.12 it is observed that under most engine conditions studied here, there is reasonable agreement between the Livengood-Wu integral prediction and the simulated engine ignition times using the detailed model.

We think that the discrepancies observed are more related to the Livengood-Wu method of accounting for the changing thermodynamic states in the simulation, than to the ability of the correlation to predict ignition delay times at a given thermodynamic state. The consistence of deviations showing in Fig. 4.12 suggests that more work needs to

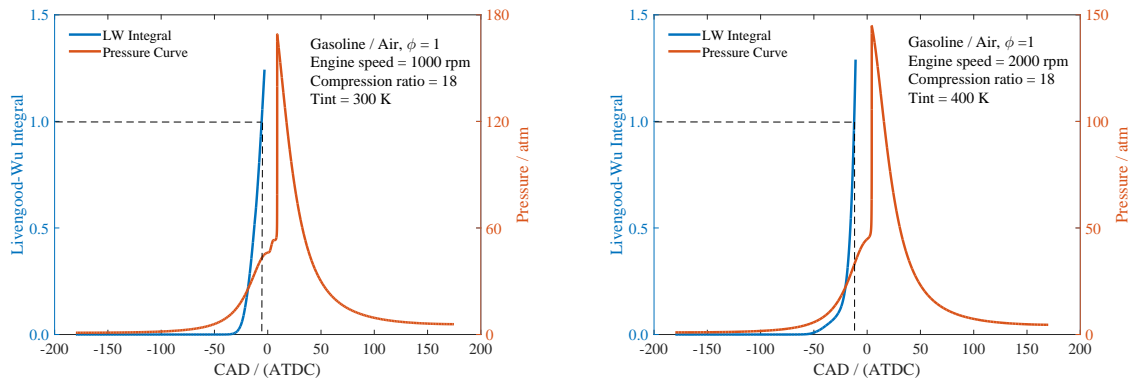


Fig. 4.11.: Cases for comparison between Livengood-Wu integral ignition prediction and engine combustion pressure profiles.

be done to modify the Livengood-Wu approach for ignition prediction. One other aspect that needs to be modified is to account for possible temperature increase as a result of first stage ignition. However, it is still expected that a more broad ignition database and optimization of correlation parameters selection might provide further improvement in the correlation prediction performance.

Modern engines often run at lean and diluted conditions to improve the efficiency and emission performance. However, to further demonstrate the necessity of incorporating low temperature chemistry into full HCCI engine conditions simulation which includes undiluted and near stoichiometric conditions for maximum power density, we also solved Livengood-Wu integral under these conditions using only high temperature ignition correlation. We found that because of the relatively shorter ignition delay time predicted from the high temperature ignition correlation, the integral which involves reciprocal of the ignition delay reaches unity at a faster rate. The erroneous percentages between LW

Integral using only high temperature ignition correlation and simulation results for some cases are around 100%, which are significantly higher than the results presented before with a generalized ignition correlation including both low and high temperature ignitions.

The correlations developed in this work are for stoichiometric mixtures; they could be extended in each region to incorporate the effects of equivalence ratio and dilution. The proposed correlation therefore has limitations that should be mentioned here. Power law dependence of ignition delay times on equivalence ratios and on dilution levels is often assumed, for instance in previous works by one of the authors [25, 53].

If it is desired that these effects be captured by the generalized correlation, the three separate correlations can be modified to include equivalence ratios and dilution levels as variables. However, if the temperature range is wide (low- to high-temperature through NTC), the dependence of ignition delay times on equivalence ratio varies from one region to another, such that a strong dependence is observed in the NTC region, with ignition

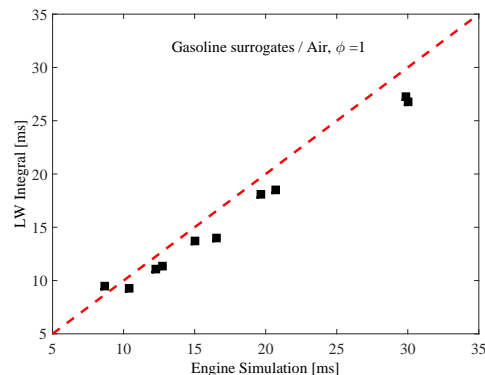


Fig. 4.12.: Comparison of the predicted ignition times for gasoline surrogates using Livengood-Wu integral method and engine simulation results.

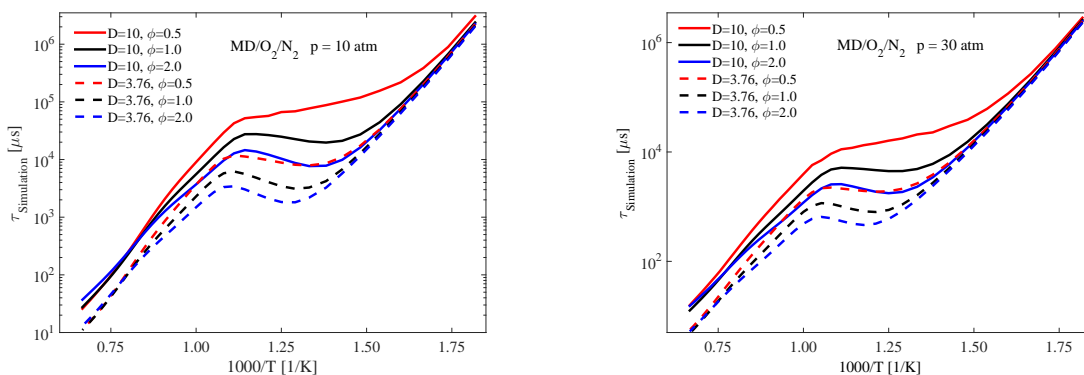


Fig. 4.13.: Simulation for MD ignition under various dilution and equivalence ratios.

delay times decreasing with increasing equivalence ratio. This dependence is much weaker at higher temperatures and can even lead to a reversal of the NTC trend at high enough temperatures around 1400 K.

Regarding dilution, when more inert gases are present, the competition between reactions of fuel radicals with oxygen and high temperature decomposition of radicals is weaker, so much so that the NTC region can completely disappear. These points are illustrated in Fig. 4.13 by simulated ignition delay times of methyl decanoate at two different dilution levels, three equivalence ratios, and two pressures. It can be seen that the effect of equivalence ratio is well defined in the NTC region but weaker at high-temperatures with possible cross-overs. Dilution also reduces the NTC behavior, especially for lean mixtures, where the behavior is absent.

## 5. CONCLUSION AND OUTLOOK

This thesis set out to explore ignition-resistant fuels, validate chemical kinetic models and develop simpler ignition models with respect to these goals, it has established the following main results:

- From the study of bioalcohols, propanol isomers, it is found that *iso*-propanol is more resistant to ignition than *n*-propanol. This accords with previous studies and raises the prospect of using *iso*-propanol to boost the ignition resistance of the engine fuel.
- From the comparative study of MTBE and ETBE ignition, it is established the more environmentally benign ETBE has comparable ignition behavior to the regulated ignition-resistant MTBE. This raises the prospect of more extensive use of ETBE as a fuel component to increase the ignition resistance of the resulting fuel. The similarity of the ignition behavior of the two ethers is explained on the basis of the bond strengths of the molecular structures as revealed by simple electronic structure calculations.
- Using *iso*-octane as a gasoline representative, the effect of adding *iso*-propanol or ETBE to the fuel is explored. No substantial differences are observed partly owing to the high temperature of the reactor and the fact that *iso*-octane actually has a higher ignition resistance than conventional gasoline. Combined models for *iso*-octane and the additives are also developed.

- Reduced chemical kinetic models of the fuels studied here are obtained on the basis of the Alternate Species Elimination method. A generalized ignition correlation method is also proposed to attain yet simpler ignition model for engine combustion analysis. This correlation method relies on a database of ignition delay times obtained from kinetic simulations or statistically significant number of experimentally determined ignition delay times.

This work contributes to the growing body of knowledge on biofuels combustion, especially those biofuels which exhibit higher ignition-resistant behavior. The comparative reactivity study bridges the gap in our understanding of the reactivity of propanol isomers and MTBE/ETBE. The combined model development and analysis will be useful to the understanding of fuel blend combustion, involving gasoline surrogate and potential anti-knock agents. The reduced combustion models and simplified ignition correlation work contributes to the incorporation of chemical kinetic effects in combustion analysis of practical systems, for instance, engine knock prediction and control.

Beyond the current work, further blending effects of *iso*-propanol and ETBE on gasoline could be explored using a surrogate fuel which has three or more fuel components. The generalized ignition correlation could be extended to capture the effect of equivalence ratio and dilution.

## LIST OF REFERENCES

- [1] G. Kalghatgi, "Developments in internal combustion engines and implications for combustion science and future transport fuels," *Proceedings of the Combustion Institute*, 2014.
- [2] R. Malhotra, "Fossil energy," Springer, 2013.
- [3] R. D. Reitz, "Directions in internal combustion engine research," *Combustion and Flame*, vol. 160, no. 1, pp. 1–8, 2013.
- [4] Y. Qi, Z. Wang, J. Wang, and X. He, "Effects of thermodynamic conditions on the end gas combustion mode associated with engine knock," *Combustion and Flame*, vol. 162, no. 11, pp. 4119 – 4128, 2015.
- [5] X. Zhen, Y. Wang, S. Xu, Y. Zhu, C. Tao, T. Xu, and M. Song, "The engine knock analysis - an overview," *Applied Energy*, vol. 92, no. 0, pp. 628 – 636, 2012.
- [6] E. Dem'yanenko, A. Sachivko, V. Tverdokhlebov, P. Deineko, A. Bakaleinik, V. Manaenkov, V. Emel'yanov, and S. Onoichenko, "Antiknock agent for unleaded gasolines," *Chemistry and Technology of Fuels and Oils*, vol. 29, no. 6, pp. 267–270, 1993.
- [7] H. Hamid and M. A. Ali, *Handbook of MTBE and Other Gasoline Oxygenates*. CRC Press, 2004.
- [8] R. Sawangkeaw and S. Ngamprasertsith, "A review of lipid-based biomasses as feedstocks for biofuels production," *Renewable and Sustainable Energy Reviews*, vol. 25, pp. 97 – 108, 2013.
- [9] N. Pragma, K. K. Pandey, and P. Sahoo, "A review on harvesting, oil extraction and biofuels production technologies from microalgae," *Renewable and Sustainable Energy Reviews*, vol. 24, pp. 159 – 171, 2013.
- [10] D. Klass, *Biomass for Renewable Energy, Fuels, and Chemicals*. Elsevier, 1998.
- [11] Y. Chen and R. Raine, "A study on the influence of burning rate on engine knock from empirical data and simulation," *Combustion and Flame*, vol. 162, no. 5, pp. 2108 – 2118, 2015.
- [12] J. N. Mattavi, *Combustion modelling in reciprocating engines*. Plenum Press, 1980.
- [13] E. Moses, A. L. Yarin, and P. Bar-Yoseph, "On knocking prediction in spark ignition engines," *Combustion and Flame*, vol. 101, no. 3, pp. 239 – 261, 1995.
- [14] N. Kawahara and E. Tomita, "Visualization of auto-ignition and pressure wave during knocking in a hydrogen spark-ignition engine," *International Journal of Hydrogen Energy*, vol. 34, no. 7, pp. 3156 – 3163, 2009.

- [15] M. Poschl and T. Sattelmayer, "Influence of temperature inhomogeneities on knocking combustion," *Combustion and Flame*, vol. 153, no. 4, pp. 562–573, 2008. cited By 23.
- [16] A. Groysman, *Corrosion in systems for storage and transportation of petroleum products and biofuels*. Springer, 2014.
- [17] K. Owen and T. Coley, "Automotive fuels reference book," 1995.
- [18] A. Demirbas, "Biofuels sources, biofuel policy, biofuel economy and global biofuel projections," *Energy conversion and management*, vol. 49, no. 8, pp. 2106–2116, 2008.
- [19] A. Demirbas, "Competitive liquid biofuels from biomass," *Applied Energy*, vol. 88, no. 1, pp. 17–28, 2011.
- [20] R. Arvidsson, K. Fransson, M. Fröling, M. Svanström, and S. Molander, "Energy use indicators in energy and life cycle assessments of biofuels: review and recommendations," *Journal of Cleaner Production*, vol. 31, pp. 54–61, 2012.
- [21] P. Lamers, C. Hamelinck, M. Junginger, and A. Faaij, "International bioenergy trade—a review of past developments in the liquid biofuel market," *Renewable and Sustainable Energy Reviews*, vol. 15, no. 6, pp. 2655 – 2676, 2011.
- [22] J. M. Bergthorson and M. J. Thomson, "A review of the combustion and emissions properties of advanced transportation biofuels and their impact on existing and future engines," *Renewable and Sustainable Energy Reviews*, vol. 42, pp. 1393–1417, 2015.
- [23] V. H. Rapp, J. H. Mack, P. Tschann, W. Hable, R. J. Cattolica, and R. W. Dibble, "Research octane numbers of primary and mixed alcohols from biomass-based syngas," *Energy & Fuels*, vol. 28, no. 5, pp. 3185–3191, 2014.
- [24] A. Frassoldati, A. Cuoci, T. Faravelli, U. Niemann, E. Ranzi, R. Seiser, and K. Seshadri, "An experimental and kinetic modeling study of n-propanol and iso-propanol combustion," *Combustion and Flame*, vol. 157, no. 1, pp. 2–16, 2010.
- [25] K. E. Noorani, B. Akih-Kumgeh, and J. M. Bergthorson, "Comparative high temperature shock tube ignition of c1- c4 primary alcohols," *Energy & fuels*, vol. 24, no. 11, pp. 5834–5843, 2010.
- [26] J. Zhang, S. Niu, Y. Zhang, C. Tang, X. Jiang, E. Hu, and Z. Huang, "Experimental and modeling study of the auto-ignition of n-heptane/n-butanol mixtures," *Combustion and Flame*, vol. 160, no. 1, pp. 31–39, 2013.
- [27] L. Cai and H. Pitsch, "Optimized chemical mechanism for combustion of gasoline surrogate fuels," *Combustion and Flame*, vol. 162, no. 5, pp. 1623 – 1637, 2015.
- [28] C. Tang, L. Wei, X. Man, J. Zhang, Z. Huang, and C. K. Law, "High temperature ignition delay times of {C5} primary alcohols," *Combustion and Flame*, vol. 160, no. 3, pp. 520 – 529, 2013.
- [29] K. A. Heufer, S. M. Sarathy, H. J. Curran, A. C. Davis, C. K. Westbrook, and W. J. Pitz, "Detailed kinetic modeling study of n-pentanol oxidation," *Energy & Fuels*, vol. 26, no. 11, pp. 6678–6685, 2012.
- [30] X. Gu, Z. Huang, S. Wu, and Q. Li, "Laminar burning velocities and flame instabilities of butanol isomers–air mixtures," *Combustion and Flame*, vol. 157, no. 12, pp. 2318–2325, 2010.



- [31] Q. Li, E. Hu, X. Zhang, Y. Cheng, and Z. Huang, "Laminar flame speeds and flame instabilities of pentanol isomer-air mixtures at elevated temperatures and pressures," *Energy & Fuels*, vol. 27, no. 2, pp. 1141–1150, 2013.
- [32] Q. Li, C. Tang, Y. Cheng, L. Guan, and Z. Huang, "Laminar flame speeds and kinetic modeling of n-pentanol and its isomers," *Energy & Fuels*, vol. 29, no. 8, pp. 5334–5348, 2015.
- [33] C. R. Shen and J. C. Liao, "Metabolic engineering of escherichia coli for 1-butanol and 1-propanol production via the keto-acid pathways," *Metabolic engineering*, vol. 10, no. 6, pp. 312–320, 2008.
- [34] S. Atsumi and J. C. Liao, "Metabolic engineering for advanced biofuels production from escherichia coli," *Current Opinion in Biotechnology*, vol. 19, no. 5, pp. 414 – 419, 2008. Tissue, cell and pathway engineering.
- [35] M. Eyidogan, A. Ozsezen, M. Canakci, and A. Turkcan, "Impact of alcohol-gasoline fuel blends on the performance and combustion characteristics of an {SI} engine," *Fuel*, vol. 89, no. 10, pp. 2713 – 2720, 2010.
- [36] T. Wallner, A. Ickes, and K. Lawyer, "Analytical assessment of c2-c8 alcohols as spark-ignition engine fuels," in *Proceedings of the FISITA 2012 World Automotive Congress*, pp. 15–26, Springer, 2013.
- [37] A. Keskin and M. Gürü, "The effects of ethanol and propanol additions into unleaded gasoline on exhaust and noise emissions of a spark ignition engine," *Energy Sources, Part A: Recovery, Utilization, and Environmental Effects*, vol. 33, no. 23, pp. 2194–2205, 2011.
- [38] B. Masum, H. Masjuki, M. A. Kalam, S. Palash, and M. Habibullah, "Effect of alcohol-gasoline blends optimization on fuel properties, performance and emissions of a si engine," *Journal of Cleaner Production*, vol. 86, pp. 230–237, 2015.
- [39] S. Smith and A. Gordon, "Studies of diffusion flames. ii. diffusion flames of some simple alcohols.," *The Journal of Physical Chemistry*, vol. 60, no. 8, pp. 1059–1062, 1956.
- [40] K. Kohse-Höinghaus, P. Oßwald, T. A. Cool, T. Kasper, N. Hansen, F. Qi, C. K. Westbrook, and P. R. Westmoreland, "Biofuel combustion chemistry: from ethanol to biodiesel," *Angewandte Chemie International Edition*, vol. 49, no. 21, pp. 3572–3597, 2010.
- [41] X. Lu, Y. Hou, L. Ji, L. Zu, and Z. Huang, "Heat release analysis on combustion and parametric study on emissions of hcci engines fueled with 2-propanol/n-heptane blend fuels," *Energy and Fuels*, vol. 20, no. 5, pp. 1870–1878, 2006. cited By 33.
- [42] A. Uyumaz, "An experimental investigation into combustion and performance characteristics of an hcci gasoline engine fueled with n-heptane, isopropanol and n-butanol fuel blends at different inlet air temperatures," *Energy Conversion and Management*, vol. 98, pp. 199–207, 2015.
- [43] T. Balamurugan and R. Nalini, "Experimental investigation on performance, combustion and emission characteristics of four stroke diesel engine using diesel blended with alcohol as fuel," *Energy*, vol. 78, pp. 356–363, 2014.
- [44] A. Atmanli, "Comparative analyses of diesel-waste oil biodiesel and propanol, n-butanol or 1-pentanol blends in a diesel engine," *Fuel*, vol. 176, pp. 209–215, 2016.

- [45] Y. Li, L. Wei, Z. Tian, B. Yang, J. Wang, T. Zhang, and F. Qi, "A comprehensive experimental study of low-pressure premixed c 3-oxygenated hydrocarbon flames with tunable synchrotron photoionization," *Combustion and Flame*, vol. 152, no. 3, pp. 336–359, 2008.
- [46] T. Kasper, P. Oßwald, U. Struckmeier, K. Kohse-Höinghaus, C. A. Taatjes, J. Wang, T. Cool, M. Law, A. Morel, and P. R. Westmoreland, "Combustion chemistry of the propanol isomers investigated by electron ionization and vuv-photoionization molecular-beam mass spectrometry," *Combustion and Flame*, vol. 156, no. 6, pp. 1181–1201, 2009.
- [47] C. Togbe, P. Dagaut, F. Halter, and F. Foucher, "2-propanol oxidation in a pressurized jet-stirred reactor (jsr) and combustion bomb: Experimental and detailed kinetic modeling study," *Energy and Fuels*, vol. 25, no. 2, pp. 676–683, 2011. cited By 9.
- [48] B. Galmiche, C. Togblé, P. Dagaut, F. Halter, and F. Foucher, "Experimental and detailed kinetic modeling study of the oxidation of 1-propanol in a pressurized jet-stirred reactor (jsr) and a combustion bomb," *Energy and Fuels*, vol. 25, no. 5, pp. 2013–2021, 2011. cited By 13.
- [49] P. S. Veloo and F. N. Egolfopoulos, "Studies of n-propanol, iso-propanol, and propane flames," *Combustion and Flame*, vol. 158, no. 3, pp. 501–510, 2011.
- [50] J. Beeckmann, L. Cai, and H. Pitsch, "Experimental investigation of the laminar burning velocities of methanol, ethanol, n-propanol, and n-butanol at high pressure," *Fuel*, vol. 117, pp. 340–350, 2014.
- [51] J. Gong, S. Zhang, Y. Cheng, Z. Huang, C. Tang, and J. Zhang, "A comparative study of n-propanol, propanal, acetone, and propane combustion in laminar flames," *Proceedings of the Combustion Institute*, vol. 35, no. 1, pp. 795–801, 2015.
- [52] M. Johnson, S. Goldsborough, Z. Serinyel, P. O'Toole, E. Larkin, G. O'Malley, and H. Curran, "A shock tube study of n- and iso-propanol ignition," *Energy and Fuels*, vol. 23, no. 12, pp. 5886–5898, 2009. cited By 46.
- [53] B. Akih-Kumgeh and J. M. Bergthorson, "Structure-reactivity trends of c1–c4 alkanolic acid methyl esters," *Combustion and Flame*, vol. 158, no. 6, pp. 1037–1048, 2011.
- [54] X. Man, C. Tang, J. Zhang, Y. Zhang, L. Pan, Z. Huang, and C. K. Law, "An experimental and kinetic modeling study of n-propanol and i-propanol ignition at high temperatures," *Combustion and Flame*, vol. 161, no. 3, pp. 644–656, 2014.
- [55] K. Yang, C. Zhan, X. Man, L. Guan, Z. Huang, and C. Tang, "Shock tube study on propanal ignition and the comparison to propane, n-propanol and i-propanol," *Energy & Fuels*, 2015.
- [56] S. M. Sarathy, P. Oswald, N. Hansen, and K. Kohse-Hoinghaus, "Alcohol combustion chemistry," *Progress in Energy and Combustion Science*, vol. 44, pp. 40–102, 2014.
- [57] G. Kalghatgi, *Fuel/Engine Interactions*. SAE International, 2013.
- [58] P. Richards, *Automotive Fuels Reference Book*. SAE International, 2014.
- [59] I. E. Agency, "Fuel ethers for gasoline."  
[http://iea-amf.org/content/fuel\\_information/ethanol/ethers](http://iea-amf.org/content/fuel_information/ethanol/ethers).

- [60] ICIS, "Methyl tertiary butyl ether (mtbe) production and manufacturing process." <http://www.icis.com/resources/news/2007/11/05/9076055/methyl-tertiary-butyl-ether-mtbe-production-and-manufacturing-process/>.
- [61] K. F. Yee, A. R. Mohamed, and S. H. Tan, "A review on the evolution of ethyl tert-butyl ether (etbe) and its future prospects," *Renewable and Sustainable Energy Reviews*, vol. 22, pp. 604 – 620, 2013.
- [62] E. P. Agency, "1990 clean air act amendment summary." <https://www.epa.gov/clean-air-act-overview/1990-clean-air-act-amendment-summary>.
- [63] T. C. Schmidt, "Analysis of methyl tert-butyl ether (mtbe) and tert-butyl alcohol (tba) in ground and surface water," *TrAC Trends in Analytical Chemistry*, vol. 22, no. 10, pp. 776 – 784, 2003.
- [64] B.-L. Yang, S.-B. Yang, and R. qing Yao, "Synthesis of ethyl tert-butyl ether from tert-butyl alcohol and ethanol on strong acid cation-exchange resins," *Reactive and Functional Polymers*, vol. 44, no. 2, pp. 167 – 175, 2000.
- [65] C. J. Donahue, T. D'Amico, and J. A. Exline, "Synthesis and characterization of a gasoline oxygenate, ethyl tert-butyl ether," *J. Chem. Educ.*, vol. 79, no. 6, p. 724, 2002.
- [66] E. F. O. Association, "European ether market and outlook." <http://www.efoa.eu/en/markets.aspx>.
- [67] M. T. Noorman, "The effect of mtbe, dipe and tame on vehicle emissions," tech. rep., SAE Technical Paper, 1993.
- [68] T. Cerri, G. DañErrico, and A. Onorati, "Experimental investigations on high octane number gasoline formulations for internal combustion engines," *Fuel*, vol. 111, pp. 305–315, 2013.
- [69] C. AnishRaman, K. Varatharajan, P. Abinesh, and N. Venkatachalapathi, "Analysis of mtbe as an oxygenate additive to gasoline,"
- [70] T. Topgül, "The effects of mtbe blends on engine performance and exhaust emissions in a spark ignition engine," *Fuel Processing Technology*, vol. 138, pp. 483–489, 2015.
- [71] I. Schifter, U. González, L. Díaz, C. González-Macías, and I. Mejía-Centeno, "Experimental and vehicle (on road) test investigations of spark-ignited engine performance and emissions using high concentration of mtbe as oxygenated additive," *Fuel*, vol. 187, pp. 276–284, 2017.
- [72] M. Hamdan and T. Al-Subaih, "Improvement of locally produced gasoline and studying its effects on both the performance of the engine and the environment," *Energy conversion and management*, vol. 43, no. 14, pp. 1811–1820, 2002.
- [73] J. Milpied, N. Jeuland, G. Plassat, S. Guichaous, N. Dioc, A. Marchal, and P. Schmelzle, "Impact of fuel properties on the performances and knock behaviour of a downsized turbocharged di si engine-focus on octane numbers and latent heat of vaporization," *SAE International Journal of Fuels and Lubricants*, vol. 2, no. 2009-01-0324, pp. 118–126, 2009.
- [74] R. Magnusson and C. Nilsson, "The influence of oxygenated fuels on emissions of aldehydes and ketones from a two-stroke spark ignition engine," *Fuel*, vol. 90, no. 3, pp. 1145–1154, 2011.

- [75] I. Schifter, U. González, and C. González-Macías, “Effects of ethanol, ethyl-tert-butyl ether and dimethyl-carbonate blends with gasoline on si engine,” *Fuel*, vol. 183, pp. 253–261, 2016.
- [76] O. I. Awad, R. Mamat, M. Noor, T. K. Ibrahim, I. Yusri, and A. Yusop, “The impacts of compression ratio on the performance and emissions of ice powered by oxygenated fuels: A review,” *Journal of the Energy Institute*, 2016.
- [77] G. Wallace, J. Blondy, W. Mirabella, E. Schulte-Körne, and J. Viljanen, “Ethyl tertiary butyl ether-a review of the technical literature,” *SAE International Journal of Fuels and Lubricants*, vol. 2, no. 2009-01-1951, pp. 940–952, 2009.
- [78] A. Arteconi, A. Mazzarini, and G. Di Nicola, “Emissions from ethers and organic carbonate fuel additives: a review,” *Water, Air, & Soil Pollution*, vol. 221, no. 1-4, pp. 405–423, 2011.
- [79] J. Brocard, F. Baronnet, and H. O’Neal, “Chemical kinetics of the oxidation of methyl tert-butyl ether (mtbe),” *Combustion and Flame*, vol. 52, pp. 25 – 35, 1983.
- [80] T. S. Norton and F. L. Dryer, “Twenty-third symposium (international) on combustion the flow reactor oxidation of c1?c4 alcohols and mtbe,” *Symposium (International) on Combustion*, vol. 23, no. 1, pp. 179 – 185, 1991.
- [81] H. J. Curran, M. P. Dunphy, J. M. Simmie, C. K. Westbrook, and W. J. Pitz, “Twenty-fourth symposium on combustion shock tube ignition of ethanol, isobutene and mtbe: Experiments and modeling,” *Symposium (International) on Combustion*, vol. 24, no. 1, pp. 769 – 776, 1992.
- [82] M. Yahyaoui, N. Djebaili-Chaumeix, P. Dagaut, and C.-E. Paillard, “Ethyl tertiary butyl ether ignition and combustion using a shock tube and spherical bomb,” *Energy and Fuels*, vol. 22, no. 6, pp. 3701–3708, 2008. cited By 10.
- [83] K. Yasunaga, J. Simmie, H. Curran, T. Koike, O. Takahashi, Y. Kuraguchi, and Y. Hidaka, “Detailed chemical kinetic mechanisms of ethyl methyl, methyl tert-butyl and ethyl tert-butyl ethers: The importance of uni-molecular elimination reactions,” *Combustion and Flame*, vol. 158, no. 6, pp. 1032 – 1036, 2011.
- [84] E. Kaiser, J. Andino, W. Siegl, R. Hammerle, and J. Butler, “Hydrocarbon and aldehyde emissions from an engine fueled with ethyl-t-butyl ether,” *Journal of the Air and Waste Management Association*, vol. 41, no. 2, pp. 195–197, 1991. cited By 14.
- [85] A. Ciajolo, A. D’Anna, and M. Kurz, “Low-temperature oxidation of mtbe in a high-pressure jet-stirred flow reactor,” *Combustion Science and Technology*, vol. 123, no. 1-6, pp. 49–61, 1997. cited By 0.
- [86] A. Goldaniga, T. Faravelli, E. Ranzi, P. Dagaut, and M. Cathonnet, “Oxidation of oxygenated octane improvers: Mtbe, etbe, dipe, and {TAME},” *Symposium (International) on Combustion*, vol. 27, no. 1, pp. 353 – 360, 1998. Twenty-Seventh Symposium (International) on Combustion Volume One.
- [87] P. Glaude, F. Battin-Leclerc, B. Judenherc, V. Warth, R. Fournet, G. C?me, G. Scacchi, P. Dagaut, and M. Cathonnet, “Experimental and modeling study of the gas-phase oxidation of methyl and ethyl tertiary butyl ethers,” *Combustion and Flame*, vol. 121, no. 1C2, pp. 345 – 355, 2000.
- [88] X. Liu, S. Ito, and Y. Wada, “Oxidation characteristic and products of etbe (ethyl tert-butyl ether),” *Energy*, vol. 82, pp. 184–192, 2015.

- [89] X. Liu, Q. Zhang, S. Ito, and Y. Wada, "Oxidation characteristics and products of five ethers at low temperature," *Fuel*, vol. 165, pp. 513–525, 2016.
- [90] M. D. Boot, M. Tian, E. J. Hensen, and S. M. Sarathy, "Impact of fuel molecular structure on auto-ignition behavior: Design rules for future high performance gasolines," *Progress in Energy and Combustion Science*, vol. 60, pp. 1 – 25, 2017.
- [91] P. Dagaut, R. Koch, and M. Cathonnet, "The oxidation of n-heptane in the presence of oxygenated octane improvers: Mtbe and etbe," *Combustion Science and Technology*, vol. 122, no. 1-6, pp. 345–361, 1997. cited By 0.
- [92] F. Battin-Leclerc, P. Glaude, V. Warth, R. Fournet, G. Scacchi, and G. C. me, "Computer tools for modelling the chemical phenomena related to combustion," *Chemical Engineering Science*, vol. 55, no. 15, pp. 2883 – 2893, 2000.
- [93] T. Ogura, Y. Sakai, A. Miyoshi, M. Koshi, and P. Dagaut, "Modeling of the oxidation of primary reference fuel in the presence of oxygenated octane improvers: ethyl tert-butyl ether and ethanol," *Energy & Fuels*, vol. 21, no. 6, pp. 3233–3239, 2007.
- [94] M. P. Dunphy and J. M. Simmie, "Combustion of methyl tert-butyl ether. part i: Ignition in shock waves," *Combustion and Flame*, vol. 85, no. 3-4, pp. 489–498, 1991.
- [95] K. Fieweger, R. Blumenthal, and G. Adomeit, "Shock-tube investigations on the self-ignition of hydrocarbon-air mixtures at high pressures," in *Symposium (International) on Combustion*, vol. 25, pp. 1579–1585, Elsevier, 1994.
- [96] K. Fieweger, R. Blumenthal, and G. Adomeit, "Self-ignition of si engine model fuels: a shock tube investigation at high pressure," *Combustion and Flame*, vol. 109, no. 4, pp. 599–619, 1997.
- [97] F. Battin-Leclerc, "Detailed chemical kinetic models for the low-temperature combustion of hydrocarbons with application to gasoline and diesel fuel surrogates," *Progress in Energy and Combustion Science*, vol. 34, no. 4, pp. 440–498, 2008.
- [98] L. S. Tran, B. Sirjean, P.-A. Glaude, R. Fournet, and F. Battin-Leclerc, "Progress in detailed kinetic modeling of the combustion of oxygenated components of biofuels," *Energy*, vol. 43, no. 1, pp. 4–18, 2012.
- [99] F. Battin-Leclerc, J. M. Simmie, and E. Blurock, *Cleaner Combustion: Developing Detailed Chemical Kinetic Models*. Springer Science & Business Media, 2013.
- [100] E. Ranzi, "A wide-range kinetic modeling study of oxidation and combustion of transportation fuels and surrogate mixtures," *Energy & fuels*, vol. 20, no. 3, pp. 1024–1032, 2006.
- [101] C. J. Mueller, W. J. Cannella, T. J. Bruno, B. Bunting, H. D. Dettman, J. A. Franz, M. L. Huber, M. Natarajan, W. J. Pitz, M. A. Ratcliff, *et al.*, "Methodology for formulating diesel surrogate fuels with accurate compositional, ignition-quality, and volatility characteristics," *Energy & Fuels*, vol. 26, no. 6, pp. 3284–3303, 2012.
- [102] W. J. Pitz, N. P. Cernansky, F. L. Dryer, F. Egolfopoulos, J. Farrell, D. Friend, and H. Pitsch, "Development of an experimental database and chemical kinetic models for surrogate gasoline fuels," tech. rep., SAE Technical Paper, 2007.
- [103] M. Yao, Z. Zheng, and H. Liu, "Progress and recent trends in homogeneous charge compression ignition (hcci) engines," *Progress in Energy and Combustion Science*, vol. 35, no. 5, pp. 398 – 437, 2009.

- [104] N. Komninos and C. Rakopoulos, "Modeling HCCI combustion of biofuels: A review," *Renewable and Sustainable Energy Reviews*, vol. 16, no. 3, pp. 1588 – 1610, 2012.
- [105] L. Chen, T. Li, T. Yin, and B. Zheng, "A predictive model for knock onset in spark-ignition engines with cooled EGR," *Energy Conversion and Management*, vol. 87, no. 0, pp. 946 – 955, 2014.
- [106] W. J. Pitz and C. J. Mueller, "Recent progress in the development of diesel surrogate fuels," *Progress in Energy and Combustion Science*, vol. 37, no. 3, pp. 330 – 350, 2011.
- [107] M. Mehl, W. J. Pitz, C. K. Westbrook, and H. J. Curran, "Kinetic modeling of gasoline surrogate components and mixtures under engine conditions," *Proceedings of the Combustion Institute*, vol. 33, no. 1, pp. 193 – 200, 2011.
- [108] E. Ranzi, A. Frassoldati, R. Grana, A. Cuoci, T. Faravelli, A. Kelley, and C. Law, "Hierarchical and comparative kinetic modeling of laminar flame speeds of hydrocarbon and oxygenated fuels," *Progress in Energy and Combustion Science*, vol. 38, no. 4, pp. 468–501, 2012.
- [109] S. Dooley, S. H. Won, M. Chaos, J. Heyne, Y. Ju, F. L. Dryer, K. Kumar, C.-J. Sung, H. Wang, M. A. Oehlschlaeger, *et al.*, "A jet fuel surrogate formulated by real fuel properties," *Combustion and Flame*, vol. 157, no. 12, pp. 2333–2339, 2010.
- [110] H. Wang, E. Dames, B. Sirjean, D. Sheen, R. Tangko, A. Violi, J. Lai, F. Egolfopoulos, D. Davidson, R. Hanson, *et al.*, "Jetsurf version 2.0: A high-temperature chemical kinetic model of n-alkane (up to n-dodecane), cyclohexane, and methyl-, ethyl-, n-propyl and n-butyl-cyclohexane oxidation at high temperatures," 2010.
- [111] T. Lu and C. Law, "A directed relation graph method for mechanism reduction," *Proceedings of the Combustion Institute*, vol. 30, no. 1, pp. 1333–1341, 2005.
- [112] P. Pepiot-Desjardins and H. Pitsch, "An efficient error-propagation-based reduction method for large chemical kinetic mechanisms," *Combustion and Flame*, vol. 154, no. 1, pp. 67–81, 2008.
- [113] K. E. Niemeyer, C.-J. Sung, and M. P. Raju, "Skeletal mechanism generation for surrogate fuels using directed relation graph with error propagation and sensitivity analysis," *Combustion and flame*, vol. 157, no. 9, pp. 1760–1770, 2010.
- [114] G. Esposito and H. Chelliah, "Skeletal reaction models based on principal component analysis: Application to ethylene/air ignition, propagation, and extinction phenomena," *Combustion and Flame*, vol. 158, no. 3, pp. 477–489, 2011.
- [115] B. Akih-Kumgeh and J. Bergthorson, "Skeletal chemical kinetic mechanisms for syngas, methyl butanoate, n-heptane, and n-decane," *Energy & Fuels*, vol. 27, no. 4, pp. 2316–2326, 2013.
- [116] X. Zou, H. Wang, Z. Zheng, R. Reitz, and M. Yao, "Numerical study of the rcci combustion processes fuelled with methanol, ethanol, n-butanol and diesel," tech. rep., SAE Technical Paper, 2016.
- [117] V. Sivasankaralingam, V. Raman, M. Ali, A. Alfazazi, T. Lu, H. Im, S. Sarathy, and R. Dibble, "Experimental and numerical investigation of ethanol/diethyl ether mixtures in a ci engine," tech. rep., SAE Technical Paper, 2016.

- [118] H. Wang, R. D. Reitz, M. Yao, B. Yang, Q. Jiao, and L. Qiu, "Development of an n-heptane-n-butanol-pah mechanism and its application for combustion and soot prediction," *Combustion and Flame*, vol. 160, no. 3, pp. 504–519, 2013.
- [119] J. Munzar, B. Akih-Kumgeh, B. Denman, A. Zia, and J. Bergthorson, "An experimental and reduced modeling study of the laminar flame speed of jet fuel surrogate components," *Fuel*, vol. 113, pp. 586–597, 2013.
- [120] N. Peters, B. Akih-Kumgeh, and J. Bergthorson., "Comparative analysis of chemical kinetic models using the alternate species elimination (ASE) approach," *Journal of Engineering for Gas Turbines and Power*, 2014. In Press.
- [121] A. Vandersickel, M. Hartmann, K. Vogel, Y. Wright, M. Fikri, R. Starke, C. Schulz, and K. Boulouchos, "The autoignition of practical fuels at HCCI conditions: High-pressure shock tube experiments and phenomenological modeling," *Fuel*, vol. 93, no. 0, pp. 492 – 501, 2012.
- [122] A. Vandersickel, Y. Wright, and K. Boulouchos, "Global reaction mechanism for the auto-ignition of full boiling range gasoline and kerosene fuels," *Combustion Theory and Modelling*, vol. 17, no. 6, pp. 1020–1052, 2013.
- [123] S. Gowdagiri and M. Oehlschlaeger, "Global reduced model for conventional and alternative jet and diesel fuel autoignition," *Energy & Fuels*, vol. 28, no. 4, pp. 2795–2801, 2014.
- [124] J. M. Simmie, "Detailed chemical kinetic models for the combustion of hydrocarbon fuels," *Progress in Energy and Combustion Science*, vol. 29, no. 6, pp. 599 – 634, 2003.
- [125] K. Bhaskaran and P. Roth, "The shock tube as wave reactor for kinetic studies and material systems," *Progress in Energy and Combustion Science*, vol. 28, no. 2, pp. 151–192, 2002.
- [126] A. G. Gaydon and I. R. Hurle, *The shock tube in high-temperature chemical physics*. Chapman and Hall, 1963.
- [127] D. Davidson and R. Hanson, "Interpreting shock tube ignition data," *International Journal of Chemical Kinetics*, vol. 36, no. 9, pp. 510–523, 2004. cited By 102.
- [128] P. Cadman, G. Thomas, and P. Butler, "The auto-ignition of propane at intermediate temperatures and high pressures," *Physical Chemistry Chemical Physics*, vol. 2, no. 23, pp. 5411–5419, 2000. cited By 46.
- [129] A. Amadio, M. Crofton, and E. Petersen, "Test-time extension behind reflected shock waves using co<sub>2</sub>-he and c<sub>3</sub>h<sub>8</sub>-he driver mixtures," *Shock Waves*, vol. 16, no. 2, pp. 157–165, 2006. cited By 0.
- [130] H. Li, A. Farooq, J. Jeffries, and R. Hanson, "Near-infrared diode laser absorption sensor for rapid measurements of temperature and water vapor in a shock tube," *Applied Physics B: Lasers and Optics*, vol. 89, no. 2, pp. 407–416, 2007.
- [131] A. Farooq, J. B. Jeffries, and R. Hanson, "Co<sub>2</sub> concentration and temperature sensor for combustion gases using diode-laser absorption near 2.7  $\mu\text{m}$ ," *Applied Physics B: Lasers and Optics*, vol. 90, no. 3, pp. 619–628, 2008.
- [132] C. Goldenstein, R. Spearrin, J. Jeffries, and R. Hanson, "Wavelength-modulation spectroscopy near 2.5  $\mu\text{m}$  for h<sub>2</sub>o and temperature in high-pressure and-temperature gases," *Applied Physics B*, vol. 116, no. 3, pp. 705–716, 2014.

- [133] D. F. Davidson and R. K. Hanson, "Real gas corrections in shock tube studies at high pressures," *Israel journal of chemistry*, vol. 36, no. 3, pp. 321–326, 1996.
- [134] W. Tsang, "Comparative rate single pulse shock tube studies on the thermal stability of polyatomic molecules," *Shock waVes in chemistry*, pp. 59–129, 1981.
- [135] R. Tranter, R. Sivaramakrishnan, N. Srinivasan, and K. Brezinsky, "Calibration of reaction temperatures in a very high pressure shock tube using chemical thermometers," *International Journal of Chemical Kinetics*, vol. 33, no. 11, pp. 722–731, 2001.
- [136] S. W. Benson and J. H. Buss, "Additivity rules for the estimation of molecular properties. thermodynamic properties," *The Journal of Chemical Physics*, vol. 29, no. 3, pp. 546–572, 1958.
- [137] M. A. Eldeeb and B. Akih-Kumgeh, "Reactivity trends in furan and alkyl furan combustion," *Energy & Fuels*, vol. 28, no. 10, pp. 6618–6626, 2014.
- [138] M. A. Eldeeb and B. Akih-Kumgeh, "Investigation of 2, 5-dimethyl furan and iso-octane ignition," *Combustion and Flame*, vol. 162, no. 6, pp. 2454–2465, 2015.
- [139] M. A. Eldeeb, *Characterization and Chemical Kinetic Analysis of the Ignition of Representative Conventional and Bio-Derived Fuels*. PhD thesis, SYRACUSE UNIVERSITY, 2015.
- [140] E. Petersen, M. Rickard, M. Crofton, E. Abbey, M. Traum, and D. Kalitan, "A facility for gas-and condensed-phase measurements behind shock waves," *Measurement Science and Technology*, vol. 16, no. 9, p. 1716, 2005.
- [141] V. P. Zhukov, V. A. Sechenov, and A. Y. Starikovskiy, "Autoignition of kerosene (jet-a)/air mixtures behind reflected shock waves," *Fuel*, vol. 126, pp. 169–176, 2014.
- [142] J. P. Holman and W. J. Gajda, *Experimental methods for engineers*, vol. 2. McGraw-Hill New York, 1994.
- [143] J. R. Taylor and W. Thompson, *An introduction to error analysis: the study of uncertainties in physical measurements*. AIP, 1998.
- [144] M. Eldeeb and B. Akih-Kumgeh, "Reactivity trends in furan and alkyl furan combustion," *Energy and Fuels*, vol. 28, no. 10, pp. 6618–6626, 2014. cited By 0.
- [145] J. A. Miller, R. J. Kee, and C. K. Westbrook, "Chemical kinetics and combustion modeling," *Annual Review of Physical Chemistry*, vol. 41, no. 1, pp. 345–387, 1990.
- [146] T. Turányi and A. S. Tomlin, *Analysis of kinetic reaction mechanisms*. Springer, 2014.
- [147] J. B. Heywood, *Internal combustion engine fundamentals*, vol. 930. Mcgraw-hill New York, 1988.
- [148] R. D. Reitz, "Grand challenges in engine and automotive engineering," *Frontiers in Mechanical Engineering*, vol. 2, p. 1, 2015.
- [149] O. Herbinet, W. J. Pitz, and C. K. Westbrook, "Detailed chemical kinetic mechanism for the oxidation of biodiesel fuels blend surrogate," *Combustion and Flame*, vol. 157, no. 5, pp. 893 – 908, 2010.



- [150] S. Honnet, K. Seshadri, U. Niemann, and N. Peters, "A surrogate fuel for kerosene," *Proceedings of the Combustion Institute*, vol. 32, no. 1, pp. 485–492, 2009.
- [151] L. Cai, Y. Uygun, C. Togblé, H. Pitsch, H. Olivier, P. Dagaut, and S. M. Sarathy, "An experimental and modeling study of n-octanol combustion," *Proceedings of the Combustion Institute*, vol. 35, no. 1, pp. 419 – 427, 2015.
- [152] B. Gauthier, D. Davidson, and R. Hanson, "Shock tube determination of ignition delay times in full-blend and surrogate fuel mixtures," *Combustion and Flame*, vol. 139, no. 4, pp. 300 – 311, 2004.
- [153] M. Fikri, J. Herzler, R. Starke, C. Schulz, P. Roth, and G. Kalghatgi, "Autoignition of gasoline surrogates mixtures at intermediate temperatures and high pressures," *Combustion and Flame*, vol. 152, no. 11C2, pp. 276 – 281, 2008.
- [154] N. Peters, G. Paczko, R. Seiser, and K. Seshadri, "Temperature cross-over and non-thermal runaway at two-stage ignition of n-heptane," *Combustion and Flame*, vol. 128, pp. 38–59, 2002.
- [155] S. Jouzdani, A. Zhou, and B. Akih-Kumgeh, "Propanol isomers: Investigation of ignition and pyrolysis time scales," *Combustion and Flame*, vol. 176, pp. 229 – 244, 2017.
- [156] N. Peters, B. Akih-Kumgeh, and J. Bergthorson, "Comparative analysis of chemical kinetic models using the alternate species elimination approach," *Journal of Engineering for Gas Turbines and Power*, vol. 137, no. 2, p. 021505, 2015.
- [157] M. Frisch, G. Trucks, H. Schlegel, G. Scuseria, M. Robb, J. Cheeseman, G. Scalmani, V. Barone, B. Mennucci, G. Petersson, *et al.*, "Gaussian 09, revision a. 1; gaussian: Wallingford, ct, 2009," *There is no corresponding record for this reference*.
- [158] T. Ogura, A. Miyoshi, and M. Koshi, "Rate coefficients of h-atom abstraction from ethers and isomerization of alkoxyalkylperoxy radicals," *Physical Chemistry Chemical Physics*, vol. 9, no. 37, pp. 5133–5142, 2007.
- [159] S. M. Sarathy, P. Oßwald, N. Hansen, and K. Kohse-Höinghaus, "Alcohol combustion chemistry," *Progress in Energy and Combustion Science*, vol. 44, pp. 40–102, 2014.
- [160] S. Klotz, K. Brezinsky, and I. Glassman, "Symp.(int.) comb," Proc, 1998.
- [161] H. J. Curran, W. Pitz, C. Westbrook, G. Callahan, and F. Dryer, "Oxidation of automotive primary reference fuels at elevated pressures," in *Symposium (International) on Combustion*, vol. 27, pp. 379–387, Elsevier, 1998.
- [162] P. Dagaut and C. Togbé, "Experimental and modeling study of the kinetics of oxidation of ethanol- gasoline surrogate mixtures (e85 surrogate) in a jet-stirred reactor," *Energy & Fuels*, vol. 22, no. 5, pp. 3499–3505, 2008.
- [163] P. Dagaut and C. Togbé, "Experimental and modeling study of the kinetics of oxidation of butanol- n-heptane mixtures in a jet-stirred reactor," *Energy & Fuels*, vol. 23, no. 7, pp. 3527–3535, 2009.
- [164] J. Zhang, S. Niu, Y. Zhang, C. Tang, X. Jiang, E. Hu, and Z. Huang, "Experimental and modeling study of the auto-ignition of n-heptane/n-butanol mixtures," *Combustion and Flame*, vol. 160, no. 1, pp. 31–39, 2013.
- [165] Reaction Design: San Diego, "CHEMKIN-PRO," 2013.

- [166] M. Mehl, J.-Y. Chen, W. J. Pitz, S. M. Sarathy, and C. K. Westbrook, "An approach for formulating surrogates for gasoline with application toward a reduced surrogate mechanism for cfd engine modeling," *Energy & Fuels*, vol. 25, no. 11, pp. 5215–5223, 2011.
- [167] W. Wang and M. A. Oehlschlaeger, "A shock tube study of methyl decanoate autoignition at elevated pressures," *Combustion and Flame*, vol. 159, no. 2, pp. 476 – 481, 2012.
- [168] Z. Li, W. Wang, Z. Huang, and M. A. Oehlschlaeger, "Autoignition of methyl decanoate, a biodiesel surrogate, under high-pressure exhaust gas recirculation conditions," *Energy & Fuels*, vol. 26, no. 8, pp. 4887–4895, 2012.
- [169] G. Kukkadapu, K. Kumar, C.-J. Sung, M. Mehl, and W. J. Pitz, "Autoignition of gasoline and its surrogates in a rapid compression machine," *Proceedings of the Combustion Institute*, vol. 34, no. 1, pp. 345 – 352, 2013.
- [170] J. Livengood and P. Wu, "Correlation of autoignition phenomena in internal combustion engines and rapid compression machines," *Symposium (International) on Combustion*, vol. 5, no. 1, pp. 347 – 356, 1955.

**Vita**

Author's Name: Apeng Zhou

Place of Birth: Fuyang, Anhui, China

Date of Birth: October 24, 1989

Degrees Awarded:

Bachelor of Science, Hefei University of Technology, 2010

Master of Science, Xi'an Jiaotong University, 2013

Professional Experience:

Research and Teaching Assistant, Syracuse University Department of MAE, 2013-2017

Summer Research Intern, Fulton Companies, 2015